

100



LEVEL

AD A100794



DTIC FILE COPY

UNITED STATES AIR FORCE  
AIR UNIVERSITY

AIR FORCE INSTITUTE OF TECHNOLOGY

Wright-Patterson Air Force Base, Ohio

DTIC  
ELECTE  
JUL 1 1981

A

This document has been approved  
for public release and sale; its  
distribution is unlimited.

81 6

30 077

14

AFIT/GE/EE/80D-36

11 Dec 80

12 144

6 Direct Digital Design Method For  
Reconfigurable Multivariable Control Laws  
for the A-7D Digitac II Aircraft.

9 ~~master's~~ Thesis

AFIT/GE/EE/80D-36

10 David W. Potts  
1st Lt USAF

DTIC  
ELECTE  
JUL 1 1981

A

012225

gwr

DIRECT DIGITAL DESIGN METHOD FOR RECONFIGURABLE  
MULTIVARIABLE CONTROL LAWS FOR  
THE A-7D DIGITAC II AIRCRAFT

THESIS

Presented to the Faculty of the School of Engineering  
of the Air Force Institute of Technology  
Air University  
in Partial Fulfillment of the  
Requirements for the Degree of  
Master of Science

by

David W. Potts, B.S.E.E.

1st Lt USAF

Graduate Electrical Engineering

December 1980

Accession For	
MIS CRUI	<input checked="checked" type="checkbox"/>
PMIC TAB	<input type="checkbox"/>
Unprocessed	<input type="checkbox"/>
Post Migration	
Date of	
Availability Codes	
and, or	
Special	

A

Approved for public release; distribution unlimited

In my search for a thesis topic, I wanted one that paralleled my graduate courses in the flight control sequence. The topic of reconfigurable control laws was a perfect area for research. This is a new area of study and meets the needs of future Air Force aircraft. This study was proposed by the AFWAL/Flight Dynamics Laboratory (FDL) and investigates how the inherently redundant control surfaces of future aircraft could be utilized after a surface failure by employing a digital flight control system (DFCS).

This thesis provides an accurate aircraft model for further research into the area of reconfigurable control laws. I also attempt to show how a direct digital design method using the entire eigenstructure assignment can be implemented to design a state feedback control law.

I want to express my gratitude to Dr. J. D'Azzo for his guidance in the thesis development and unending effort in the reading of this thesis for accuracy and completeness. My appreciation to Mr. Jerry Jenkins, Flight Dynamics Laboratory (FDL), for his assistance in deriving the essential aircraft data that was needed to complete this report.

I also wish to thank my sponsor, Mr. Duane Robertus (FDL), Professor C. H. Houppis, and Capt. J. Silverthorn for their assistance and suggestions.

## Contents

	Page
Preface . . . . .	ii
List of Figures . . . . .	v
List of Symbols . . . . .	viii
Abstract . . . . .	xii
I. Introduction . . . . .	1
Background . . . . .	1
Problem . . . . .	3
Scope . . . . .	3
Assumptions . . . . .	4
Approach and Presentation . . . . .	4
II. The Aircraft Model . . . . .	7
Introduction . . . . .	7
General Description . . . . .	7
System Model . . . . .	8
Control Derivatives . . . . .	9
Summary . . . . .	9
III. Theory of Entire Eigenstructure Assignment . . . . .	10
Introduction . . . . .	10
Distinct Eigenvalue Assignment . . . . .	11
Multiple Eigenvalue Assignment . . . . .	17
Tracker . . . . .	24
Continuous Simulation . . . . .	26
Summary . . . . .	26
IV. Design of Reconfigurable Multivariable Control Law . . . . .	28
Introduction . . . . .	28
CESA Modification . . . . .	29
Controllability . . . . .	30
Control Law Design . . . . .	33
Regulator Control Law . . . . .	37
Summary . . . . .	90a
V. Conclusion and Recommendation . . . . .	97
Bibliography . . . . .	100

## Contents

	Page
Appendix A, Aircraft Equations of Motion . . . . .	102
Appendix B, Control Derivatives . . . . .	117
Vita . . . . .	128

# List of Figures

<u>Figure</u>		<u>Page</u>
1	Continuous-Time System Block Diagram . . . . .	12
2	Discrete-Time System Block Diagram . . . . .	12
3	Regulator Design Example Time Responses	
	a. $X_1(t)$ vs. $t$ . . . . .	18
	b. $X_2(t)$ vs. $t$ . . . . .	19
	c. $X_3(t)$ vs. $t$ . . . . .	20
	d. $y_1(t)$ vs. $t$ . . . . .	21
	e. $y_2(t)$ vs. $t$ . . . . .	22
4	Control Surface Failure vs. Reconfigured Input (9) Matrix	34
5	Output Signals of (a) Original System and (b) Internally Balanced System . . . . .	39
6	Continuous-Time Simulation Responses for the Original System Equations	
	a. Pitch Angle for 0.1 Rad Impulse $\delta_{h_1}$ Input . . . . .	41
	b. Pitch Rate for 0.1 Rad Impulse $\delta_{h_1}$ Input . . . . .	42
	c. Roll Angle for 0.2 Rad Impulse $\delta_{a_1}$ Input . . . . .	43
	d. Roll Rate for 0.2 Rad Impulse $\delta_{a_1}$ Input . . . . .	44
	e. Roll Angle for 0.1 Rad Impulse $\delta_{h_1}$ Input . . . . .	45
	f. Roll Angle for 0.1 Rad Impulse $\delta_{h_r}$ Input . . . . .	46
	g. Sideslip Angle for 0.07 Rad Impulse $\delta_r$ Input . . . . .	47
	h. Yaw Angle for 0.2 Rad Impulse $\delta_{a_1}$ Input . . . . .	48
7	Continuous-Time Simulation Responses for the Balanced System Equations	
	a. Pitch Angle for 0.1 Rad Impulse $\delta_{h_1}$ Input . . . . .	50
	b. Pitch Rate for 0.1 Rad Impulse $\delta_{h_1}$ Input . . . . .	51
	c. Roll Angle for 0.2 Rad Impulse $\delta_{a_1}$ Input . . . . .	52
	d. Roll Rate for 0.2 Rad Impulse $\delta_{a_1}$ Input . . . . .	53
	e. Sideslip Angle for 0.07 Rad Impulse $\delta_r$ Input . . . . .	54
	f. Yaw Angle for 0.07 Rad Impulse $\delta_{a_1}$ Input . . . . .	55

## List of Figures

(Continued)

<u>Figure</u>		<u>Page</u>
8	Continuous-Time Simulation Responses for the Reduced Balanced System Equations	
	a. Pitch Angle for 0.1 Rad Impulse $\delta_{h_1}$ Input . . . . .	56
	b. Pitch Rate for 0.1 Rad Impulse $\delta_{h_1}$ Input . . . . .	57
	c. Roll Angle for 0.2 Rad Impulse $\delta_{a_1}$ Input . . . . .	58
	d. Roll Rate for 0.2 Rad Impulse $\delta_{a_1}$ Input . . . . .	59
	e. Sideslip Angle for 0.07 Rad Impulse $\delta_r$ Input . . . . .	60
	f. Yaw Angle for 0.07 Rad Impulse $\delta_{a_1}$ Input . . . . .	61
9	Control Surface Failure vs. Reconfigured Input (7) Matrix	62
10	State Feedback Block Diagram of the Original System . . .	64
11	State Feedback Block Diagram of the Balanced System . . .	64
12	Continuous-Time Simulation Responses for the Regulator Design of the Original System	
	a. Pitch Angle, Initial Condition 0.1 Rad vs. t . . . . .	69
	b. Pitch Rate vs. t . . . . .	70
	c. Roll Angle, Initial Conditions 0.2 Rad vs. t . . . . .	71
	d. Roll Rate vs. t . . . . .	72
	e. Sideslip Angle vs. t . . . . .	73
	f. Yaw Rate vs. t . . . . .	74
13	Continuous-Time Simulation Responses for the Regulator Design of the Balanced System	
	a. Pitch Angle vs. t . . . . .	81
	b. Pitch Rate vs. t . . . . .	82
	c. Roll Angle vs. t . . . . .	83
	d. Roll Rate vs. t . . . . .	84
	e. Sideslip Angle vs. t . . . . .	85
	f. Yaw Rate vs. t . . . . .	86

## List of Figures

(Continued)

<u>Figure</u>		<u>Page</u>
14	Continuous-Time Simulation Responses for the Regulator Design of the Reduced Balanced System	
	a. Pitch Angle vs. $t$ . . . . .	91
	b. Pitch Rate vs. $t$ . . . . .	92
	c. Roll Angle vs. $t$ . . . . .	93
	d. Roll Rate vs. $t$ . . . . .	94
	e. Sideslip Angle vs. $t$ . . . . .	95
	f. Yaw Rate vs. $t$ . . . . .	96

# List of Symbols

$b$	(Wing) span	ft
$\bar{c}$	Mean aerodynamic (geometric) chord	ft
$C_L = \frac{L}{\bar{q}S}$	Lift coefficient (airplane)	
$C_D = \frac{D}{\bar{q}S}$	Drag coefficient (airplane)	
$C_m = \frac{M}{\bar{q}S\bar{c}}$	Pitching moment coefficient (airplane, planform)	
$C_{\ell} = \frac{L}{\bar{q}Sb}$	Rolling moment coefficient	
$C_n = \frac{N}{\bar{q}Sb}$	Yawing moment coefficient	
$C_y = \frac{F_y}{\bar{q}S}$	Side force coefficient	
$C_{D_\delta} = \frac{\partial C_D}{\partial \delta}$	Variation of drag coefficient with control surface angle	$\text{deg}^{-1},$ $\text{rad}^{-1}$
$C_{L_{i_h}} = \frac{\partial C_L}{\partial i_h}$	Variation of lift coefficient with stabilizer angle	$\text{deg}^{-1},$ $\text{rad}^{-1}$
$C_{L_\delta} = \frac{\partial C_L}{\partial \delta}$	Variation of lift coefficient with control surface angle	$\text{deg}^{-1},$ $\text{rad}^{-1}$
$C_{m_\alpha} = \frac{\partial C_m}{\partial \alpha}$	Variation of Pitching moment co- efficient with angle of attack (i.e. static longitudinal stability)	$\text{rad}^{-1}$
$C_{m_{i_h}} = \frac{\partial C_m}{\partial i_h}$	Variation of pitching moment co- efficient with stabilizer angle (i.e. longitudinal control power)	$\text{deg}^{-1},$ $\text{rad}^{-1}$
$C_{m_\delta} = \frac{\partial C_m}{\partial \delta}$	Variation of pitching moment co- efficient with control surface angle	$\text{deg}^{-1},$ $\text{rad}^{-1}$

$C_{l_\delta} = \frac{\partial C_l}{\partial \delta}$	Variation of rolling moment coefficient with control surface angle	deg <sup>-1</sup> , rad <sup>-1</sup>
$C_{y_\delta} = \frac{\partial C_y}{\partial \delta}$	Variation of side force coefficient with control surface angle	deg <sup>-1</sup> , rad <sup>-1</sup>
$C_{n_\delta} = \frac{\partial C_n}{\partial \delta}$	Variation of yawing moment coefficient with control surface angle	deg <sup>-1</sup> , rad <sup>-1</sup>
$g$	Acceleration of gravity	ft/sec <sup>2</sup>
$I_{xx}, I_{yy}, I_{zz}$	Moments of inertia about X, Y, Z axes respectively	slug ft <sup>2</sup>
$I_{xz}$	Product of inertia in XYZ system	slug ft <sup>2</sup>
$i_H$	Stabilizer incidence angle	deg
$L_\beta$	Dimensional variation of rolling moment about $X_S$ with sideslip angle	sec <sup>-2</sup>
$L_p$	Dimensional variation of rolling moment about $X_S$ with roll rate	sec <sup>-1</sup>
$L_r$	Dimensional variation of rolling moment about $X_S$ with yaw rate	sec <sup>-1</sup>
$L_\delta$	Dimensional variation of rolling moment about $X_S$ with stabilizer, aileron, flap, rudder, and spoiler where $\delta = \delta_{it}, \delta_a, \delta_f, \delta_r, \delta_s$ angle	sec <sup>-2</sup>
$m$	Mass (airplane)	slugs
$M_u$	Dimensional variation of pitching moment with speed	ft <sup>-1</sup> sec <sup>-1</sup>
$M_\alpha$	Dimensional variation of pitching moment with angle of attack	sec <sup>-2</sup>
$M_{\dot{\alpha}}$	Dimensional variation of pitching moment with rate of change of angle of attack	sec <sup>-1</sup>
$M_q$	Dimensional variation of pitching moment with pitch rate	sec <sup>-1</sup>
$M_\delta$	Dimensional variation of pitching moment with a stabilizer, aileron, flap, rudder, spoiler where $\delta = \delta_{it}, \delta_a, \delta_f, \delta_r, \delta_s$ angle	sec <sup>-2</sup>

$n$	Perturbed yawing moment	ft lbs
$N_\beta$	Dimensional variation of yawing moment about $Z_s$ with sideslip angle	$\text{sec}^{-2}$
$N_p$	Dimensional variation of yawing moment about $Z_s$ with roll rate	$\text{sec}^{-1}$
$N_r$	Dimensional variation of yawing moment about $Z_s$ with yaw rate	$\text{sec}^{-1}$
$N_\delta$	Dimensional variation of yawing moment about $Z_s$ with stabilizer, aileron, flap, rudder, and spoiler, where $\delta = \delta_{it}, \delta_a, \delta_f, \delta_r, \delta_s$ angle	$\text{sec}^{-2}$
$p$	Perturbed roll rate (about x)	rad/sec
$\bar{q}$	Dynamic pressure	$\text{lbs/ft}^2$
$r$	Perturbed yaw rate	rad/sec
$S$	Surface area, Reference (wing) area	$\text{ft}^2$
$U_1$	Forward velocity (along X) steady state	ft/sec
$u$	Perturbed forward velocity (along X)	ft/sec
$v$	Perturbed side velocity	ft/sec
$w$	Perturbed downward velocity	ft/sec
$X_u$	Dimensional variation of $X_s$ -force with speed	$\text{sec}^{-1}$
$X_\alpha$	Dimensional variation of $X_s$ -force with angle of attack	$\text{ft/sec}^2$
$X_{\dot{\alpha}}$	Dimensional variation of $X_s$ -force with rate of change of angle of attack	ft/sec
$X_\delta$	Dimensional variation of $X_s$ -force with stabilizer, aileron, flap, rudder, and spoiler where $\delta = \delta_{it}, \delta_a, \delta_f, \delta_r, \delta_s$ angle	$\text{ft/sec}^2$
$Y_\beta$	Dimensional variation of $Y_s$ -force with sideslip angle	$\text{ft/sec}^2$

$Y_p$	Dimensional variation of $Y_S$ -force with roll rate	ft/sec
$Y_r$	Dimensional variation of $Y_S$ -force with yaw rate	ft/sec
$Y_\delta$	Dimensional variation of $Y_S$ -force with stabilizer, aileron, flap rudder, and spoiler where $\delta = \delta_{it}, \delta_a, \delta_f, \delta_r, \delta_s$ angle	ft/sec <sup>2</sup>
$Z_u$	Dimensional variation of $Z_S$ -force with speed	sec <sup>-1</sup>
$Z_\alpha$	Dimensional variation of $Z_S$ -force with angle of attack	ft/sec <sup>2</sup>
$Z_{\dot{\alpha}}$	Dimensional variation of $Z_S$ -force with rate of change of angle of attack	ft/sec
$Z_q$	Dimensional variation of $Z_S$ -force with pitch rate	ft/sec
$Z_\delta$	Dimensional variation of $Z_S$ -force with stabilizer, aileron, flap, rudder, and spoiler where $\delta = \delta_{it}, \delta_a, \delta_f, \delta_r, \delta_s$ angle	ft/sec <sup>2</sup>
$\theta, \theta_1, \theta$	Pitch attitude angle (total, steady state, perturbed)	rad
$\phi, \phi$	Bank (roll) angle (total, perturbed)	rad
$\alpha$	Angle of attack	rad
$\lambda$	Closed-loop eigenvalue	
$\Delta$	Incremental value	
$\delta_j$	Deflection of the $j$ th surface (See Appendix A)	
$X_S, Y_S, Z_S$	Stability axes system of coordinates	

## Abstract

This thesis investigates control of an aircraft when there is a primary control surface failure. The object of this study is to reconfigure the remaining control surfaces to compensate for the additional forces and moments generated by the inoperative control surface. To study this flight control problem, a comprehensive aircraft model is required which considers each control surface operating individually.

A six degree-of-freedom aircraft model is developed, including all the individual control surfaces. A control surface input can produce both a lateral and/or a longitudinal response. Thus, the equations of motion cannot be decoupled for the design of the control laws. The coupling between the axes requires the derivation of several new non-dimensional control derivatives. Using the geometrical properties of the aircraft and the Digital Datcom computer program, the needed control derivatives are derived.

With a comprehensive aircraft model now available, the entire eigenstructure assignment method is used to assign both the eigenvalues and the eigenvectors to the closed-loop plant matrix. This method is used for the direct digital design of a multivariable discrete regulator and tracker control law. The effect of increasing the number of control inputs on the relative degree of controllability of the states was determined by singular value decomposition.

This thesis concludes that a direct digital design for reconfiguring the multivariable control law is feasible. However, more wind tunnel data is essential to derive the additional control derivatives for a more accurate aircraft model driven by individual control surfaces. Further work is also necessary to perfect the assignment of the closed-loop eigenvalues and eigenvectors.

# DIRECT DIGITAL DESIGN METHOD FOR RECONFIGURABLE MULTIVARIABLE CONTROL LAWS FOR THE A-7D DIGITAC II AIRCRAFT

## I. Introduction

The increased flexibility and miniaturization of digital computers make it possible to use digital flight control systems (DFCS) on future aircraft. These aircraft, whether they are inherently stable or unstable, will have the normal sets of primary control surfaces (ailerons, spoilers, flaps, and horizontal stabilizers), split into independently controllable surfaces. The combination of a DFCS and independently movable control surfaces suggest that a method for redesigning the control laws be developed. A set of reconfigured multivariable control laws could then be stored in the DFCS. In the event a primary control surface becomes inoperative or blown away due to battle damage, a reconfigured multivariable control law would be implemented by the DFCS upon the detection and isolation of the failure. The design method developed in this thesis results in reconfigured multivariable control laws using state variable feedback and complete eigenstructure assignment.

This chapter presents the background, problem, scope, assumptions and approach associated with this thesis.

### Background

Due to recent advancements in digital technology, there is improved computational speed and lower cost for digital computers used in flight control systems. By replacing the analog flight control system (AFCS) with a DFCS, it has been shown one can achieve a faster reaction to an input disturbance and increased flexibility in control surface

utilization (Ref 10).

The DFCS used in the A-7D Digitac II aircraft is an experimental test system which is being used to determine if the mission capabilities are improved when compared to the AFCS. The test program is also intended to provide a technology base for future development of digital and multimode flight control functions. The results of a 92 hour flight test program conducted between February 1975 to March 1976 showed that the DFCS had the same desired high degree of reliability and flexibility as the AFCS and provided a significant improvement in the aircraft handling qualities (Ref 10:9). Therefore, a DFCS with the proper detection and isolation of the loss or failure of the primary control surface is capable of responding faster to the implementation of a reconfigured control law.

Reconfiguration of the control laws implies reconfiguration of the control surface utilization to compensate for a surface failure by battle damage and using the remaining surfaces to control the aircraft. In the past, this has been done manually by pilots with some success, particularly in aircraft with a high degree of aerodynamic stability. In the future, however, the loss or partial loss of a control surface could result in an unrecoverable flight condition in inherently unstable aircraft. The pilot would not have time to identify, analyze, and take corrective action after a control surface failure. Even in fly-by-wire (FBW) controlled configured vehicles (CCV) of the future, manual control without automated assistance to achieve effective reconfiguration does not appear feasible (Ref 3:114). Once a reconfigured control law is implemented and control of the aircraft is regained, the capabilities and response of the aircraft may be

degraded. Even if the degradation of the flying qualities only allows the pilot a get home and land capability, the reconfiguration of the control laws will have served its purpose of saving the pilot and aircraft.

Since modern aircraft designs tend to have more movable control surfaces, this suggests that more inherent redundancy is available if these control surfaces can be properly used. With a DFCS and utilization of the inherent redundancy of the control surfaces, it is feasible to design reconfigurable control laws.

#### Problem

The Flight Dynamics Laboratory is presently investigating the feasibility of reconfiguring the aircraft flight control laws in the event of a primary surface failure. For example, when the right aileron or the left horizontal stabilizer become inoperative, additional forces and moments are generated that are not normally present. The aileron commands would produce unwanted longitudinal forces and moments, while stabilator commands would produce lateral-directional inputs. The object of this thesis is to use the remaining control surfaces to compensate for the inoperative control surface. To study this flight problem, a comprehensive aircraft model is required to consider each control surface individually. At present, data is not available for consideration of each individual control surface input in each equation of motion.

#### Scope

This investigation is limited to proposing a method for redesigning the control laws of an aircraft after one of the primary control

surfaces becomes inoperative. This study determines which new dimensional control derivatives are required in the aircraft equations of motion in order to ensure the coupling of the longitudinal and lateral motion between the axes. This is accomplished by the use of additional independent control surface inputs. Next, the entire eigenstructure assignment is used to specify a method for redesigning the control laws. Only continuous time simulation is used in evaluating the system responses when checking a system configuration or control law.

#### Assumptions

A number of assumptions are made to simplify the complexity of this problem. First, the aircraft is assumed to make small perturbations about a trimmed straight and level flight condition. Secondly, the aircraft equations of motion developed are used in the stability axis. Thirdly, the coefficients of the control derivatives are normally for a set of control surfaces, i.e., ailerons, flaps, horizontal stabilizers, but only half the value of the control derivative coefficient, with the proper sign is used when the control surface set is split into two independent control surfaces, e.g., left and right aileron.

#### Approach and Presentation

The design approach or method for reconfiguring the control laws in this thesis looks at using all control surfaces independently of one another. This means that each aileron, each horizontal stabilizer, each spoiler, and each flap is controlled independently. This allows for maximum utilization of all the surfaces when a primary surface fails. To make use of these additional control surfaces, the lateral

and longitudinal inputs are present in all the state equations of the aircraft model. By doing so, one can compensate for a surface failure by using state variable feedback. To accomplish this, additional control derivatives are required to realize the effects of the additional control inputs in each of the axes as the aircraft equations are developed. With the additional control inputs, the degree of controllability of the  $(A,B)$  matrix pair is examined to determine if a state(s) requires a large magnitude of control input in order to retain control of the aircraft after a surface failure.

With a controllable and, perhaps, a reduced order plant, the reconfigured control law is designed using the complete eigenstructure assignment (CESA) design technique. The interactive program CESA is used to generate the state feedback design. This is an iterative process of assigning the closed-loop eigenvalues and selecting the eigenvectors from the controllable subspace for the assigned eigenvalues. Then, a continuous simulation analysis of the closed-loop system responses checks the reconfigured control law implemented.

This thesis is composed of five chapters. Chapter II develops the aircraft model and references Appendices A for the derivation of the aircraft equations of motion. The method used to obtain the additional control derivatives is described in the Appendix B. Because each segment of the control surface is operated independently, there is coupling between the lateral and longitudinal axes. This coupling is not encountered when the two ailerons, the two horizontal stabilizers, and the two spoilers are controlled from the same control signal. Chapter III presents the theory associated with entire eigenstructure assignment for distinct and multiple eigenvalue assignment. A

regulator design example is used to illustrate that the assigned closed-loop eigenvalues and eigenvectors can be obtained from a generated control law. Chapter IV looks at the modifications required for the interactive program CESA. Also discussed are the problems encountered with the controllability of the  $(A,B)$  matrix pair and the solutions used to obtain a higher degree of controllability. Chapter V presents the conclusions and recommendations.

## II. The Aircraft Model

### Introduction

An accurate model is desirable for any control design method; however, limitations and assumptions are necessary to derive a model that is manageable and accurate. This thesis uses a six degree-of-freedom (D-O-F) aircraft model. The model includes the effect of individual control surfaces, many of which are traditionally considered to act together as a set. For example, this thesis considers the right and left horizontal stabilizer as independent control surfaces. A linear model is formed by linearizing the nonlinear 6 D-O-F equations of motion about a nominal operating point or flight condition.

This chapter presents a general description of the A-7D aircraft, a discussion on the linearized aircraft equations of motion and a discussion on the new control derivatives required for the aircraft model.

### General Description

The A-7D is a single seat, land based, light attack aircraft with moderately swept wing and tail surfaces. The fuselage is 45.4 feet long with an underslung nose inlet duct, and is powered by a single TF41-A-1 engine (Ref 8:3.1). The wing area is 375 square feet and the mean geometric chord (m.g.c.) is 10.8 feet. The horizontal stabilizer is a slab tail with 56.2 square feet of area and a m.g.c. of 6.1 feet. The distance from 25 percent of the wing m.g.c. to 25 percent of the tail's m.g.c. is 16.2 feet. At a cruise configuration, the aircraft weight is 25,238 pounds, and is flying at 0.6 Mach at an altitude of 15,000 feet. Details of this flight condition are given in (Ref 20:A.5).

### System Model

The aircraft model in this thesis uses the 6 D-O-F equations of motion for an accurate model without approximations. The development of the aircraft equations is in Appendix A. In the derivation of the aircraft model, a method is presented to resolve the problem of how to achieve control of the lateral-directional motion with a longitudinal control surface and the control of the longitudinal motion with a lateral control surface. This is a primary requirement in order to accomplish the reconfiguration of the control law after the loss of a primary control surface.

To achieve this control, the dimensional control derivatives not normally associated with either the lateral-directional or longitudinal axes must be considered. This coupling between the axes is realized through the non-dimensional control derivatives associated with the force and moment equations control surface inputs for the non-traditional surfaces. For example, Equation (1) is a lateral-directional input coupled into a longitudinal control derivative equation by  $C_{D_{\delta_r}}$ .

$$X_{\delta_r} = \frac{S \bar{q} C_{D_{\delta_r}}}{m} \quad (1)$$

The idea of the above example applies to all the new dimensional control derivatives in the lateral-directional and longitudinal control surface inputs of the aircraft equations of motion as shown in Appendix A.

By including the individual control surfaces, the equations cannot be decoupled to separately describe the longitudinal and lateral-directional motion. One now requires knowledge of the non-dimensional control derivatives for these control surfaces for which data is not usually available. The next section provides a method for deriving this data.

### Control Derivatives

To successfully carry out the coupling between the axes requires the derivation of several non-dimensional control derivatives for the lateral-directional and longitudinal control inputs of the equations of motion. The control derivatives that are not given in (Ref 11) or (Ref 1) are derived in Appendix B. These new control derivatives were derived by digital DATCOM, (Ref 14), and conventional aerodynamic techniques. For example; the rudder was modeled as an asymmetrical wing and  $X_{D_{\delta_r}}$  was derived from digital DATCOM data. This is explained in more detail in Appendix B.

### Summary

In this chapter, a physical description of the A-7D is presented. Then, a development of the aircraft equations of motion is presented to introduce a method that achieves coupling of the lateral and longitudinal motion into the opposite axes by using all the individual control surfaces and new non-dimensional control derivatives for the respective axes. With a comprehensive system model, the next step is to present a method to design a reconfigurable multivariable control law using the complete eigenstructure assignment design technique.

### III. Theory of Entire Eigenstructure Assignment

#### Introduction

The design method in this thesis for obtaining the reconfigured control laws uses the technique of entire eigenstructure assignment for multi-input multi-output (MIMO) control systems. The assignment of the entire eigenstructure, consisting of both eigenvalues and eigenvectors, is illustrated by application to a system design in which distinct eigenvalues are assigned. The use of multiple eigenvalue assignment is particularly important for sampled-data systems since it can produce closed-loop system responses having finite settling times. Fully exploiting the properties of a multivariable system make it a powerful design tool for the synthesis of sampled-data controllers. This enables the synthesis of a sampled-data control system which consists of a continuous-time plant and a digital controller that produces a control input signal which is piecewise-constant for each sampling period.

This chapter presents a comprehensive review of the above design technique which assigns both the eigenvalue spectrum and eigenvectors associated for the closed-loop plant matrix. First, the principles of the entire eigenstructure are developed for the case of distinct eigenvalues and then a regulator is synthesized to illustrate these principles. Then, the principles for multiple eigenvalue assignment are presented. This is followed by applying the theory to systems augmented with integrators for the design of a tracker controller and a discussion on continuous simulation (Ref 6).

### Distinct Eigenvalue Assignment

The linear multivariable time-invariant vector matrix equations governing the plant and its output in the continuous-time domain have the forms

$$\dot{x}(t) = Ax(t) + B u(t) \quad (2)$$

$$y(t) = Cx(t) \quad (3)$$

and is illustrated in Figure 1. To form the sampled-data system, a linear time invariant discrete-time MIMO system is described by the matrix difference equation (Ref 6:491)

$$\dot{x}(kT+T) = F(T) x(kT) + G(T) u(kT) \quad (4)$$

$$y(kT) = C x(kT) \quad (5)$$

where  $T$  is the sampling time and is shown in Figure 2. The control law for applying state-variable feedback for the discrete-time system is

$$u(kT) = Kx(kT). \quad (6)$$

The purpose in applying state feedback is to assign a closed-loop self-conjugate distinct eigenvalue spectrum

$$\sigma(F+GK) = \{\lambda_1, \lambda_2, \dots, \lambda_n\} \quad (7)$$

and the associated set of eigenvectors

$$\{x_{\lambda_1}, x_{\lambda_2}, \dots, x_{\lambda_n}\}. \quad (8)$$

The eigenvalues and eigenvectors for the closed-loop system are related

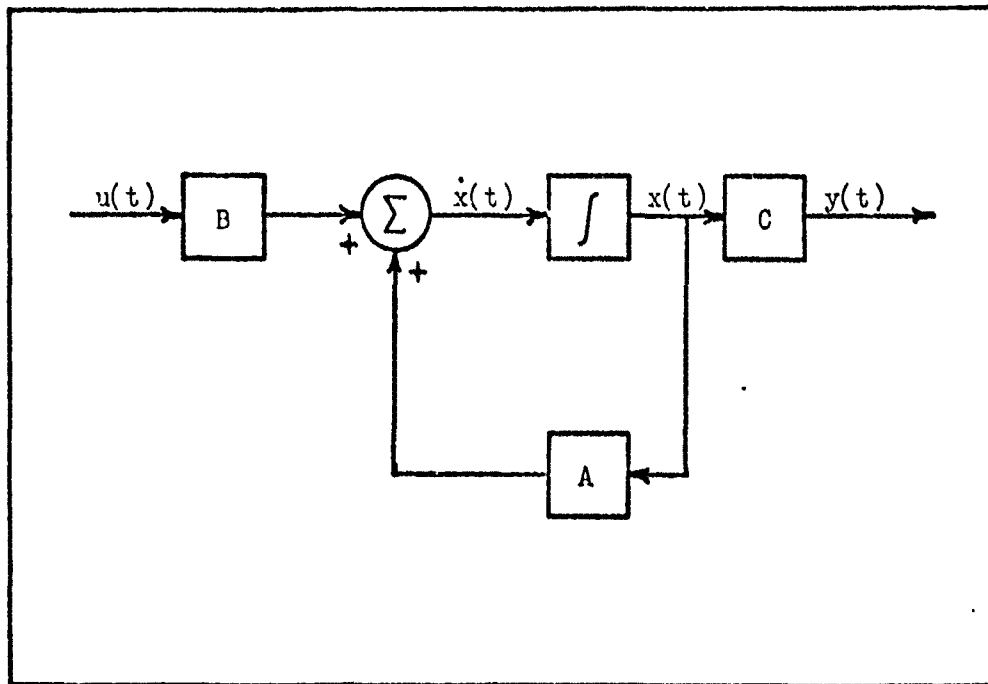


Figure 1. Continuous-Time System Block Diagram

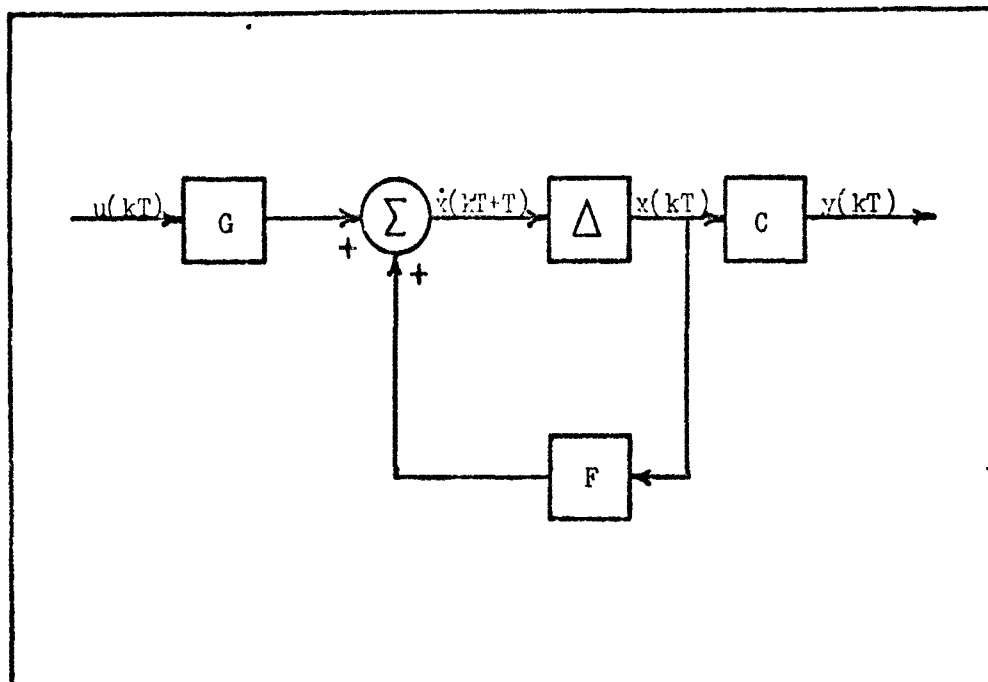


Figure 2. Discrete-Time System Block Diagram

by the equation

$$(F+GK) x_{\lambda_i} = \lambda_i x_{\lambda_i} \quad (i = 1, 2, \dots, n) \quad (9)$$

which may be put in the form

$$[F-\lambda_i I, G] \begin{bmatrix} x_{\lambda_i} \\ \omega_{\lambda_i} \end{bmatrix} = 0 \quad (i = 1, 2, \dots, n) \quad (10)$$

where

$$\omega_{\lambda_i} = Kx_{\lambda_i} \quad (11)$$

and where  $[x_{\lambda_i}^T, \omega_{\lambda_i}^T]^T$  is a vector which lies in the kernel or null space of the matrix:

$$S(\lambda_i) = [F-\lambda_i I, G] \quad (i = 1, 2, \dots, n) \quad (12)$$

It follows from Equation (11) that the required state feedback matrix K is given by

$$K = [\omega_{\lambda_1}, \omega_{\lambda_2}, \dots, \omega_{\lambda_n}] [x_{\lambda_1}, x_{\lambda_2}, \dots, x_{\lambda_n}]^{-1} \\ K = \Omega X^{-1} \quad (13)$$

The matrix K is real and simultaneously assigns both the desired set of eigenvalues and the assigned set of associated eigenvectors.

Equation (11) may also be solved directly without the requirement to obtain the inverse matrix shown in Equation (13) (Ref 22). The ker  $S(\lambda_i)$  ( $i = 1, 2, \dots, n$ ) imposes constraints on the eigenvector(s)

that may be associated with the assigned eigenvalue  $\lambda_i$  ( $i = 1, 2, \dots, n$ ) by identifying a subspace within which the eigenvector  $x_{\lambda_i}$  ( $i = 1, 2, \dots, n$ ) must be located. The eigenvectors must be linearly independent and self-conjugate so that the inverse matrix  $x^{-1}$  in Equation (13) exists and is real. Within these constraints, there is freedom in assigning the eigenstructure of the closed-loop plant matrix  $F+GK$ . This is illustrated with the following example (Ref 6:13).

Example II-1.

A continuous system is represented by the following state and output equations:

$$\begin{aligned} \dot{x}(t) &= \begin{bmatrix} 0 & 1 & 0 \\ 0 & 0 & 1 \\ -6 & -11 & -6 \end{bmatrix} x(t) + \begin{bmatrix} 0 & 0 \\ 1 & 0 \\ 0 & 1 \end{bmatrix} u(t) \\ y(t) &= \begin{bmatrix} 1 & 1 & 0 \\ 0 & 0 & 1 \end{bmatrix} x(t) \end{aligned} \quad (14)$$

The design of the regulator in this example is carried out with the interactive computer program CESA (Ref 8). The discrete-time domain representation is obtained with a sampling period of  $T = 1$  second. The eigenvectors lie in the null space of the matrix  $S(\lambda)$  of Equation (12).

$$S(\lambda) = \begin{bmatrix} 0.7474-\lambda & 0.4530 & 0.0735 & 0.3261 & 0.0421 \\ 0.4410 & -0.0611-\lambda & 0.0121 & 0.4530 & 0.0735 \\ 0.0723 & -0.5735 & -0.1334-\lambda & -1.0610 & 0.0121 \end{bmatrix} \quad (15)$$

The open-loop sampled-data eigenvalue spectrum for the discrete

plant matrix F is

$$\sigma(F) = \{0.50, 0.135, 0.368\} . \quad (16)$$

The feedback matrix K is to be computed so that the closed-loop system is asymptotically stable and has the eigenvalue spectrum

$$\sigma(F+GK) = \{0.05, 0.1, 0.15\} . \quad (17)$$

The size of the null space generated is dependent upon the column dimension of the input matrix. In this example, the null space dimension is 2 as is shown for the specified eigenvalues.

$$\ker S(0.05) = \text{span} \left\{ \begin{bmatrix} 0.11152 \\ -0.33380 \\ 1 \\ 0.00005 \\ 0 \end{bmatrix}, \begin{bmatrix} -0.34692 \\ 0.68090 \\ 0 \\ -0.33305 \\ 1 \end{bmatrix} \right\} \quad (18)$$

$$\ker S(0.10) = \text{span} \left\{ \begin{bmatrix} 0.19090 \\ -0.43770 \\ 1 \\ 0.00364 \\ 0 \end{bmatrix}, \begin{bmatrix} -0.32759 \\ 0.57450 \\ 0 \\ -0.27684 \\ 1 \end{bmatrix} \right\} \quad (19)$$

$$\ker S(0.15) = \text{span} \left\{ \begin{bmatrix} 0.27612 \\ -0.52460 \\ 1 \\ -0.00229 \\ 0 \end{bmatrix}, \begin{bmatrix} -0.32393 \\ 0.50770 \\ 0 \\ -0.24100 \\ 1 \end{bmatrix} \right\} \quad (20)$$

From each null space, one eigenvector is selected ensuring that the requirement for linear independence is met and also satisfying Equation (10). Thus, making the permissible assignment from

Equations (18), (19), and (20) of

$$\left\{ \begin{bmatrix} x_{\lambda_1} \\ \vdots \\ \omega_{\lambda_1} \end{bmatrix} \begin{bmatrix} x_{\lambda_2} \\ \vdots \\ \omega_{\lambda_2} \end{bmatrix} \begin{bmatrix} x_{\lambda_3} \\ \vdots \\ \omega_{\lambda_3} \end{bmatrix} \right\} = \left\{ \begin{bmatrix} -0.34692 \\ 0.68090 \\ 0 \\ -0.33305 \\ 1 \end{bmatrix}, \begin{bmatrix} 0.19090 \\ -0.43770 \\ 1 \\ 0.00364 \\ 0 \end{bmatrix}, \begin{bmatrix} 0.27612 \\ -0.52460 \\ 1 \\ -0.00229 \\ 0 \end{bmatrix} \right\} \quad (21)$$

The required feedback matrix is computed from Equation (13) as

$$\begin{aligned} K &= \begin{bmatrix} -0.33305 & 0.00364 & -0.00229 \\ 1 & 0 & 0 \end{bmatrix} \begin{bmatrix} -0.34692 & 0.19090 & 0.27612 \\ 0.68090 & -0.43770 & -0.52460 \\ 0 & 1 & 1 \end{bmatrix}^{-1} \\ &= \begin{bmatrix} -1.186, & -1.094, & -0.2485 \\ 3.127, & 3.062, & 0.7432 \end{bmatrix} \quad (22) \end{aligned}$$

The resulting closed-loop sampled-data plant matrix is

$$F + GK = \begin{bmatrix} 0.4992, & 0.2253, & 0.0237 \\ -0.7487, & -0.3315, & -0.0459 \\ 1.2240, & 0.6238, & 0.1393 \end{bmatrix} \quad (23)$$

The closed-loop plant matrix has the required eigenvalue spectrum of Equation (16) and the assigned set of eigenvectors of Equation (21), as required. Thus, the method of entire eigenstructure assignment permits the eigenvalues to be altered or to be left unchanged, as required. Even when an eigenvalue is left unchanged, the associated eigenvector may be reassigned within the appropriate subspace.

The continuous-time responses of the states for the closed-loop sampled-data system are plotted in Figure 3 for the initial conditions

$$X(0) = \begin{bmatrix} 1 \\ -1.5 \\ 1 \end{bmatrix} \quad (24)$$

The plant states and outputs essentially reach steady-state in approximately three sampling periods.

#### Multiple Eigenvalue Assignment

The assignment of multiple eigenvalues is especially useful for sampled-data systems since the assignment of all eigenvalues to the origin, i.e.,  $\lambda_i = 0$  ( $i = 1, 2, \dots, n$ ), results in time-optimal or finite settling time responses. When it is desired to assign multiple eigenvalues, the associated eigenvectors are related by the equation

$$(F+G)x_i = \lambda_i x_i \quad (i = 1, 2, \dots, p \leq n). \quad (25)$$

Where  $p$  is the number of different eigenvalues and, therefore, only linearly independent eigenvectors may be generated from the null space (Ref 6:2.23, 25). Depending upon the desired algebraic multiplicity,  $M_i \leq n$ , and the number of subblocks desired in the jordan normal form of the closed-loop matrix for each assigned eigenvalue  $\lambda_i$ , it may be necessary to generate chains of generalized eigenvectors  $x_{i+k}$  using the equation

$$(F+GK) x_{i+k} = \lambda_i x_{i+k} + x_{i+k-1} \quad (k = 1, 2, \dots, M_i - 1) \quad (26)$$

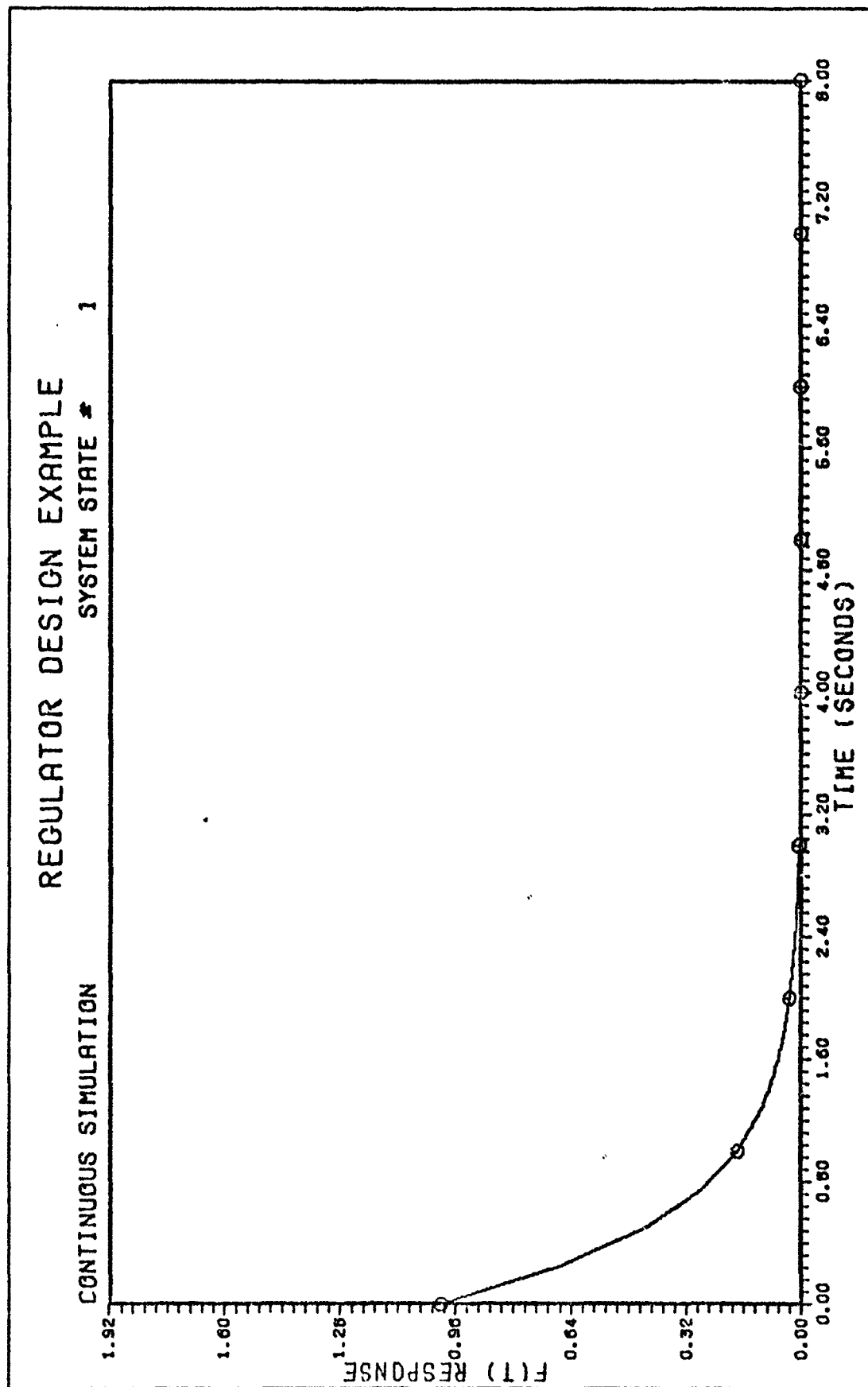


Figure 3a.  $X_1(t)$  vs.  $t$

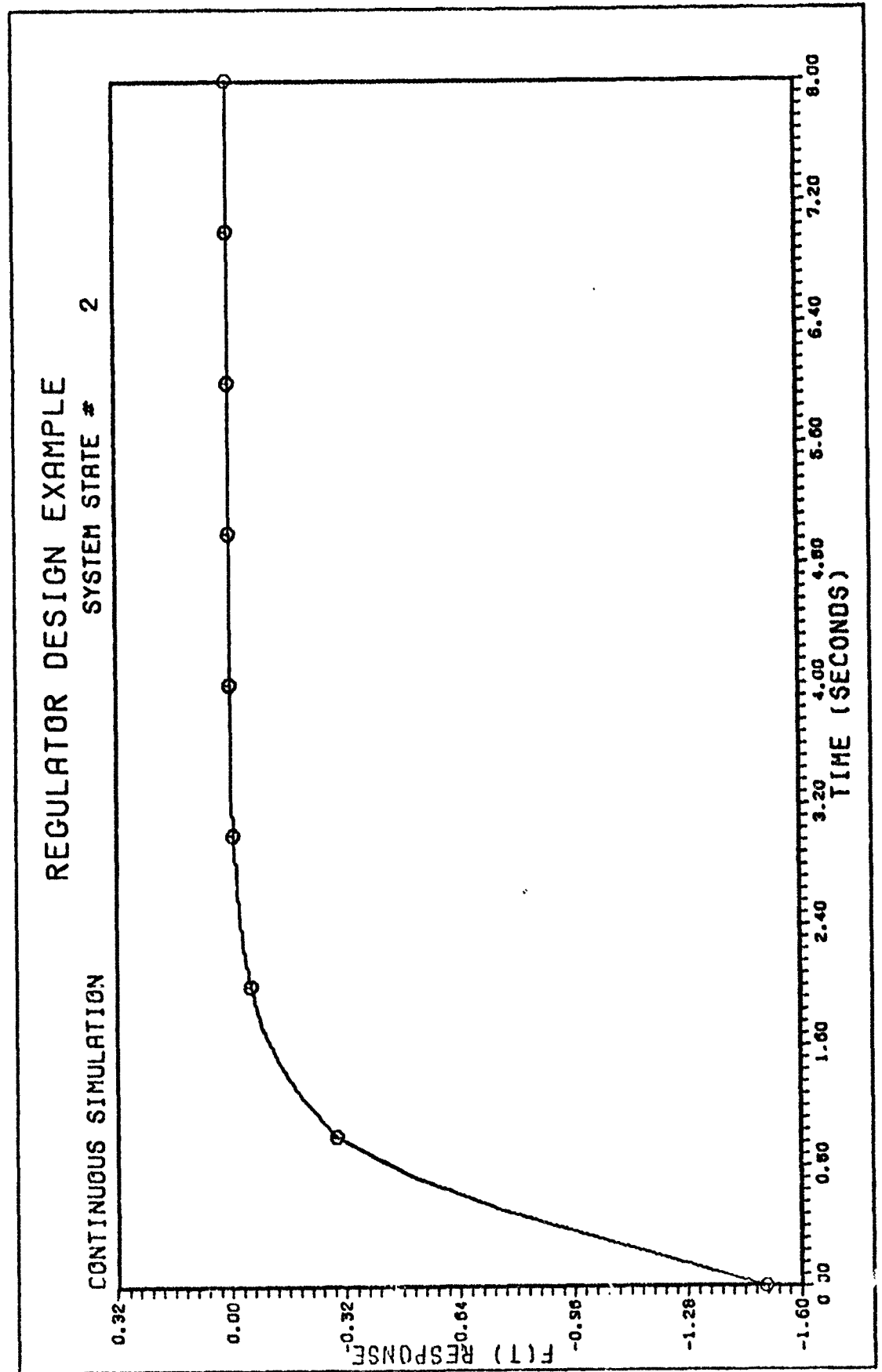


Figure 3b.  $X_2(t)$  vs.  $t$

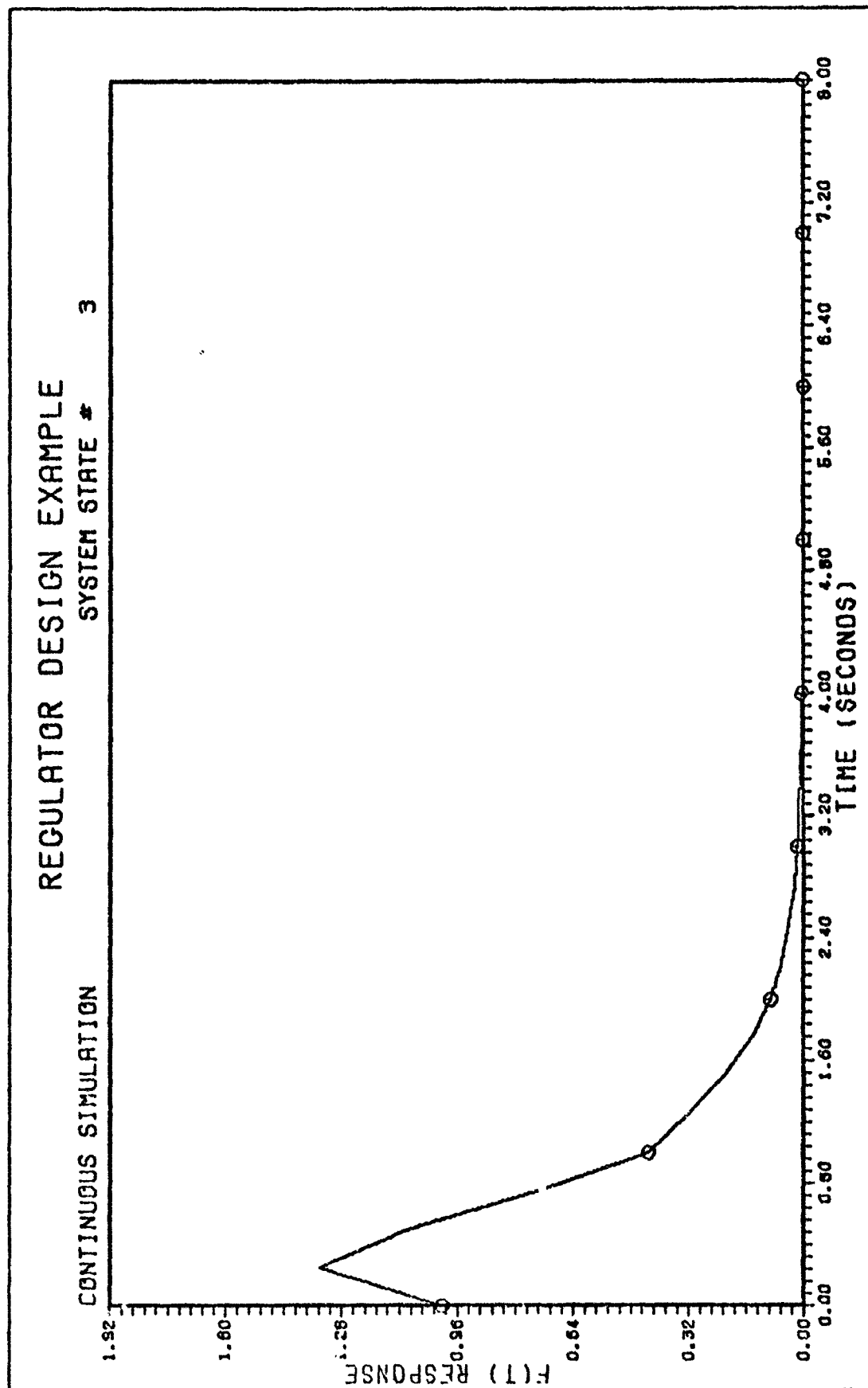


Figure 3c.  $X_3(t)$  vs.  $t$

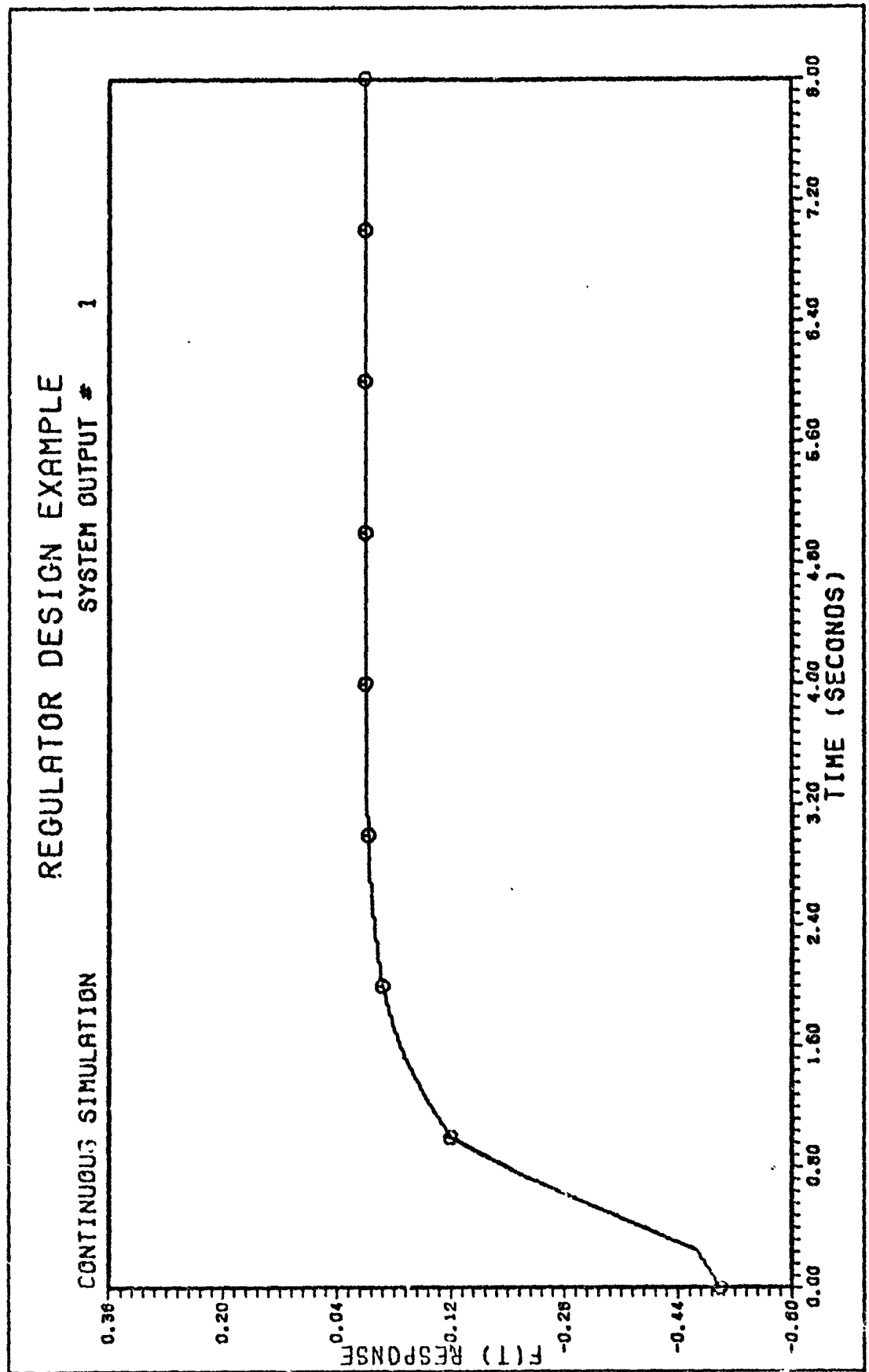


Figure 3d.  $y_1(t)$  vs.  $t$

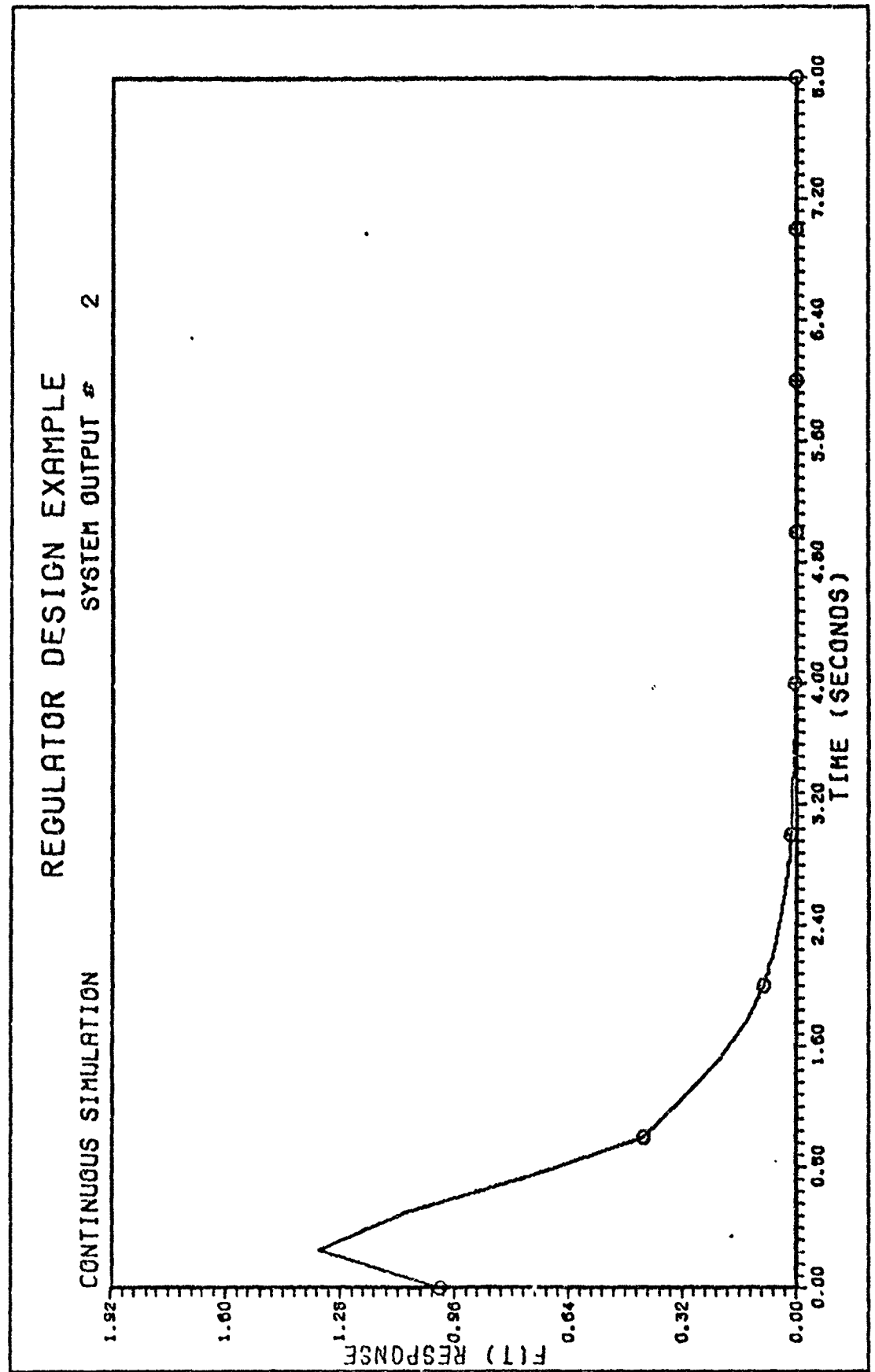


Figure 3e.  $y_2(t)$  vs.  $t$

This equation may be put in the form

$$[F - \lambda_i I, G] \begin{bmatrix} x_{\lambda_i}^{(m_{ji}, j)} \\ w_{\lambda_i}^{(m_{ji}, j)} \end{bmatrix} = x_{\lambda_i}^{(m_{ji}-1, j)} \quad (j = 1, 2, \dots, k_i; i = 1, 2, \dots, p). \quad (27)$$

This generates  $k_i$  strings of vectors associated with the eigenvalue  $\lambda_i$ , where  $x_i^{(1, j)}$  is the 1th vector in the  $j$ th string which is of length  $m_{ji}$  since the  $\ker S(\lambda_i)$  occupies a subspace of size equal to  $m$ , the number of controls.

Equation (26) allows the generation of eigenvector/generalized eigenvector chains from the original null space given by Equation (12) so that the size of the largest control index,  $d_1$ , of the open-loop system may be retained for the closed-loop system. This is possible if (1) the eigenvalue spectrum of the closed-loop system is assigned to the origin, (2) the combined length of the first eigenvector/generalized eigenvector chain is set equal to  $d_1$ . In this case, the outputs are equal to the inputs after a finite number of sampling times, that is, the system is deadbeat. This allows a deadbeat response to take place in  $q$  sampling times, where  $q$  is the order of the minimal polynomial of the closed-loop system and is equal to the largest control index of pair  $(F, G)$  (Ref 7:19).

The foregoing theory of assigning eigenvalues and selection of eigenvectors to the design of a regulator is further applied to the tracker design by augmentation of the system with integrators.

### Tracker

The synthesis of a tracking system which is required to track a command input, uses proportional plus integral state feedback in multi-variable control systems. This assures zero steady-state error for step inputs for the tracking system if the augmented system remains controllable (Ref 4). The controllable multivariable plant governed by discrete-time matrix difference and output equations are

$$x(kT+T) = Fx(kT) + Gu(kT) \quad (28)$$

and

$$y(kT) = Cx(kT) \quad (29)$$

The system is augmented by the introduction of a discrete-time vector integrator and comparator

$$z(kT+T) = z(kT) + v(kT) - y(kT) \quad (30)$$

Where the p<sub>xl</sub> output vector  $y(kT)$  is required to track the p<sub>xl</sub> piecewise constant command input vector  $v(kT)$ . The number of command inputs is less than or equal to the number of outputs. Inserting Equation (29) into (30) yields

$$z(kT+T) = -Cx(kT) + z(kT) + v(kT) \quad (31)$$

Thus, from Equation (28) and (31), the discrete composite open-loop augmented tracking system is

$$\begin{bmatrix} x(kT+T) \\ z(kT+T) \end{bmatrix} = \begin{bmatrix} F & 0 \\ -C & I_p \end{bmatrix} \begin{bmatrix} x(kT) \\ z(kT) \end{bmatrix} + \begin{bmatrix} G \\ 0 \end{bmatrix} u(kT) + \begin{bmatrix} 0 \\ I_p \end{bmatrix} v(kT) \quad (32)$$

Where  $I_p$  is a  $p \times p$  identity matrix and  $p$  is the number of integrators used.

The proportional plus integral control law is

$$u(kT) = Kx(kT) + K_1 z(kT) \quad (33)$$

where  $K$  is a  $m \times n$  matrix,  $K_1$  is a  $m \times p$  matrix, and  $m \leq n$ . The closed-loop tracking system is represented by

$$\begin{bmatrix} x(kT+T) \\ z(kT+T) \end{bmatrix} = \begin{bmatrix} F+GK, & GK_1 \\ -C & , & I \end{bmatrix} \begin{bmatrix} x(kT) \\ z(kT) \end{bmatrix} + \begin{bmatrix} 0 \\ I \end{bmatrix} v(kT) \quad (34)$$

and

$$y(kT) = [C, 0] \begin{bmatrix} x(kT) \\ z(kT) \end{bmatrix} \quad (35)$$

The output matrix  $[C, 0]$  in Equation (35) is augmented with zeros for  $z(kT)$ , since integrator outputs (Ref 6) are not system outputs.

When  $K$  and  $K_1$  are generated that produce an asymptotically stable system, the closed-loop eigenvalues are within the unit circle. The integrator state then reach constant values with a constant command  $v(kT)$ , therefore,

$$\lim_{k \rightarrow \infty} [z(kT+T) - z(kT)] = 0 \quad (36)$$

and from Equation (30),

$$\lim_{k \rightarrow \infty} [y(kT) - v(kT)] = 0 \quad (37)$$

Therefore, the desired state outputs will track the command inputs with zero steady-state error.

### Continuous Simulation

Since the aircraft plant is a continuous system, it is necessary to perform a continuous simulation of the closed-loop system in order to evaluate the effectiveness of the digital control law. This is necessary because the complete closed-loop system is partly discrete and partly continuous. Therefore, the system is simulated using the continuous state space representation with piecewise-constant control inputs.

In order to determine the continuous-time solution to the state space representation of the linear time invariant system, a discrete approximation to the exact solution is used. This method is used to discretize the plant, as explained in the preceding section on sampled data transformation, with a sampling time that is less than or equal to  $TSAMP/12$ , where  $TSAMP$  is the sampling time of the digital computer used in the control law (Ref 7:24). The state and output responses are obtained from one sampling time to the next with the control input  $u(kT)$  held constant. Then, the control input is updated at the next sampling time and the process is continued. Therefore, it is possible to determine the system responses between the sampling times. This simulation is incorporated in the computer program CESA (Ref 8).

### Summary

The use of the entire eigenstructure assignment design technique for multivariable control systems is possible by specifying the desired entire eigenstructure of a controllable closed-loop system.

There is complete freedom in assigning the eigenvalues and the corresponding eigenvectors must be assigned within a specified null space. Then, a state-variable feedback control law is determined for the discrete-time domain system.

This design method can be applied to regulators where it is desired to bring the system back to the steady state condition. Also, the system can be augmented with integrators for a tracker design where the output tracks a command input vector with zero steady-state error.

#### IV. Multivariable Control Law Design

##### Introduction

The reconfiguration of the control laws for an aircraft must compensate for the forces and moments generated by a partial primary control surface failure. The design was achieved by using the complete eigenstructure assignment design technique for a multivariable system. First, it was necessary to derive the new control derivatives for the additional independently variable control surface inputs in the six degree-of-freedom (DOF) aircraft equations of motion. In accomplishing the design, not only must the controllability of the  $(A,B)$  matrix pair be determined, but the degree of controllability is also important. The degree of controllability for this multivariable system is important since this determines the magnitude of the feedback matrix coefficients and the magnitude of the piecewise-constant control input signals. Should there be a state with a low degree of controllability, it is possible to remove that state from the model representation if the response of the original system is not affected.

This chapter presents the modification that was required to make the interactive program CESA compatible with the control input matrix of the aircraft model. Then the degree of controllability of the system is examined by using a method that balances the system matrices in a new state coordinate system, allowing for state reduction, if desired. Having established the degree of controllability of the model which was developed, the design scheme for a multivariable discrete-time tracker and regulator is presented.

### CESA Modification

The interactive computer program CESA provides the user with an interactive tool to design the control laws for regulators, disturbance rejectors, and trackers. The program has the capability for designing a multivariable control law and then evaluating the system responses by continuous or discrete simulation. Should the control law be unacceptable, it can be redesigned without having to reenter the system matrices and sampling times. However, the closed-loop eigenvalue spectrum and eigenvector assignment must be respecified. Thus, the system data is stored in memory for an interactive design process (Ref 8:157).

A program modification was required due to the dimension limitations on the continuous and discrete-time control input matrices. Also, other matrices and vectors used in the design process in the program are dependent upon the number of control inputs. This thesis required that the control input matrix dimension be increased in size to an  $m \times m$  matrix, where  $m$  is eight and this does not include the failed surface. This allows for the use of the left and right control surface input of the unit horizontal tail (UHT), ailerons, spoilers, flaps and the single vertical tail rudder. To accomplish the modification, a thorough understanding of the theory, computer program overlay structure, the programs and subroutines used in the design, and the simulation of the discrete state feedback control law generated for the A-7D aircraft model was necessary.

Once the arguments of the arrays and vectors were updated, the program was recompiled for use on the ASD Cyber computer at the Air Force Wright Aeronautical Laboratories (AFWAL) using the following

external libraries: IMSL, EISPACK, CCAUX, and CCPL0T56X. To verify and validate the updated version, the third-order system example of Chapter III and the aircraft model of Appendix A were used during testing. Then, if further corrections or parameter changes were necessary, it became an iterative process until all necessary changes were made and validated to complete the program modification.

Once the interactive program modifications were completed, the effect of increasing the number of control inputs on the degree of controllability of the (A,B) matrix pair was investigated.

#### Controllability

It is reemphasized that the interactive program CESA checks the controllability of the (F,G) matrix pair, but not the degree of controllability of the plant states. One is interested in the degree of controllability when using state feedback because it does affect the overall gain of the state feedback matrix. If the state feedback matrix produces a multivariable control law that applies large control inputs to the servo actuators, then the physical limits of the actuators are exceeded. Therefore, removing a state of low controllability from the aircraft model improves (reduces) the average gain of the feedback matrix. To improve the controllability of the model, two approaches are available. One is to determine the magnitude of the singular values of the  $H_{INF}$  matrix that are generated by the Moore balancing algorithm (Ref 12:18-20). This has been implemented in the AFIT program MIMO (Ref 13). The second approach is to reduce the number of control inputs to only those control surface inputs that have the greatest effect on the aircraft response.

The Moore algorithm (Ref 15, 16) defines a state space coordinate system which orders the state variables with respect to the controllability and observability properties, i.e., the most to the least controllable, observable state. This is done by transforming the system into an internally balanced state coordinate system, where

$$\mathbf{x} = \mathbf{T}\mathbf{x}' \quad (38)$$

Using the linear transformation matrix (Ref 16)

$$\mathbf{T} = \mathbf{U}_o \Sigma_o^{-1} \mathbf{U}_H \Sigma_H^{\frac{1}{2}} \quad (39)$$

where  $\mathbf{U}_o$  = left singular vector of the observability gramian

$\Sigma_o$  = diagonal matrix containing singular values of the observability gramian

$\mathbf{U}_H$  = left singular vectors of the  $\mathbf{H}_{INF}$  matrix

$$\mathbf{H}_{INF} = \Sigma_o \mathbf{U}_o^T \mathbf{U}_c \Sigma_c$$

$\Sigma_H$  = diagonal matrix containing singular values of the  $\mathbf{H}_{INF}$  matrix

$\mathbf{U}_c$  = left singular vectors of the controllability gramian

$\Sigma_c$  = diagonal matrix containing singular values of the controllability gramian

This transformation to the internally balanced state coordinate system results in the following equations:

$$\begin{aligned} \dot{\mathbf{x}}'(t) &= \mathbf{A}'\mathbf{x}'(t) + \mathbf{B}'\mathbf{u}(t) \\ \mathbf{y}(t) &= \mathbf{C}'\mathbf{x}'(t) \end{aligned} \quad (40)$$

where  $A' = T^{-1}AT$ ,  $B' = T^{-1}B$ , and  $C' = CT$ . However, to retain the physical inputs and output positions of the original system, which are the important physically measurable quantities desired, the  $B'$  input matrix is premultiplied by  $T$  and the  $C'$  output matrix is post multiplied by  $T^{-1}$ , so that the  $B'_0$  input and  $C'_0$  output matrices are ordered as in the original system. Then, the state and output equations are,

$$\begin{aligned}\dot{x}'(t) &= A'x'(t) + B'_0 u(t) \\ y(t) &= C'_0 x'(t)\end{aligned}\quad (41)$$

Since the internally balanced state coordinate system orders the states with respect to the controllability and observability properties, then deletion of the bottom state(s) of the balanced matrix representation is, in effect, stripping away the least controllable/observable redundant state(s). The following is an example of state reduction from a third-order to an approximately equivalent second-order system:

$$A' = \begin{bmatrix} 3 & 7 & 8 \\ 1 & 0 & 2 \\ 5 & 6 & 9 \end{bmatrix}, B'_0 = \begin{bmatrix} 8 \\ 7 \\ 2 \end{bmatrix}, C'_0 = [7, 5, 4] \quad (42)$$

$$A'_R = \begin{bmatrix} 3 & 7 \\ 1 & 0 \end{bmatrix}, B'_{0R} = \begin{bmatrix} 8 \\ 7 \end{bmatrix}, C'_{0R} = [7, 5] \quad (43)$$

where  $A'_R$ ,  $B'_{0R}$ , and  $C'_{0R}$  are the reduced matrices. This does not imply that model reduction is necessary to use the internally balanced matrices generated by Moore's algorithm effectively. The balanced matrices can be used as generated, the advantage being that the

mathematical properties of the plant matrix are improved. An example is that the condition number of the aircraft model's plant matrix is reduced from 140653 to 127 when in the balanced form.

A method has been presented which determines the degree of controllability of the states and permits model reduction of the original system, if desired. The next step in the design method for reconfigurable multivariable control laws is to develop a state feedback matrix for the aircraft model of Appendix A for a tracker and regulator controller using the entire eigenstructure assignment design technique.

#### Control Law Design

A linear multivariable discrete-time tracker or regulator controller is designed to reconfigure the control surface response to compensate for the failure of a primary control surface. This section discusses the problems and solutions encountered with the method for the tracker and regulator controller design.

The tracker design is desired because the output tracks a commanded input. With a primary control surface failure, once it is detected and isolated by a fault detection system, a control law is implemented from a family of control laws in the digital flight control system (DFCS) to reconfigure the response of the remaining independently operating control surfaces. The reconfigured tracker control law would then follow the command inputs, removing the undesired response caused by the failed surface. The open-loop Equation (32) for the tracker design is composed of Equations (A-22, A-23, A-24, and A-25) augmented with the integrator and comparator of Equation (31).

input failure	$\delta_{h_l}$	$\delta_{h_r}$	$\delta_r$	$\delta_{a_l}$	$\delta_{a_r}$	$\delta_{s_l}$	$\delta_{s_r}$	$\delta_{f_l}$	$\delta_{f_r}$
UHT <sub>l</sub>	0	X	X	X	X	X	X	X	X
UHT <sub>r</sub>	X	0	X	X	X	X	X	X	X
Rudder	X	X	0	X	X	X	X	X	X
Aileron <sub>l</sub>	X	X	X	0	X	X	X	X	X
Aileron <sub>r</sub>	X	X	X	X	0	X	X	X	X
Spoiler <sub>l</sub>	X	X	X	X	X	0	X	X	X
Spoiler <sub>r</sub>	X	X	X	X	X	X	0	X	X

\*Control Surfaces l - left, r - right  
0 - failed surface X - normal operation

Figure 4. Control Surface Failure Vs. Reconfigured Input (9) Matrix

Since the selected output was required to track four command inputs, four integrators were used. This design can be used for the failure of any primary control surface by reconfiguring the control law to use a set of control inputs as shown in Figure 4.

The desired tracker control law is

$$u(kT) = Kx(kT) + K_1 z(kT) \quad (44)$$

where the feedback matrix  $[K, K_1]$  is computed so that the closed-loop system is asymptotically stable and has the selected eigenvalue spectrum for the tracker containing 4 integrators, see (A-25),

$$\sigma[F + G(K, K_1)] = \{0.01, 0.03, 0.05, 0.06, 0.07, 0.08, 0.1, 0.15, 0.2, \dots, 0.4, 0.6\}. \quad (45)$$

The state feedback matrix is related to the eigenvalues and associated

eigenvectors of the closed-loop system by

$$[F - \lambda_i I, G] \begin{bmatrix} x_i \\ \omega_i \end{bmatrix} = 0 \quad (i = 1, 2, \dots, n) \quad (46)$$

where

$$\omega_i = K x_i \quad (i = 1, 2, \dots, n) \quad (47)$$

and

$$\begin{bmatrix} x_i \\ \omega_i \end{bmatrix} \quad (i = 1, 2, \dots, n) \quad (48)$$

is a vector that lies in the null space of the matrix

$$S(\lambda_i) = [F - \lambda_i I, G] \quad (i = 1, 2, \dots, n) \quad (49)$$

Then the feedback matrix is given as (Ref 6:17)

$$K = [\omega_1, \omega_2, \dots, \omega_n] [x_1, x_2, \dots, x_n]^{-1} \\ K = \Omega X^{-1} \quad (50)$$

As stated in Chapter III, the eigenvectors must lie within the  $\ker S(\lambda_i)$  of the specified null space. Also, the columns of the modal matrix  $X$  must be independent for the matrix  $X^{-1}$  of Equation (50) to exist. Also, if the matrix  $X$  of Equation (50) is ill-conditioned, an inverse cannot be generated, but an erroneous inverse will be produced, i.e.,  $XX^{-1} \neq I$ . This is a computer computational problem.

The initial tracker design on the interactive program CESA did generate a control law that was formed using an incorrect  $X^{-1}$ . That

tracker control law had a very high average gain of approximately  $10^9$  and the closed-loop specified eigenvalues were not contained in the characteristic equation of the closed-loop matrix  $[F+GK]$ . This was a result of the problem areas mentioned previously: (1) degree of controllability of the  $(F,G)$  matrix pair, and (2) an ill-conditioned matrix  $X$  of Equation (50). This result was not anticipated and, at first, it was not known if the subroutines and programs in CESA, the external reference, or the problems stated above caused the high gains and non-reproduction of the closed-loop eigenvalues. Extensive testing was done on the CESA subroutines since a larger number of control variables were being used which called for an even larger augmented tracking matrix of Equation (32). Also, the external reference libraries were tested to ensure that the null spaces, eigenvalues, and  $X^{-1}$  being generated were correct. During the testing it was discovered that other available library routines can calculate the feedback matrix  $K$ , i.e., solving for the  $K$  matrix for the linear algebraic equation having the form  $XK = \Omega$ . The CESA program and the external references functioned as intended and it was determined that the difficulty lay in the ill-conditioned  $X$  matrix of Equation (47).

The controllability matrix associated with the  $(F,G)$  matrix pair must have full rank. A necessary condition for the system to be controllable is that the rank of the controllability matrix be equal to  $n$ , the dimension of the plant matrix, where the controllability matrix is defined as

$$M_c = [G, FG, \dots, F^{n-1}G] \quad (51)$$

However, the degree of controllability of the states is unknown. To

drive a state to the desired steady state condition, the magnitude of the feedback gain is dependent upon the controllability of that state. The feedback matrix is related to the eigenvectors which determine the magnitude of the transient responses. The controllability problem was further investigated by considering the regulator design. The regulator does not use integrators to augment the system and involves working directly with the plant matrix and the control inputs in determining the degree of controllability of the (A,B) matrix pair.

#### Regulator Control Law

For the remainder of this study, the right aileron is the surface failure, and it is assumed to be locked in a neutral position. Before the regulator design was implemented, the Moore internally balancing algorithm was applied to Equations (A-22, A-23, and A-26) using the interactive program MEMO (Ref 13). The time responses of the original, balanced and reduced balanced system were compared to ensure that a true representation of the model was retained. Once this was established, a regulator multivariable control law was designed for the three systems. Then the time responses of the three systems were compared.

The degree of controllability of the states was determined from the singular values of the  $H_{INF}$  matrix by means of the Moore algorithm. A guideline to model reduction is the magnitude and grouping of the singular values. The singular values of the  $H_{INF}$  matrix were computed for impulse input balancing after a finite time of 20 seconds. A finite time was used due to the spiral divergence pole in the right

half S-plane. The singular values for the plant matrix are,

$$\begin{aligned}
 \sigma_1 &= 14.896 \\
 \sigma_2 &= 13.617 \\
 \sigma_3 &= 10.569 \\
 \sigma_4 &= 9.300 \\
 \sigma_5 &= 8.851 \\
 \sigma_6 &= 3.945 \\
 \sigma_7 &= 3.278 \\
 \sigma_8 &= 2.500
 \end{aligned} \tag{52}$$

These singular values of the plant indicate that at least one state corresponding to  $\sigma_8$  and possibly two others,  $\sigma_6$  and  $\sigma_7$  could be removed due to a low degree of controllability. The least controllable state is represented by the value for  $\sigma_8$ . To establish if the balanced matrices affect the time response of the system, the original system was compared with the balanced and reduced balanced system. As illustrated in Figure 5, the output responses of each system are approximately equal. Recall that  $C^*T^{-1}$  is  $C_0$  and  $T^*B^*$  is  $B_0$ , which insures the physical outputs and inputs remain the same as the original system.

The eigenvalues of the original plant are, as follows:

$$\begin{aligned}
 \lambda_{1,2} &= -0.4148E-2 \pm j \ 0.8209E-1 && \text{phugoid} \\
 \lambda_{3,4} &= -0.4358 \pm j \ 2.040 && \text{dutch roll} \\
 \lambda_{5,6} &= -0.7949 \pm j \ 2.848 && \text{short period} \\
 \lambda_7 &= 0.4934E-1 && \text{spiral divergence} \\
 \lambda_8 &= -2.878 && \text{roll subsidence}
 \end{aligned} \tag{53}$$

The time response plots for the original system, Figure 6, indicate

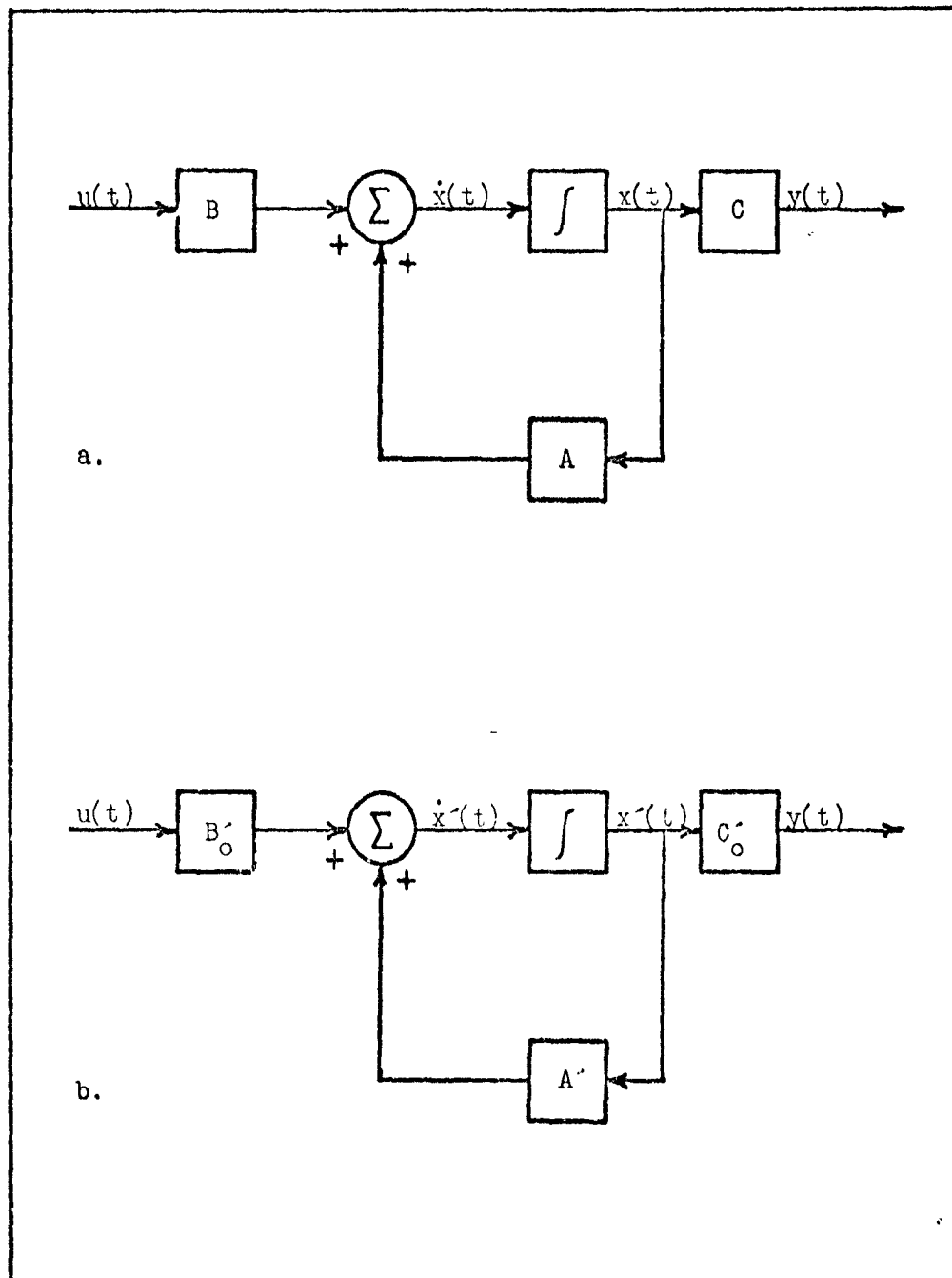


Figure 5. Output Signals of (a) Original System and (b) Internally Balanced System

that some form of compensation or feedback control is necessary to correct for the unstable spiral divergence mode present in the pitch and roll angle responses. The pitch response of Figure 6a is for an impulse of 0.1 rad and has a maximum negative pitch angle of 0.245 rad and an initial settling time of 6 seconds before slowly diverging with a constant positive pitch angle. The roll response of Figure 6c has an initial settling time of 11 seconds before a constant roll angle divergence takes over. To illustrate that the horizontal stabilizer UHT does function on the model as left and right independent control surfaces, Figures 6e and 6f show that the left stabilizer produces a positive roll and the right stabilizer a negative roll with a 0.1 rad impulse input. This illustrates the coupling between the axes as a result of longitudinal inputs into the lateral-directional equation of motion.

After balancing the system state equations with the Moore algorithm, the  $A'$ ,  $B'_o$ , and  $C'_o$  matrices are as shown in Equation (A-25 through A-27). The eigenvalues for the  $A'$  matrix remain the same as for the physical plant A matrix Equation (53) and are as follows:

$$\begin{aligned}\lambda_{1,2} &= -0.4148E-2 \pm j 0.8209E-1 \\ \lambda_{3,4} &= -0.4358 \pm j 2.040 \\ \lambda_{5,6} &= -0.7949 \pm j 2.848 \\ \lambda_7 &= 0.4934E-1 \\ \lambda_8 &= -2.878\end{aligned}\tag{54}$$

where  $\lambda_1$  to  $\lambda_8$  correspond to the same characteristic roots of the original system. Figure 7 illustrates that the time response plots of the system equations with internally balanced matrices remained the same as the original system. The yaw angle response of Figure 7f for a 0.07 rad

# ORIGINAL SYSTEM. RIGHT AILERON MISSING THETA

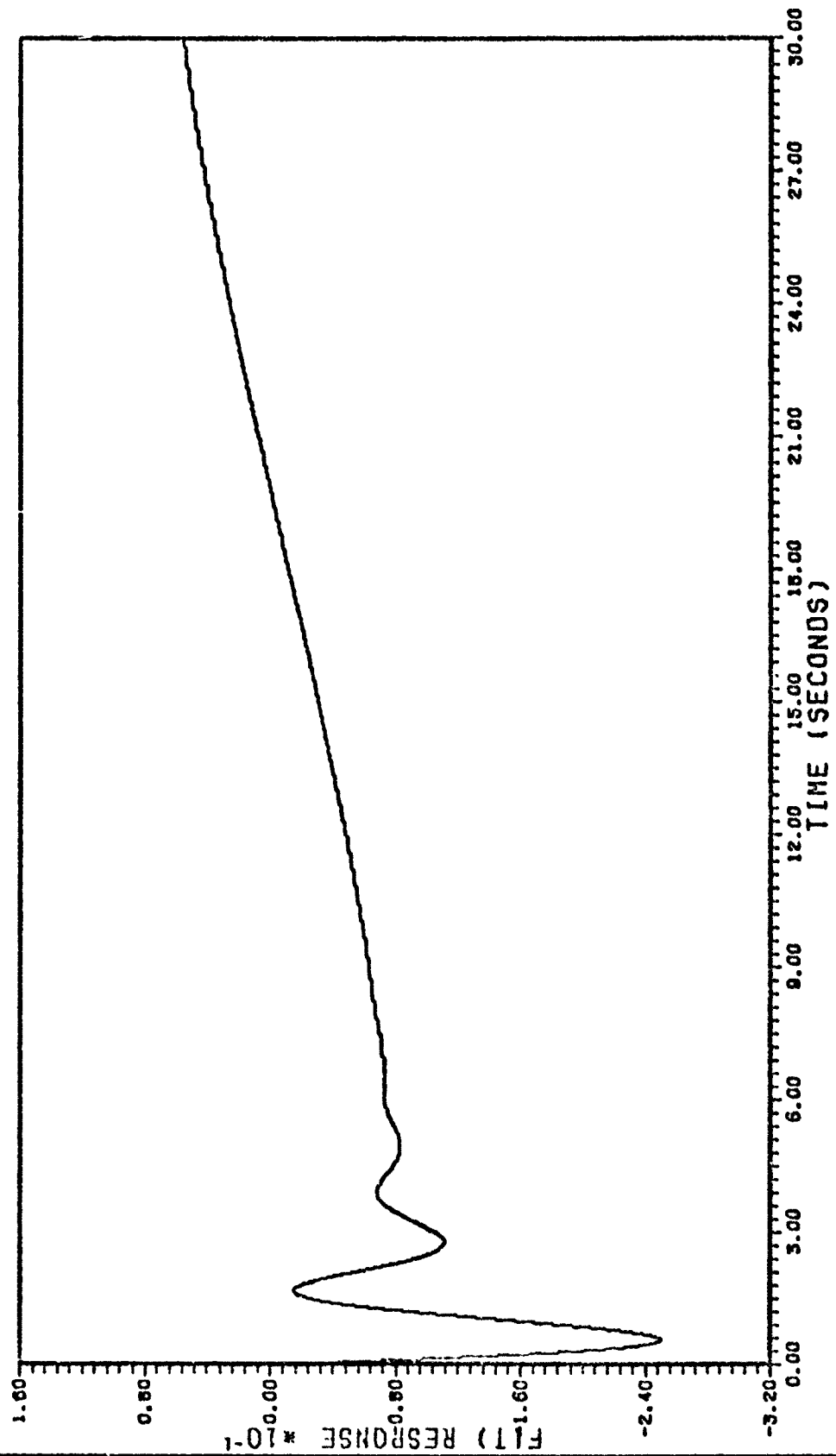


Figure 6a. Pitch Angle for 0.1 Rad Impulse  $\delta_{h_1}$  Input

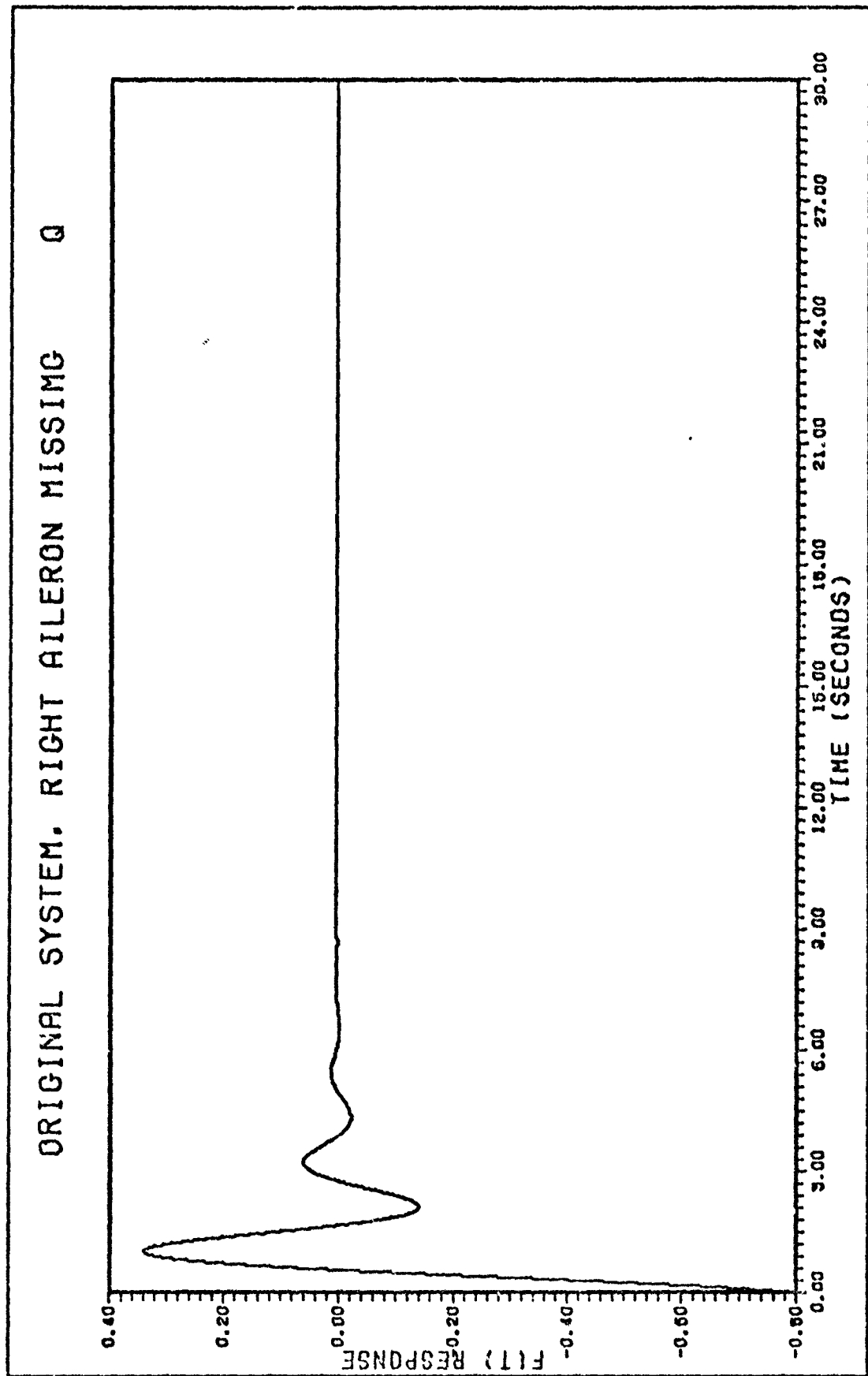


Figure 6b. Pitch Rate For 0.1 Rad Impulse  $\delta_{h_1}$  Input

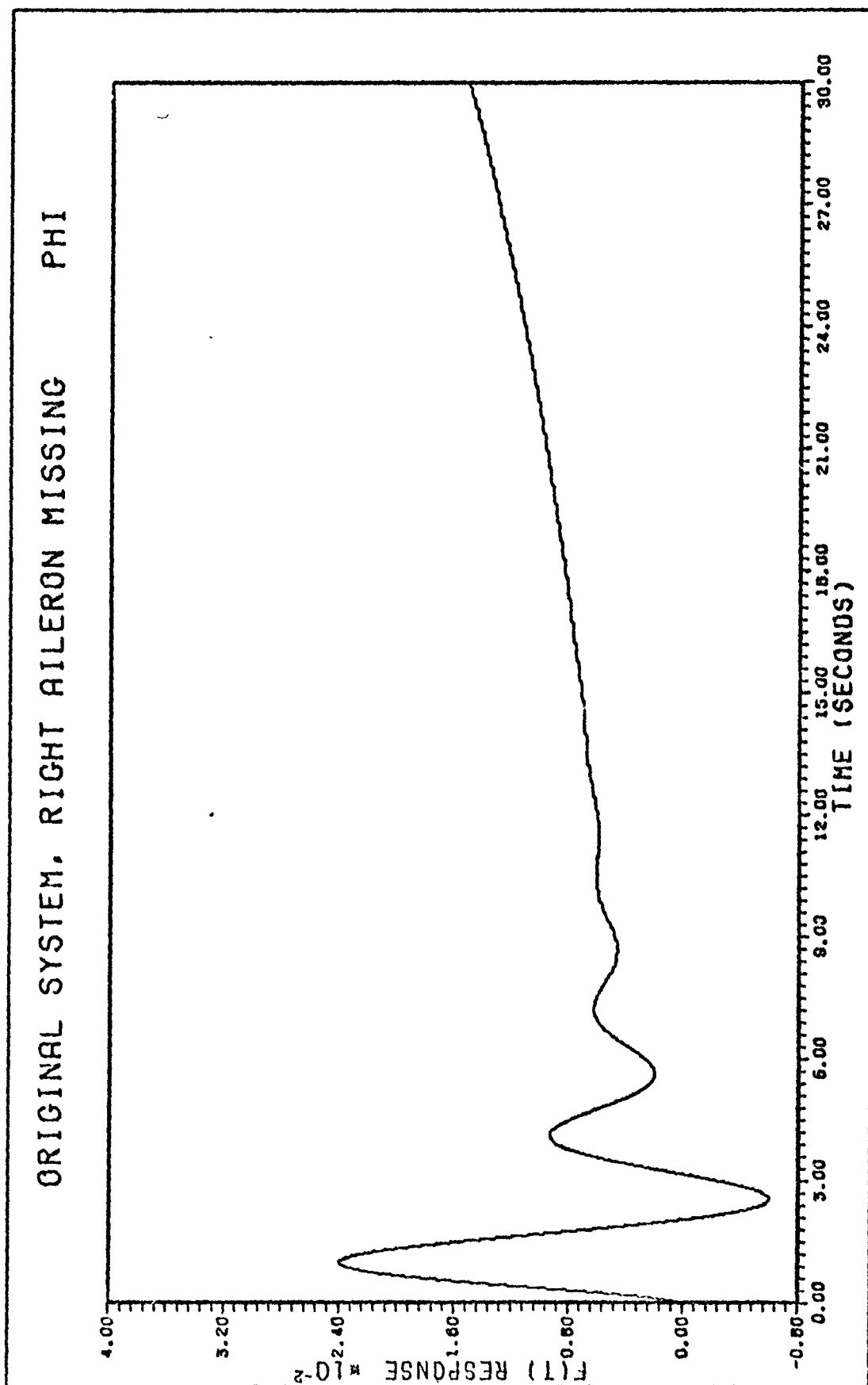


Figure 6c. Roll angle for 0.2 Rad Impulse  $\delta a_1$  Input

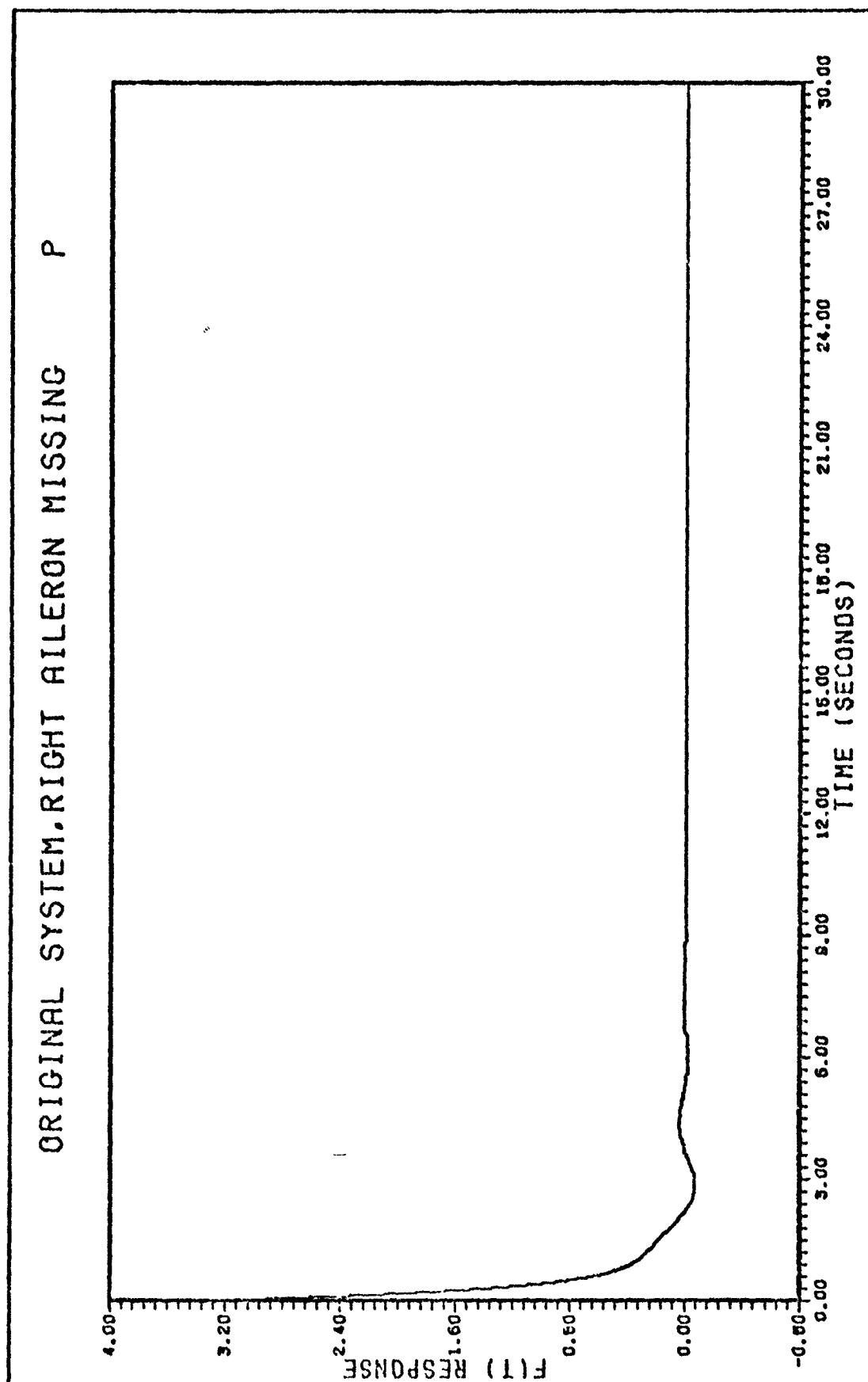


Figure 6d. Roll Rate for 0.2 Rad Impulse  $\delta_{a1}$  Input

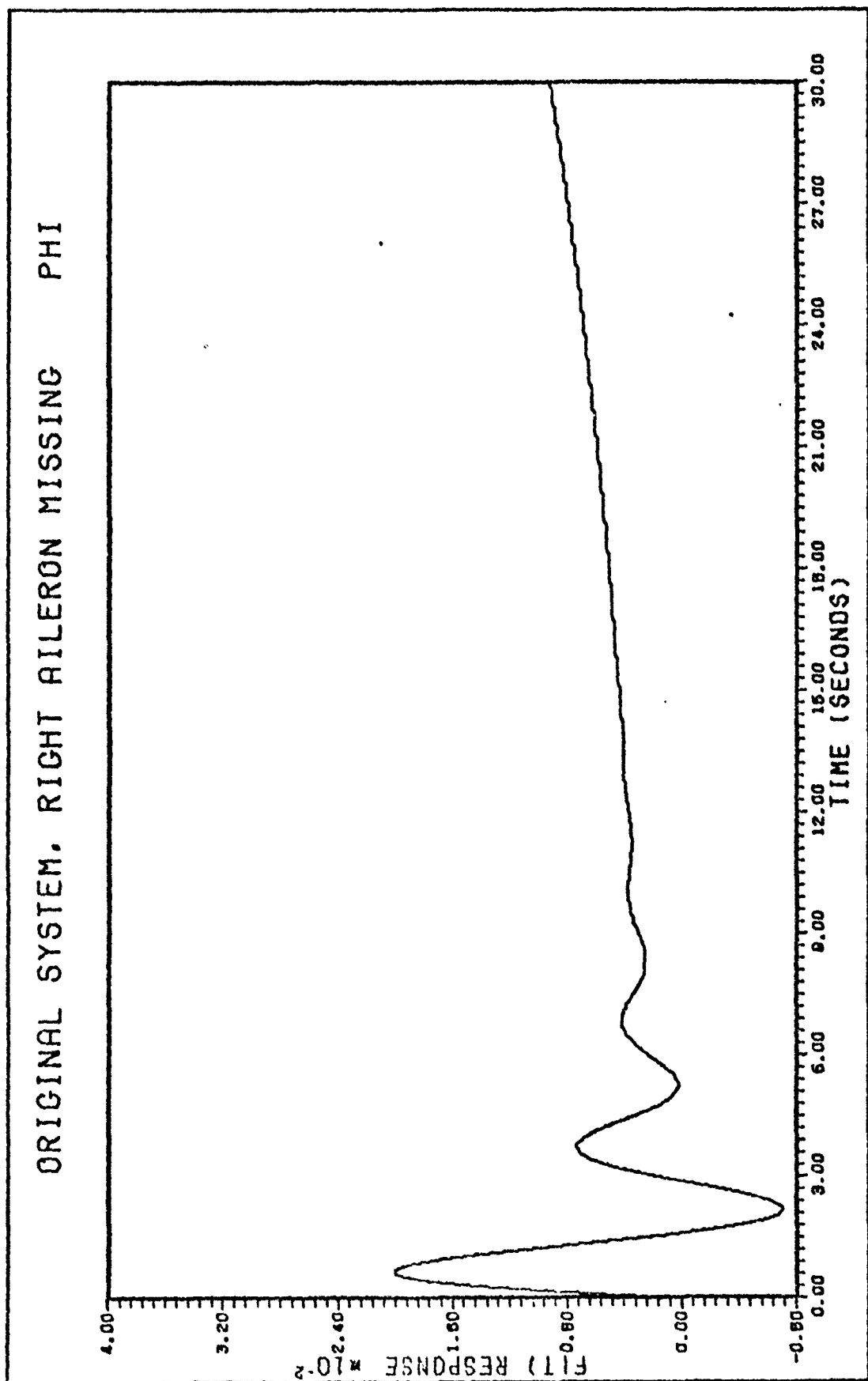


Figure 6e. Roll Angle for 0.1 Rad Impulse  $\delta_{h_1}$  Input

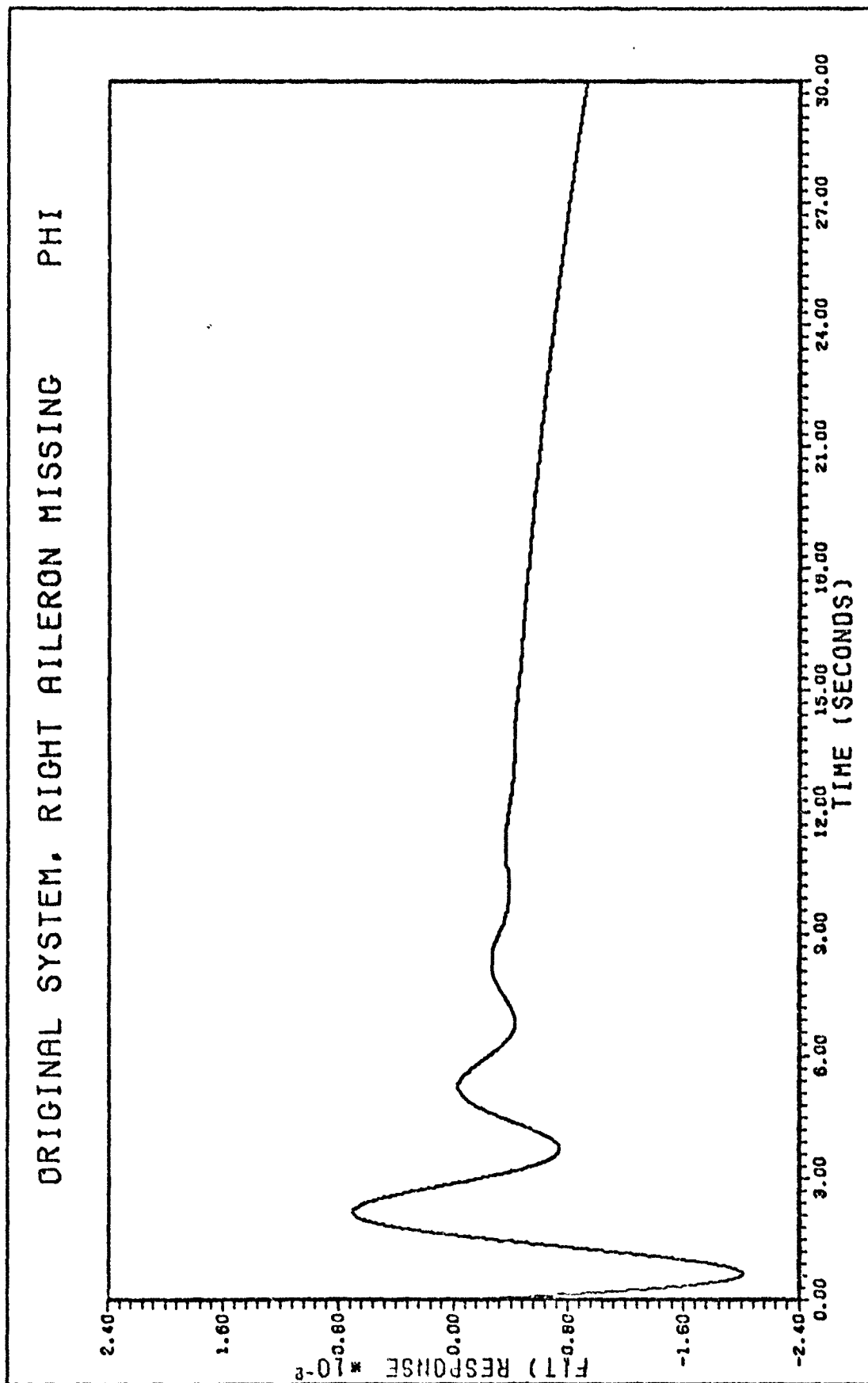


Figure 6f. Roll Angle for 0.1 Rad Impulse  $\delta_{h_r}$  Input

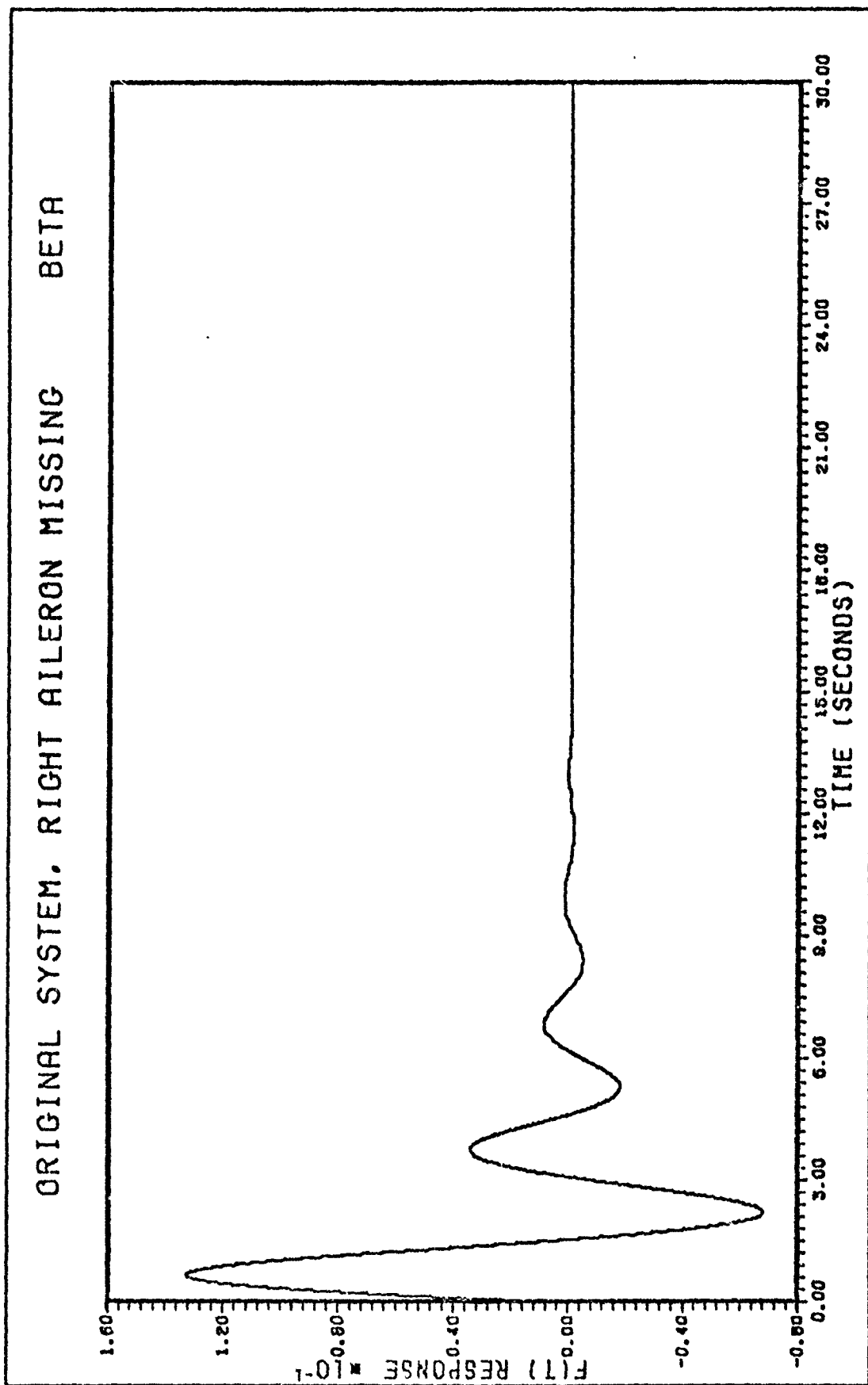


Figure 6g. Sideslip Angle for 0.07 Rad Impulse  $\delta_r$  Input

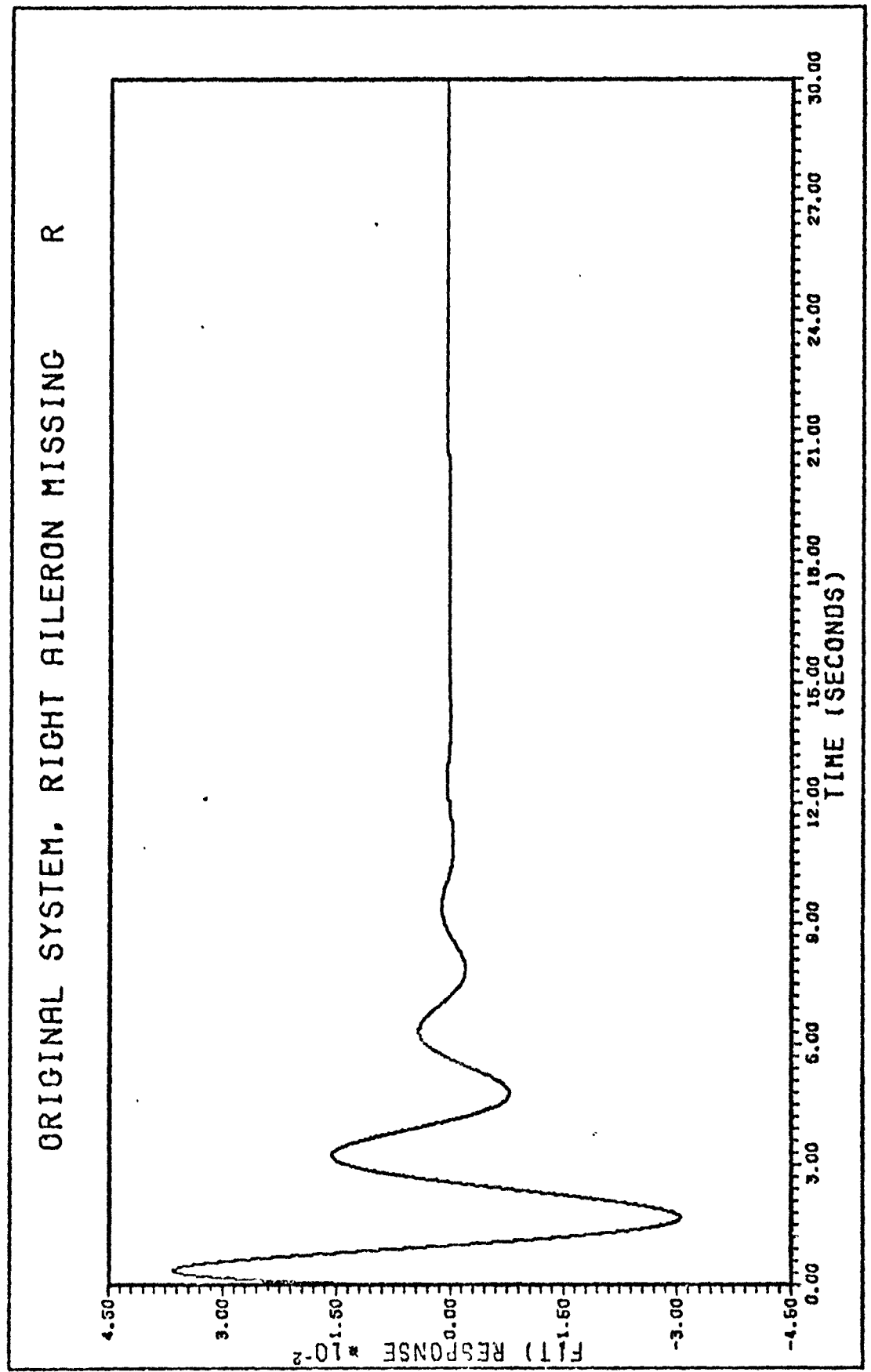


Figure 6h. Yaw Angle for 0.2 Rad Impulse  $\delta_{a_1}$  Input

impulse input results in the same form of response as for a 0.2 rad impulse input, Figure 6h, as in the original system but of a different magnitude due to the impulse input. The difference between the original and balanced matrices is that the states of the system are ordered by their degree of controllability. Thus, the redundant states can be removed as long as the system characteristics are not destroyed.

The  $A'$  matrix of Equation (A-25) was reduced to seven states, as illustrated in Equations (42 and 43) and as indicated by the singular values of Equation (52). The characteristic eigenvalues of the reduced internally balanced system are:

$$\begin{aligned}
 \lambda_{1,2} &= -0.4142E-3 \pm j \ 0.8225E-1 && \text{phugoid} \\
 \lambda_{3,4} &= -0.4731 \pm j \ 1.959 && \text{dutch roll} \\
 \lambda_{5,6} &= -0.8050 \pm j \ 2.825 && \text{short period} \\
 \lambda_7 &= 0.4935E-1 && \text{spiral divergence}
 \end{aligned} \tag{55}$$

The eigenvalues of the reduced balanced system have shifted a small amount and the roll subsidence mode is no longer present. The reduced system time response plots are shown in Figure 8.

The pitch and pitch rate time response of Figures 8a and 8b remained the same as for the original system. However, the roll angle of Figure 8c shows a phase change, an increase in magnitude from a max of 0.024 radian to 0.13 radian, and the settling time decreased by 0.5 seconds. These changes are attributed to the shifting of the poles and zeros of the  $\phi/\delta_{a1}$  transfer function. In Figure 8d, the roll rate settling time was increased from approximately 6 sec to 10 sec, while the magnitude decreased and the dutch roll oscillation decreased. The yaw rate, Figure 8f, also indicates a change in phase and magnitude.

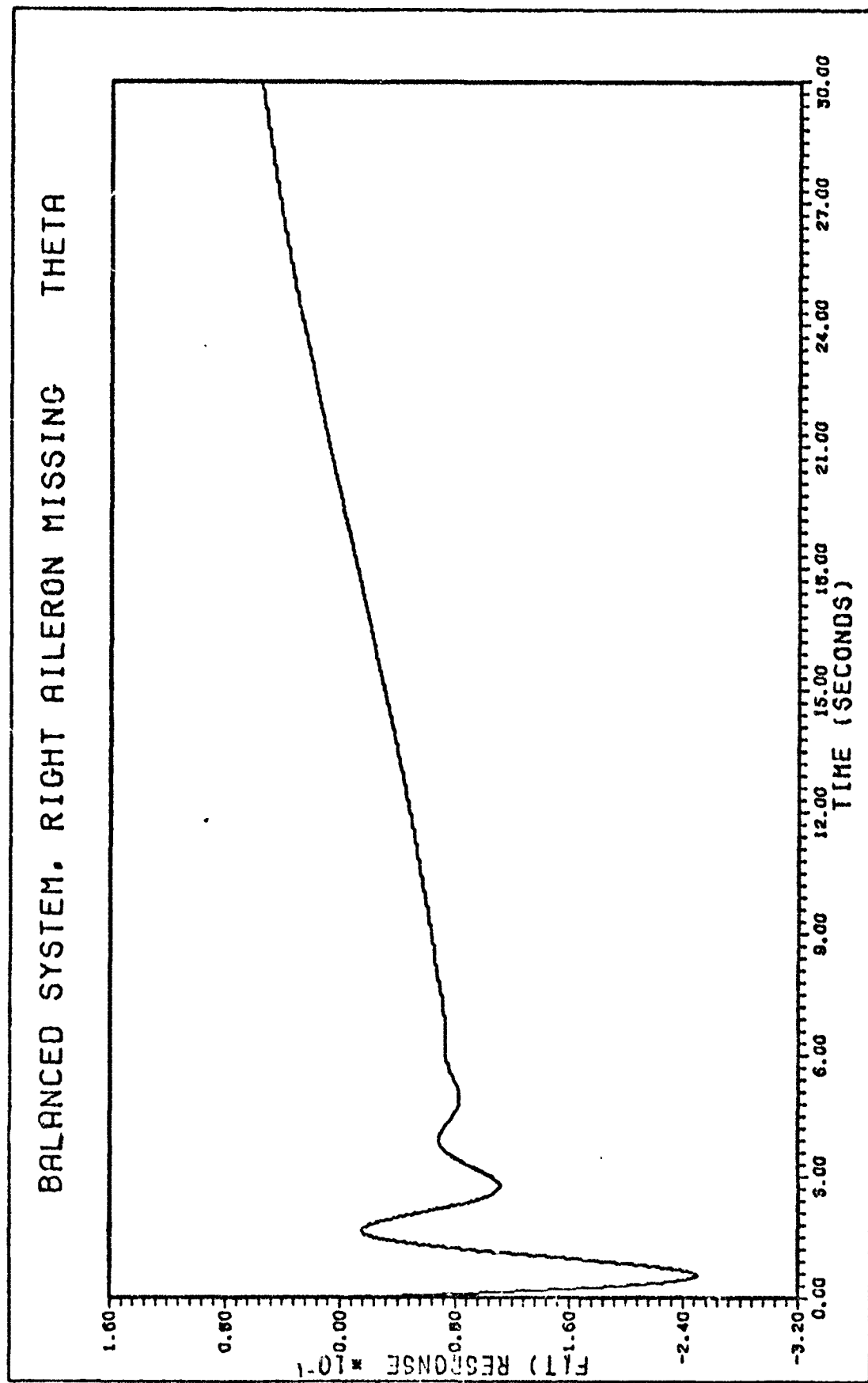


Figure 7a. Pitch Angle for 0.1 Rad Impulse  $\delta_{h1}$  Input

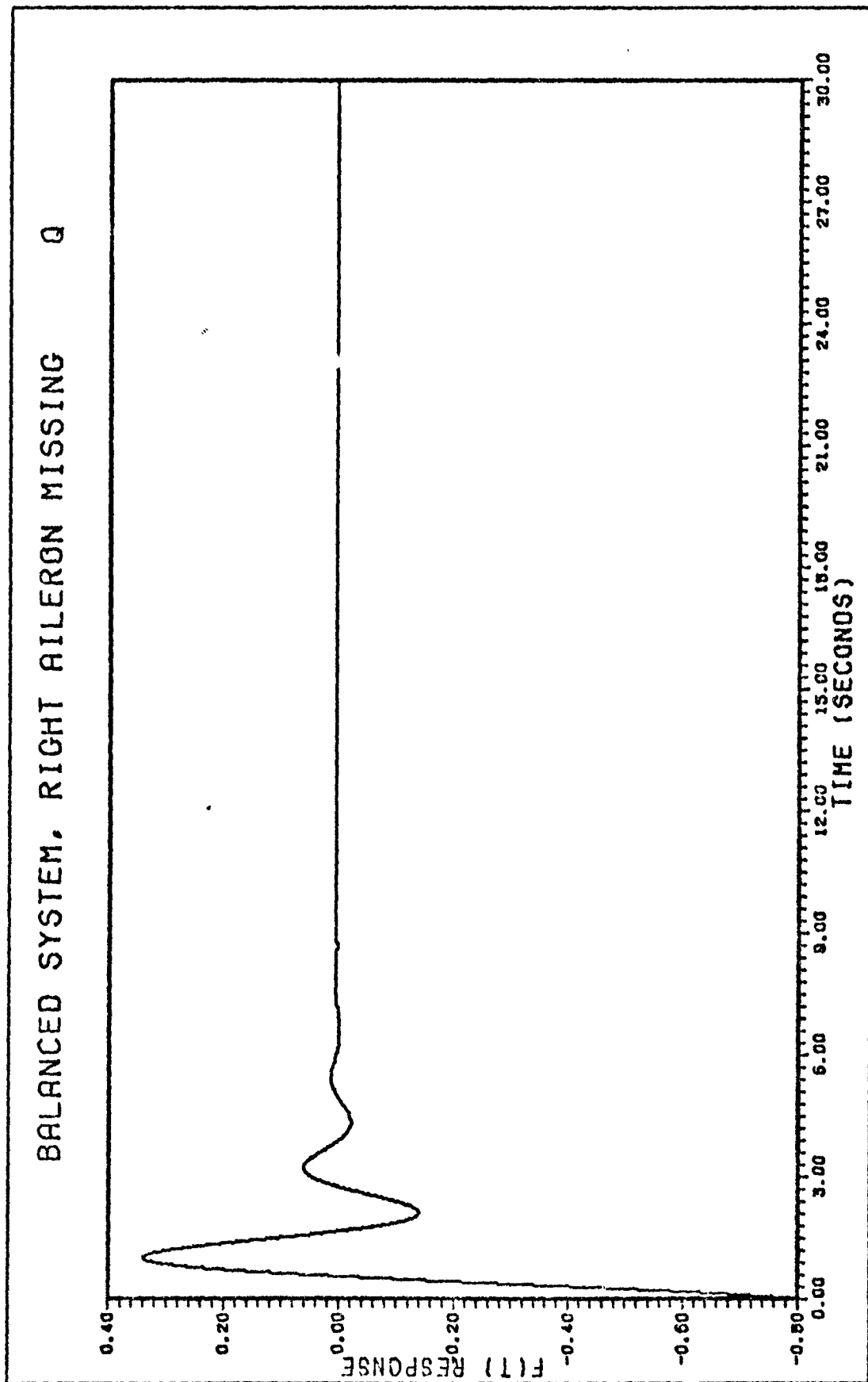


Figure 7b. Pitch Rate for 0.1 Rad Impulse  $\delta_{h_1}$  Input

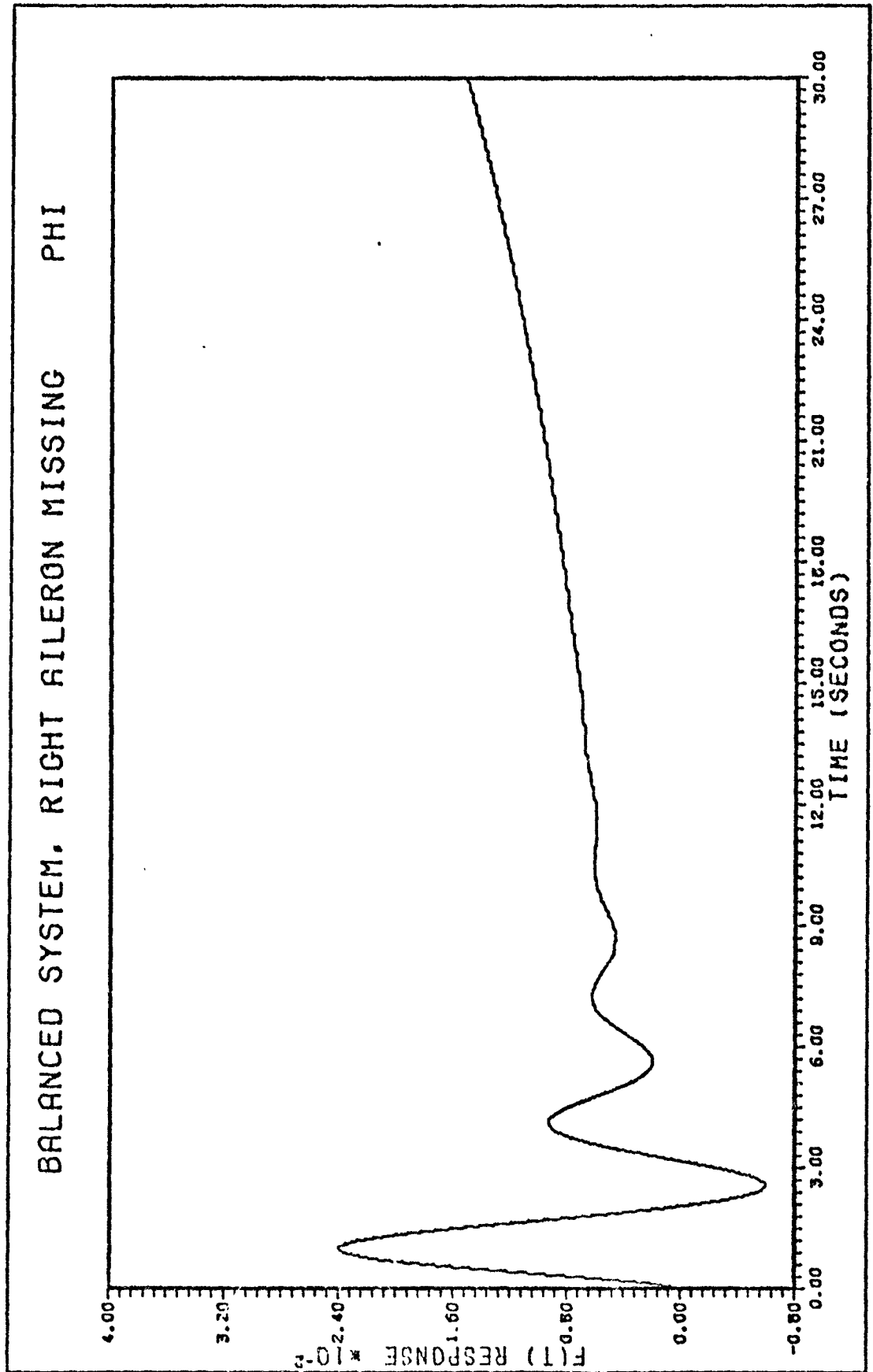


Figure 7c. Roll Angle for 0.2 Rad Impulse  $\delta_{\phi_1}$  Input

# BALANCED SYSTEM, RIGHT AILERON MISSING P

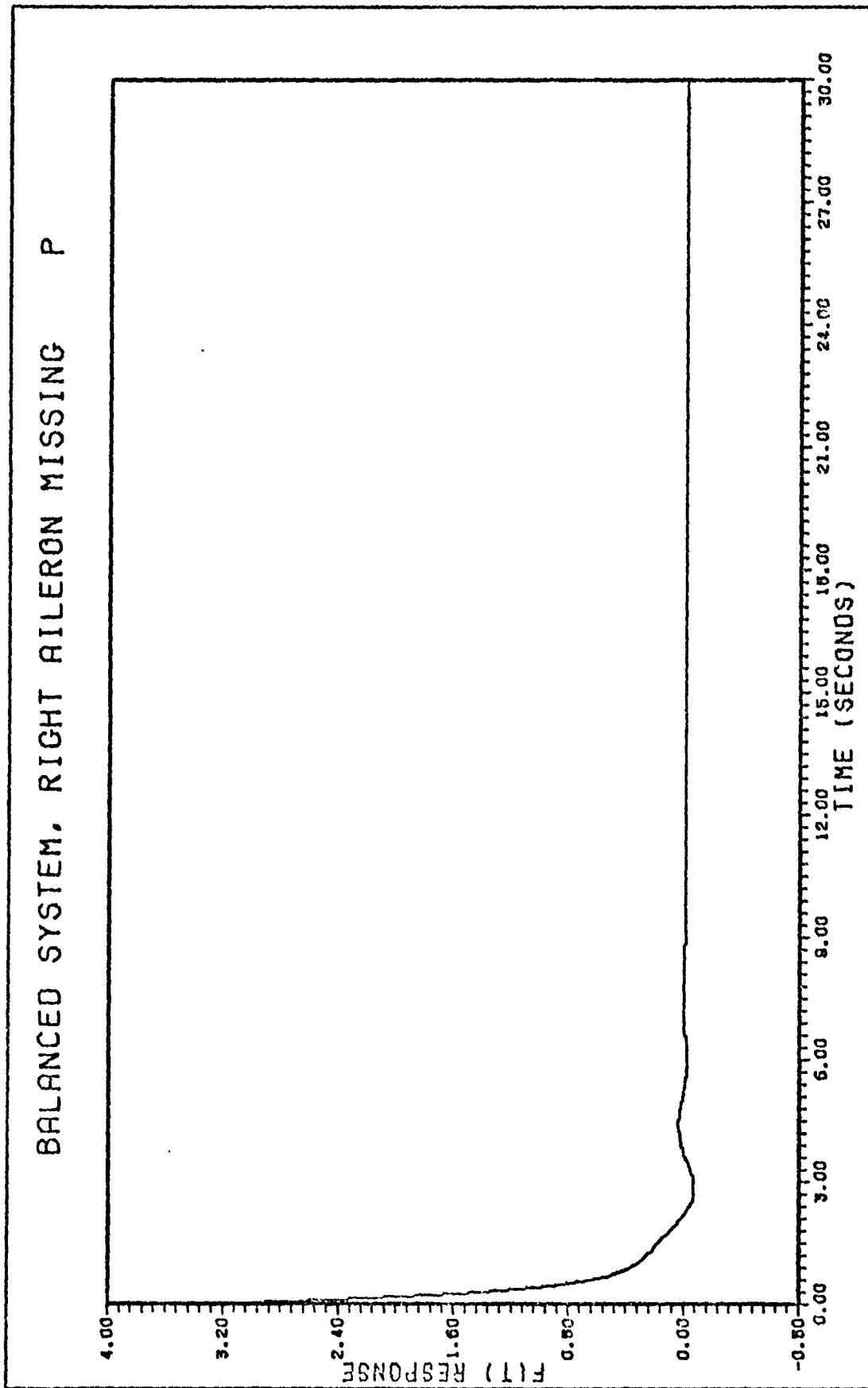


Figure 7d. Roll Rate for 0.2 Rad Impulse  $\delta_{a1}$  Input

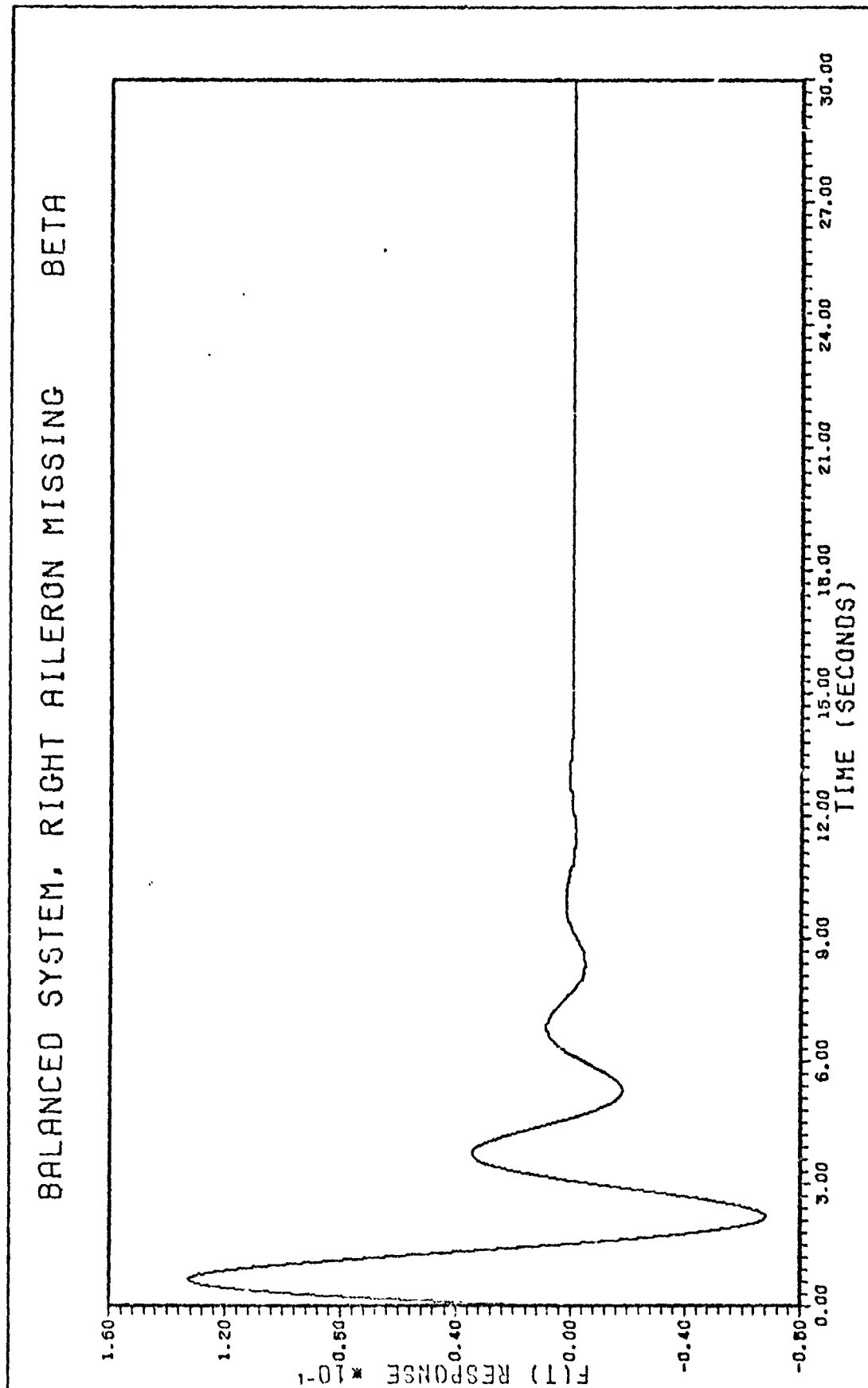


Figure 7e. Sideslip Angle for 0.07 Rad Impulse  $\delta_r$  Input

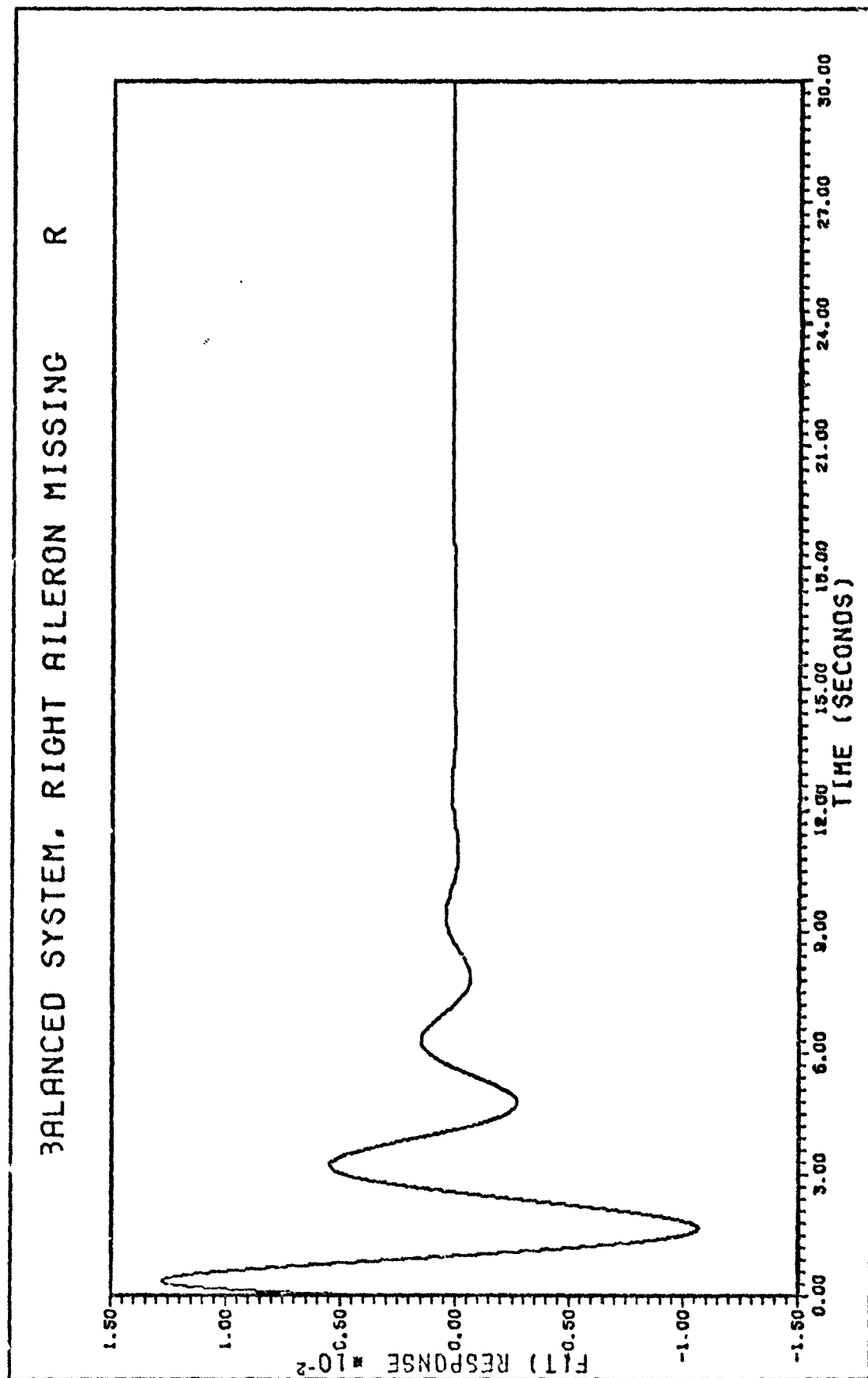


Figure 7f. Yaw Angle for 0.07 Rad Impulse  $\delta_{a_1}$  Input

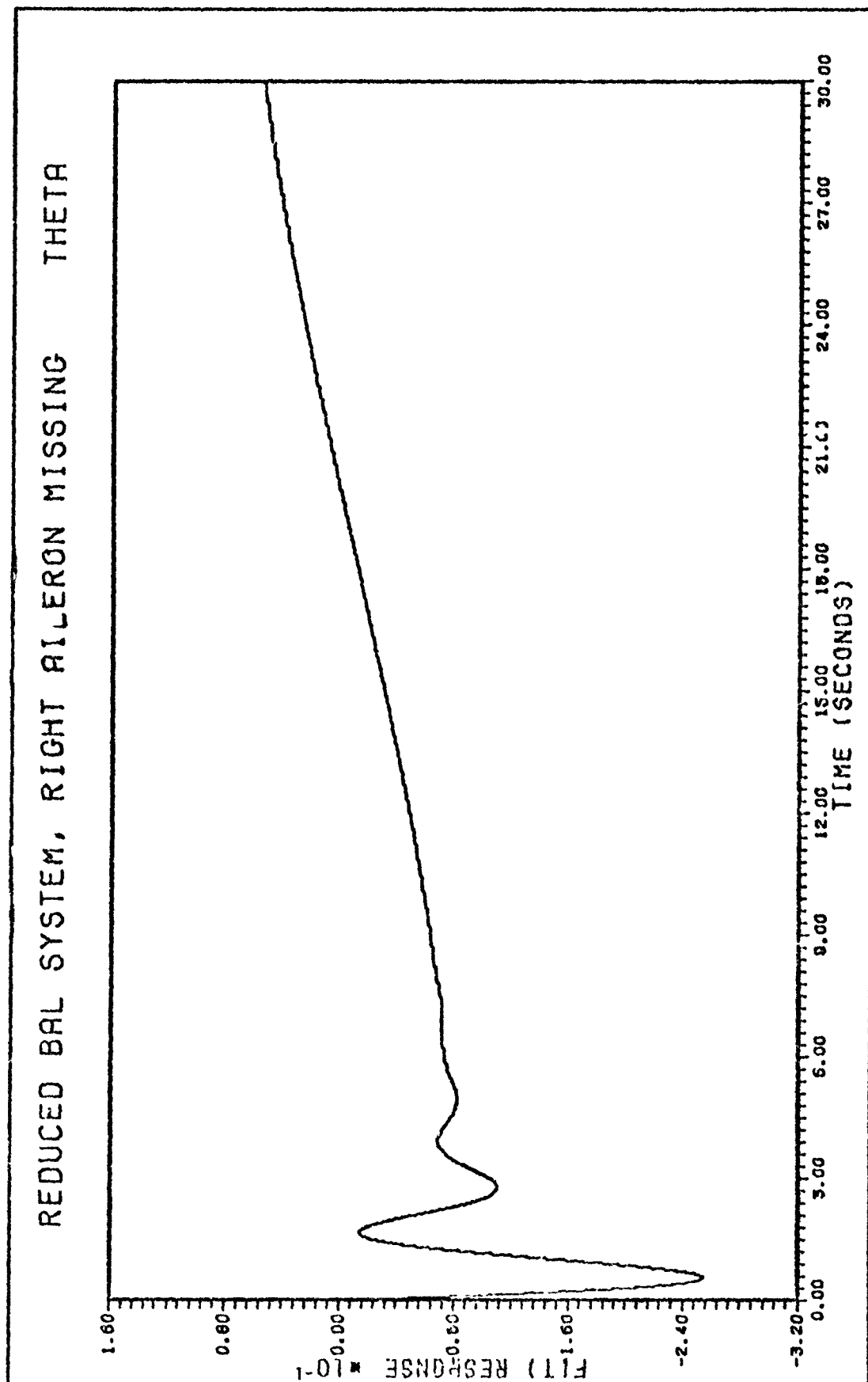
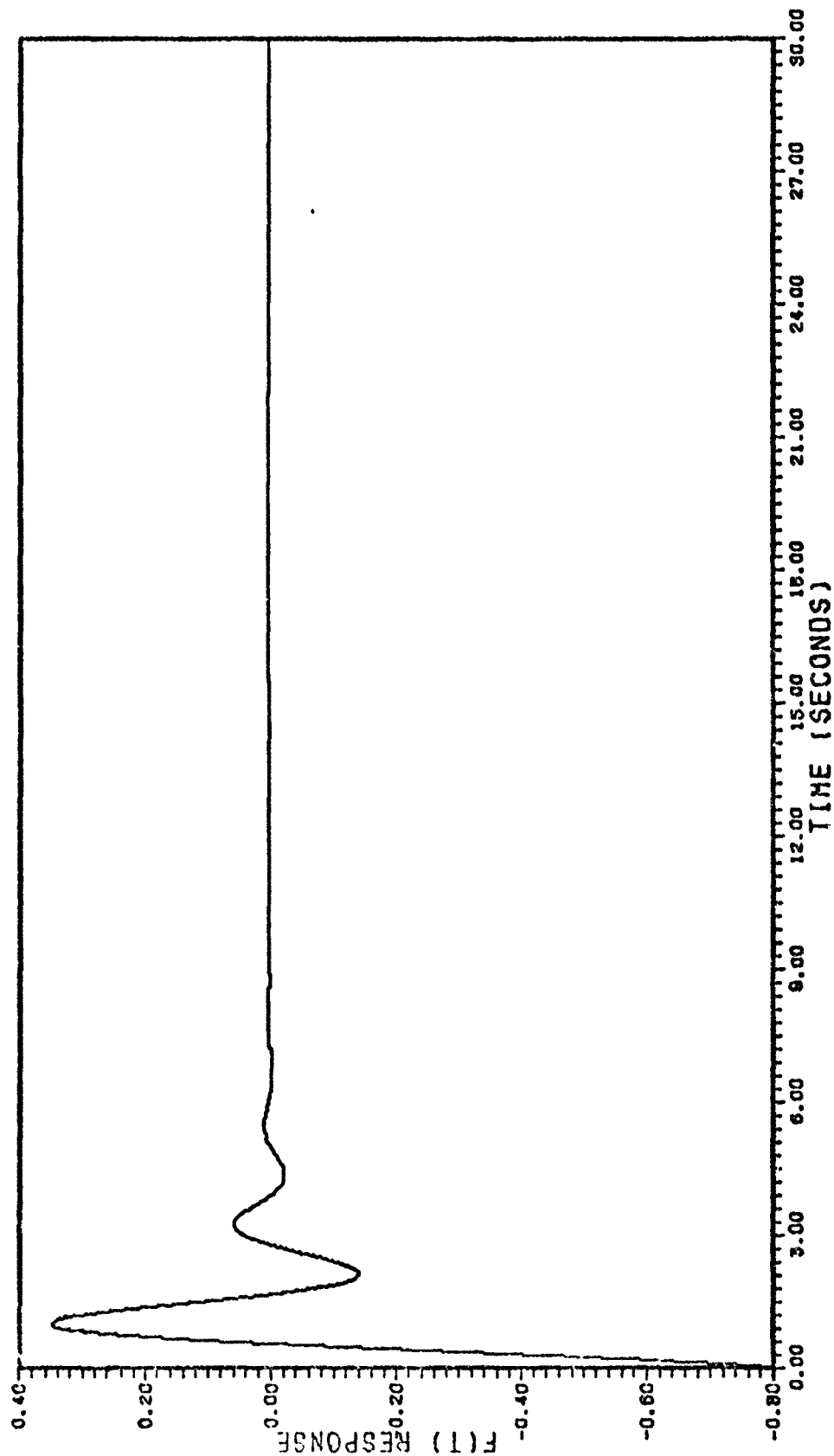


Figure 8a. Pitch Angle for 0.1 Rad Impulse  $\delta_{h1}$  Input

REDUCED BAL. SYSTEM, RIGHT AILERON MISSING Q



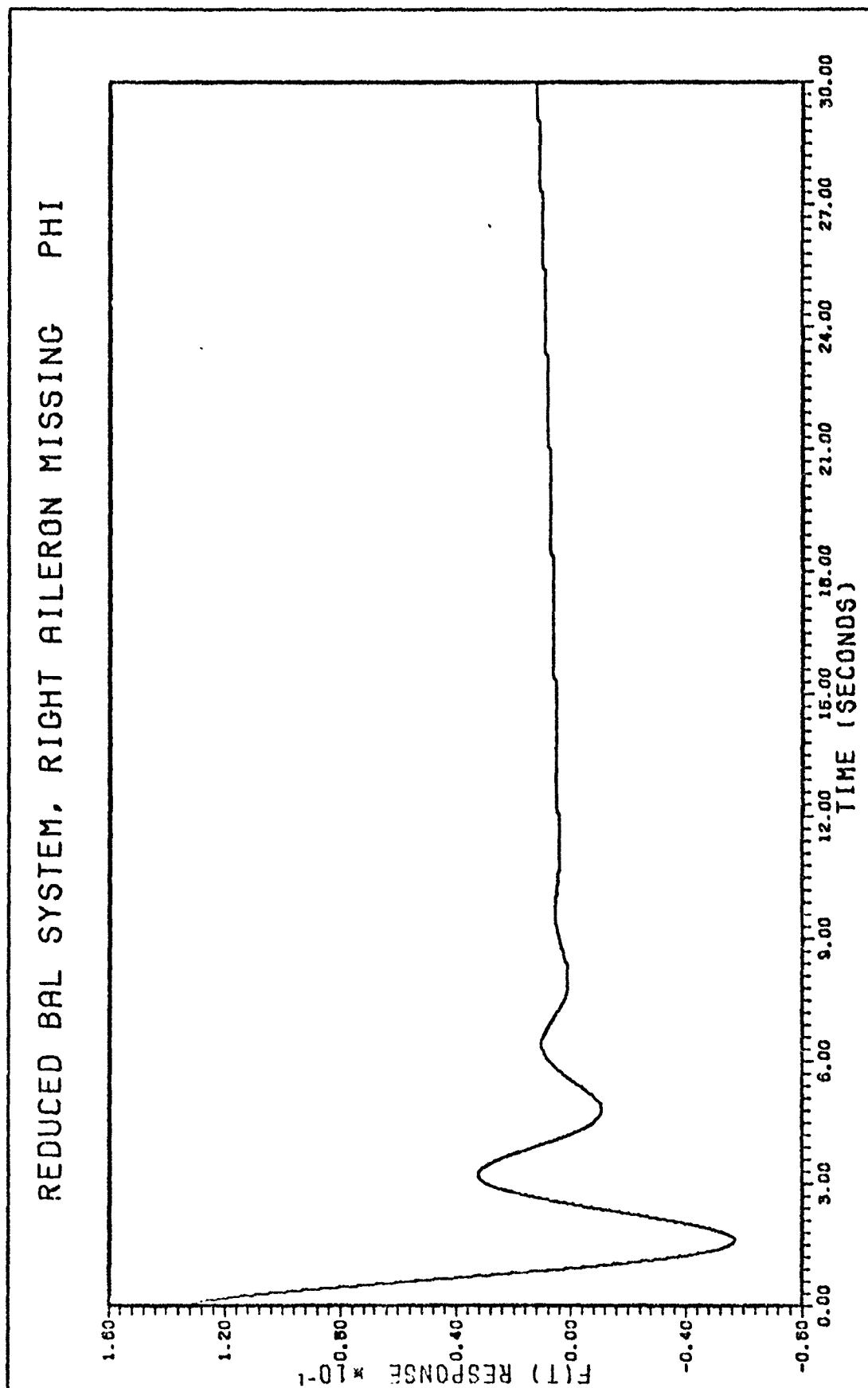


Figure 2c. Roll Angle for 0.2 Rad Impulse  $\delta_{a1}$  Input

# REDUCED BAL SYSTEM. RIGHT AILERON MISSING P

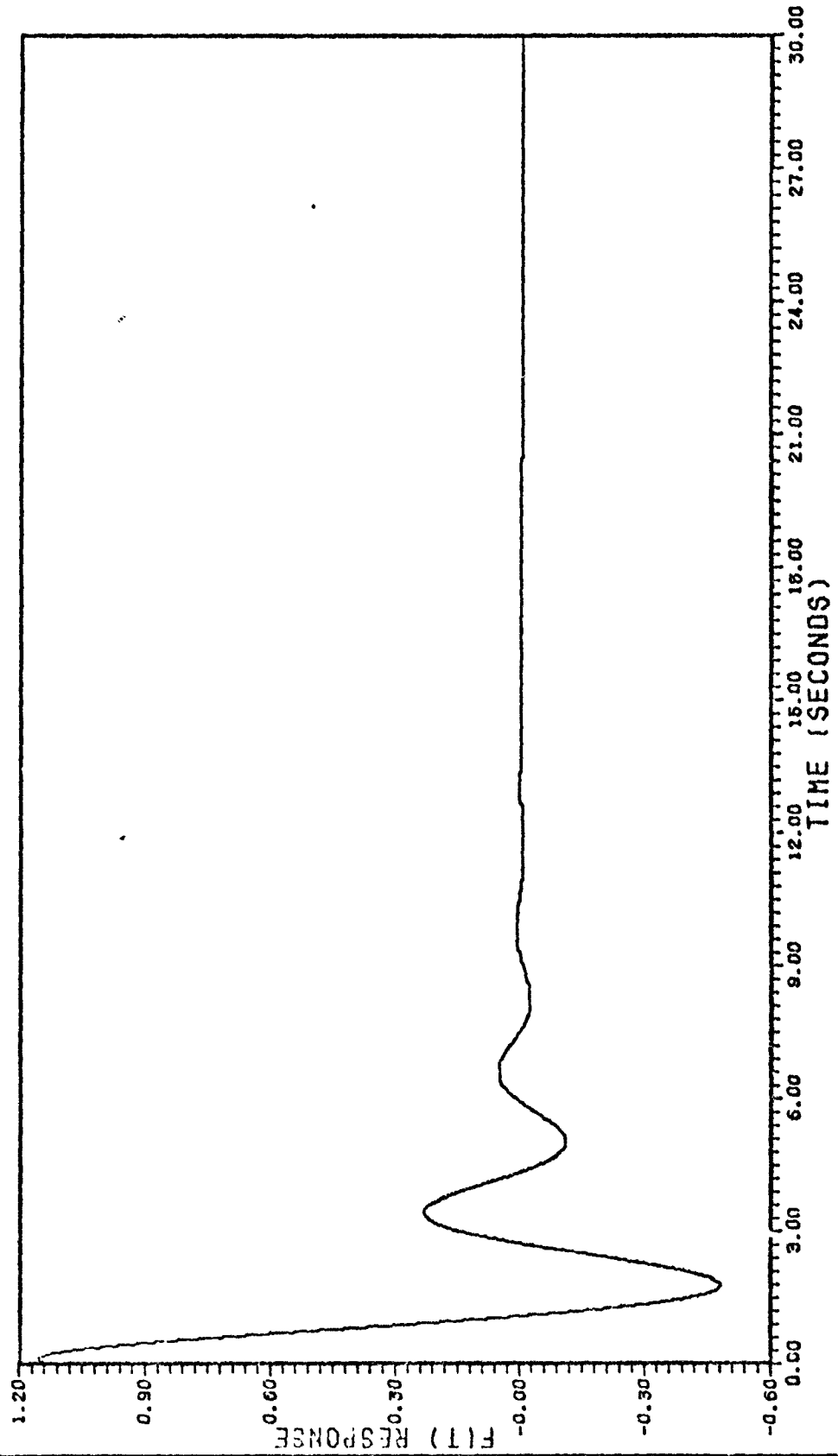


Figure 8d. Roll Rate for 0.2 Rad Impulse  $\delta_{a1}$  Input

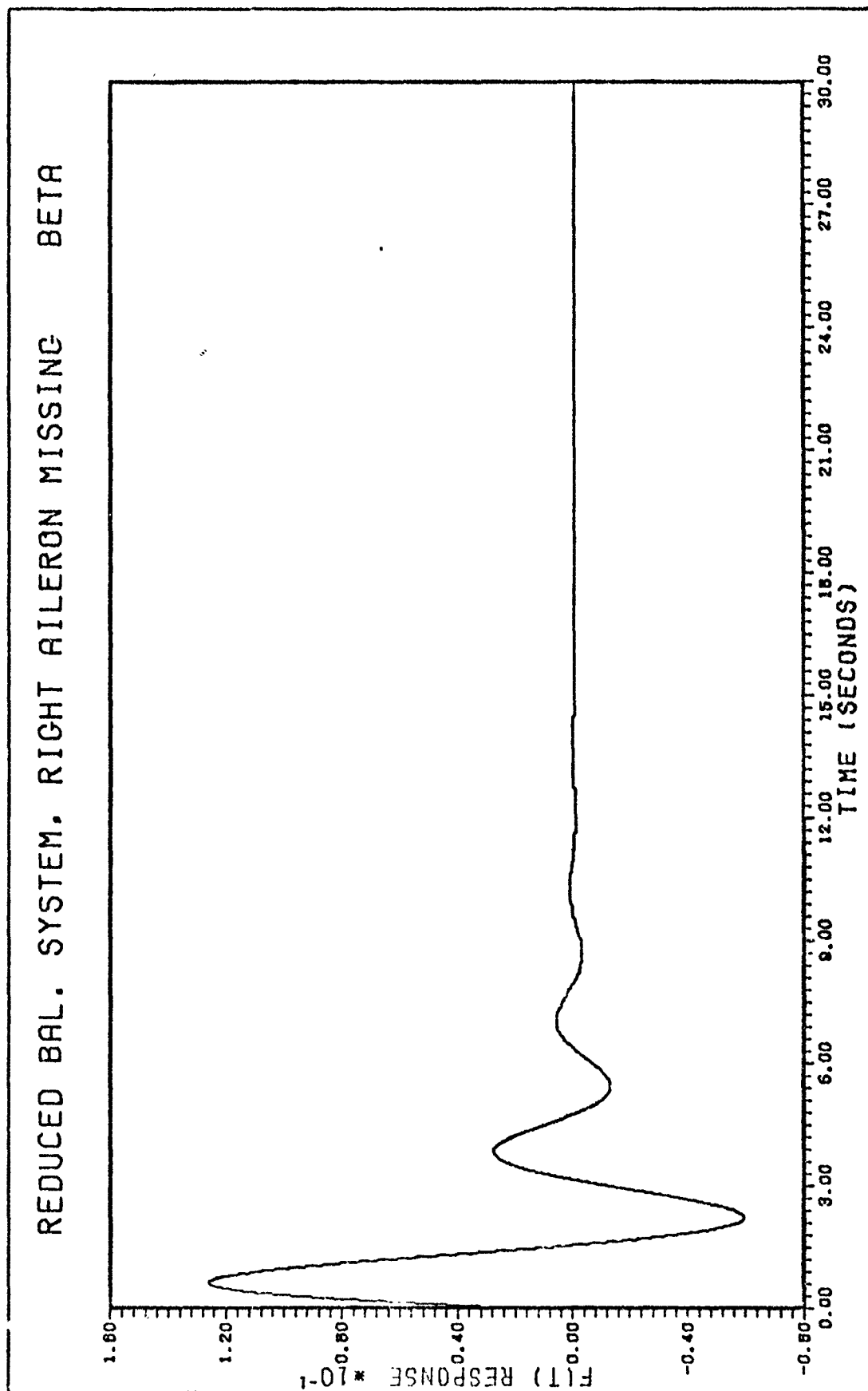


Figure 8e. Sideslip Angle for 0.07 Rad Impulse  $\delta_r$  Input

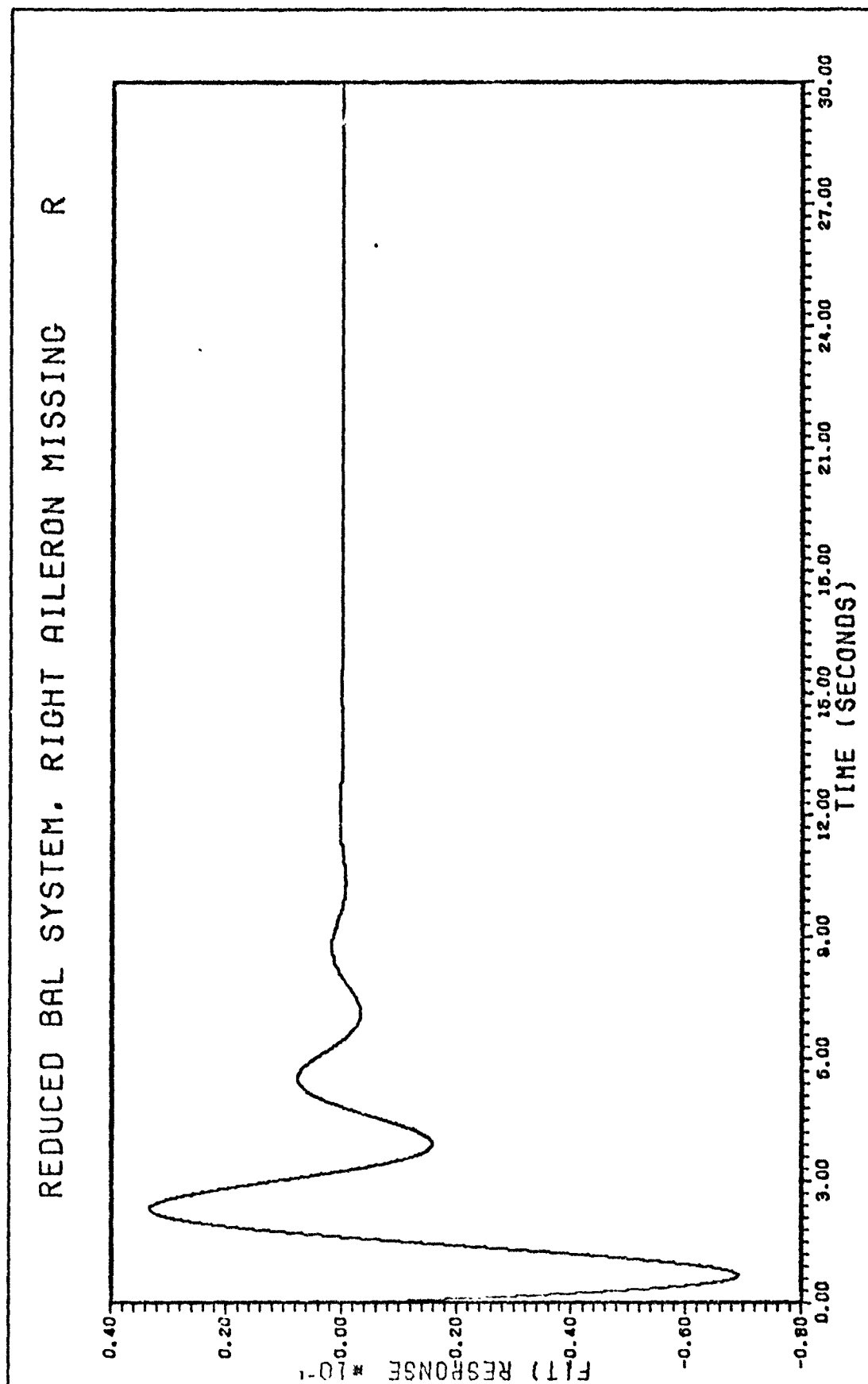


Figure 8f. Yaw Angle for 0.07 Rad Impulse  $\delta_{a_1}$  Input

Even with the system response changes pointed out, the reduced balanced system still retains all the characteristics of the aircraft model. Therefore, the removal of a state with a low degree of controllability does not affect the output response of this aircraft model.

Having established the degree of controllability of the states by the Moore algorithm, the number of control inputs was reduced to improve the controllability of the (A, B) matrix pair. A reconfigured multi-variable control law for a regulator controller was developed for the original, balanced, and reduced balanced systems using a sampling time of 0.5 seconds.

The family of reconfigured control inputs to compensate for a failed surface in the regulator design is shown in Figure 9.

input failure	$\delta_{h_l}$	$\delta_{h_r}$	$\delta_r$	$\delta_{a_l}$	$\delta_{a_r}$	$\delta_{s_l}$	$\delta_{s_r}$
UHT <sub>l</sub>	0	X	X	X	X	X	X
UHT <sub>r</sub>	X	0	X	X	X	X	X
Rudder	X	X	0	X	X	X	X
Aileron <sub>l</sub>	X	X	X	0	X	X	X
Aileron <sub>r</sub>	X	X	X	X	0	X	X
Spoiler <sub>l</sub>	X	X	X	X	X	0	X
Spoiler <sub>r</sub>	X	X	X	X	X	X	0

\*Control surfaces l - left r - right  
0 - failed surface X - normal operation

Figure 9. Control Surface Failure Vs.  
Reconfigured Input (7) Matrix

A block diagram for the state variable feedback regulator controller is shown in Figure 10 in which all the variables are vector quantities.

The regulator design uses Equations (A-20) and (A-21) except for the flap inputs, and (A-24). The outputs are  $q$ ,  $\theta$ ,  $\beta$ ,  $p$ ,  $r$ , and  $\phi$ . The feedback matrix  $K$  of Equation (47) is computed so that the closed-loop original system is asymptotically stable and has the closed-loop eigenvalue spectrum.

$$\sigma(F + GK) = \{0.001, 0.002, 0.03, 0.3, 0.4, 0.625, 0.95, 0.99\} \quad (56)$$

The vectors assigned from the null space of Equation (49) for each  $\lambda_i$  are:

$$\begin{bmatrix} x_{\lambda_1} \\ w_{\lambda_1} \end{bmatrix} \cdot \left\{ \begin{bmatrix} x_{\lambda_1} \\ w_{\lambda_1} \end{bmatrix}, \begin{bmatrix} x_{\lambda_2} \\ w_{\lambda_2} \end{bmatrix}, \dots, \begin{bmatrix} x_{\lambda_8} \\ w_{\lambda_8} \end{bmatrix} \right\} \quad (57)$$

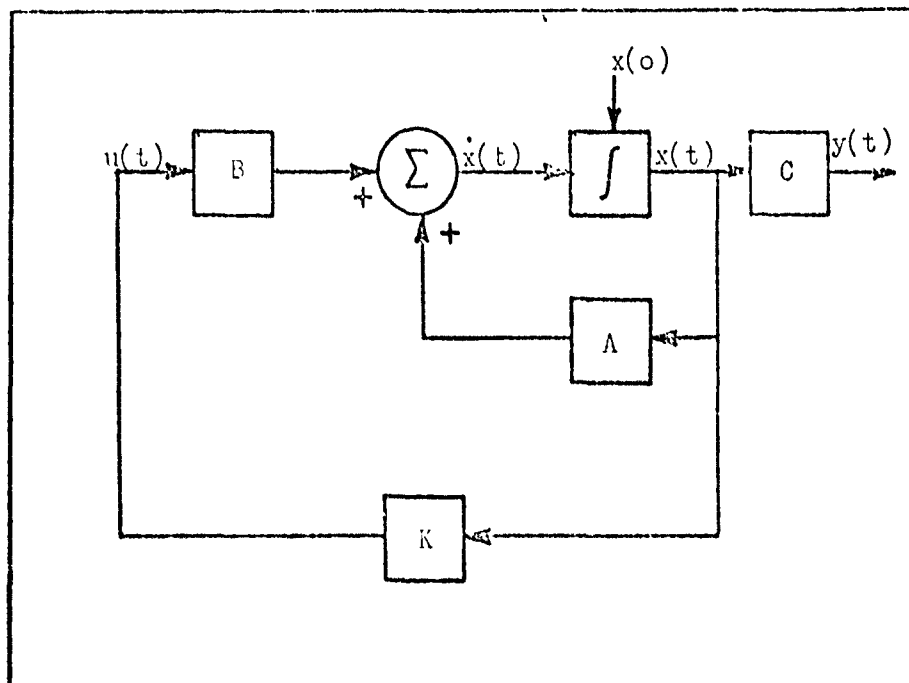


Figure 10. State Feedback Block Diagram of the Original System

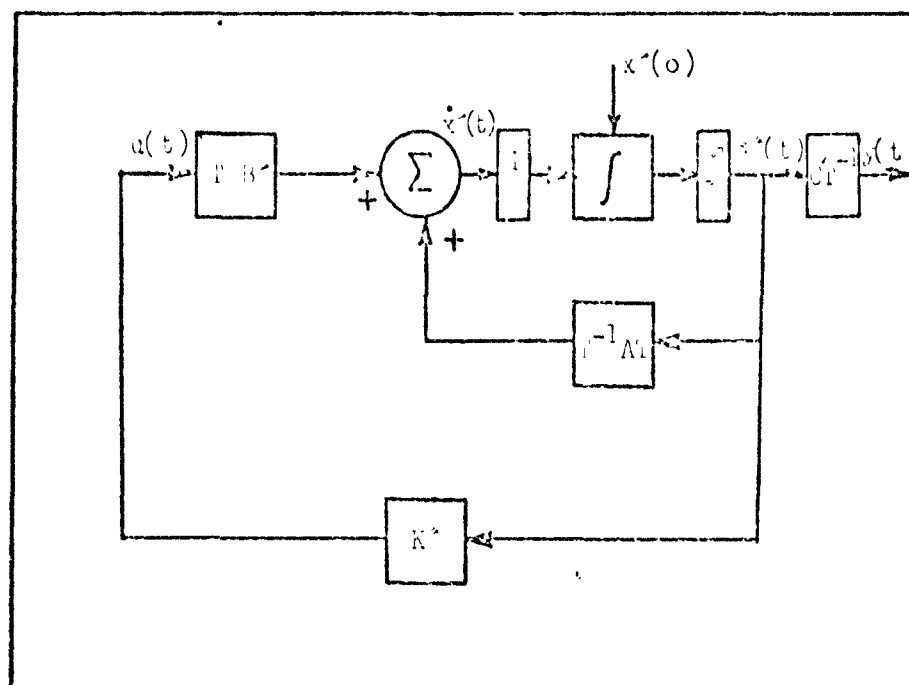


Figure 11. State Feedback Block Diagram of the Balanced System

where the X matrix of eigenvectors is

$$X = \begin{bmatrix} 1.000 & 0. & 0. & 0. \\ 0.373E-01 & -0.312E-01 & 0. & 0. \\ 0.3257E-02 & -0.5443E-02 & 0.1348E-01 & -0.6069E-02 \\ 0.392E-02 & 0.2839 & -0.1677 & 0. \\ 0. & 0. & 0. & 0. \\ 0. & 1.000 & -0.3124 & 0. \\ -0.1715E-03 & 6.1335E-03 & -0.2810 & 0.1575 \\ 0. & 0. & 0. & 0. \\ 0.8531 & 0.3117E-01 & -0.2891E-02 & 0.1693E-02 \\ -0.4633 & 0.1902E-01 & -0.2430E-02 & 0.1535E-02 \\ 0.4125 & -0.1490E-01 & .2315E-01 & -0.7605E-01 \\ 0.7000 & -0.7364E-03 & -0.364 & 0.6055 \\ 0. & 0. & 1.000 & 0. \\ 1.000 & 0.6591E-04 & 0.3950E-02 & -0.2127E-01 \\ -0.5388 & 0. & -0.2653E-01 & 1.000 \end{bmatrix} \quad (58)$$

and the associated  $\Omega$  matrix is

$$\Omega = \begin{bmatrix} -0.4294 & 0.4592 & -0.6622 & 0.1458 \\ 0.6545 & -0.3835 & 0.5430 & -0.1698 \\ -0.1273 & 0.9901E-01 & 0.2618 & -0.9987E-01 \\ -0.4618 & 0.3591 & -0.5707 & 0. \\ 0. & 0. & 0. & 0. \\ 0. & 0. & 0. & 1.000 \\ -0.5741 & -0.3831E-01 & 0.3030E-02 & -0.8611 \\ 0. & 0. & 0. & 0.3593 \\ 0.4853 & -0.1491E-01 & -0.1055 & 0.3299 \\ 0.1503 & 0.5032E-01 & 0. & 0. \\ 0. & 1.000 & 0. & 0. \\ 0. & 0. & 0. & 0. \end{bmatrix} \quad (59)$$

The size of the null space and the row dimension of the  $\Omega$  matrix is dependent upon the number of control inputs. The computed feedback matrix  $K$  of Equation (50) for the original system was

$$K = \begin{bmatrix} 0.4714 & -0.7043 & -0.5807 & 0.3532 \\ -0.3755 & -0.3578 & 0.4705 & -0.1745 \\ 0.1000 & -0.1523 & 0.2659E-01 & 0.7001 \\ 0.3585 & 0.1414 & -1.237 & -3.476 \\ -0.1627 & 15.98 & -6.894 & -42.42 \\ -0.1064 & 2.852 & 4.820 & 12.54 \\ -0.1556E-01 & -0.2957E-01 & -0.9141 & -0.8416 \\ 0.5861 & 0.9542E-01 & 0.1055 & 0.5018 \\ 0.3425 & -0.7142E-01 & 0.2144 & 0.1805 \\ 1.329 & 0.2368 & -1.252 & -1.095 \\ -1.199 & 0.7815 & -0.9945E-01 & -2.519 \\ -8.155 & -1.241 & 4.150 & 5.967 \end{bmatrix} \quad (60)$$

with an average gain of 2.97. The resulting closed-loop sampled-data plant matrix is

$$\begin{aligned}
 [F+GK] = & \begin{bmatrix} 0.2000E-02 & -0.1705E-12 & 0.2842E-13 & 0.4547E-12 \\ -0.9337E-02 & 0.5041 & 0.1754 & -0.2796E-01 \\ 0.1018E-02 & 0.9657E-01 & -0.2298 & -0.8865 \\ -0.1351E-02 & -0.6097E-01 & 0.2059 & 0.7611 \\ 0.6413E-03 & 0.1243E-01 & 0.1492E-01 & 0.3888E-01 \\ 0.3197E-13 & 0.1776E-13 & 0.7105E-13 & 0.3553E-12 \\ 0.2198E-02 & -0.3059E-01 & -0.6962E-01 & -0.1904 \\ 0.5137E-03 & -0.9197E-02 & -0.1965E-01 & -0.5355E-01 \end{bmatrix} \\
 & \begin{bmatrix} 0.2842E-13 & -0.1065E-13 & -0.2842E-13 & -0.9948E-13 \\ -0.1743E-01 & -0.2436E-02 & 0.2227E-01 & 0.9482E-02 \\ -0.4761E-01 & 0.1046E-01 & 0.1352E-02 & -0.3685E-01 \\ -0.1562E-01 & 0.2336E-02 & 0.1241E-02 & -0.8076E-02 \\ 0.7357 & -0.2537E-01 & -0.1566 & 0.1536 \\ -0.1990E-12 & 0.9500 & 0.1279E-12 & 0.1181E-12 \\ 0.6788 & 0.8965E-01 & -0.2919 & -0.4526 \\ 0.2030 & 0.2595E-01 & 0.1769 & 0.8668 \end{bmatrix} \quad (61)
 \end{aligned}$$

The closed-loop plant matrix has the specified eigenvalue spectrum of Equation (58).

A continuous-time simulation of the closed-loop system is carried out using the regulator control law designed and the following initial conditions,  $[\theta(o) = 0.1$  and  $\phi(o) = 0.2]$ ;

$$x(o)^T = [0 \ 0 \ 0 \ .1 \ 0 \ 0 \ 0 \ .2] \quad (62)$$

The responses of the aircraft to the initial condition of Equation (62) after the failure of the right aileron for the original system are shown in Figure 12. In general, the aircraft responses to the

multivariable control law are stable, settling time is faster, and oscillations of the short period, dutch roll, and the spiral divergence modes were removed from the respective outputs.

The eigenvalue spectrum of this regulator design spans the Z-plane from 0.001 to 0.99. Even though the fast eigenvalues responses have settled, the slower eigenvalues responses still drive the system with small piecewise-constant control input changes between the sampling period. The magnitude of the control inputs did not overdrive the system after the initial sampling period. Thus, a relatively smooth transition between the sampling periods from the initial conditions to the settling time of about 4 sec for the pitch angle Figure 12a and the pitch rate Figure 12b. The fast settling time of the roll angle in Figure 12c indicates that the initial control inputs for some of the control surfaces were large. Consequently,  $\phi$  was forced to approximately zero in less than half a sampling period. The left aileron and spoilers did exceed their physical limits. Also, the spoilers had a negative and positive deflection; this is impossible since the spoilers only have a negative deflection (CCW) on the A-7D. The simulation routine in CESA is for a linear system and control surface limitations are not recognized. The roll rate response of Figure 12d is well within the maximum roll rate of 200 deg/sec (Ref 1). A small initial sideslip angle (0.0017 rad), Figure 12e, and yaw rate (-0.012 rad), Figure 12f, does exist, but is negligible.

The block diagram for the internally balanced state-variable feedback controller is shown in Figure 11. The transformed state

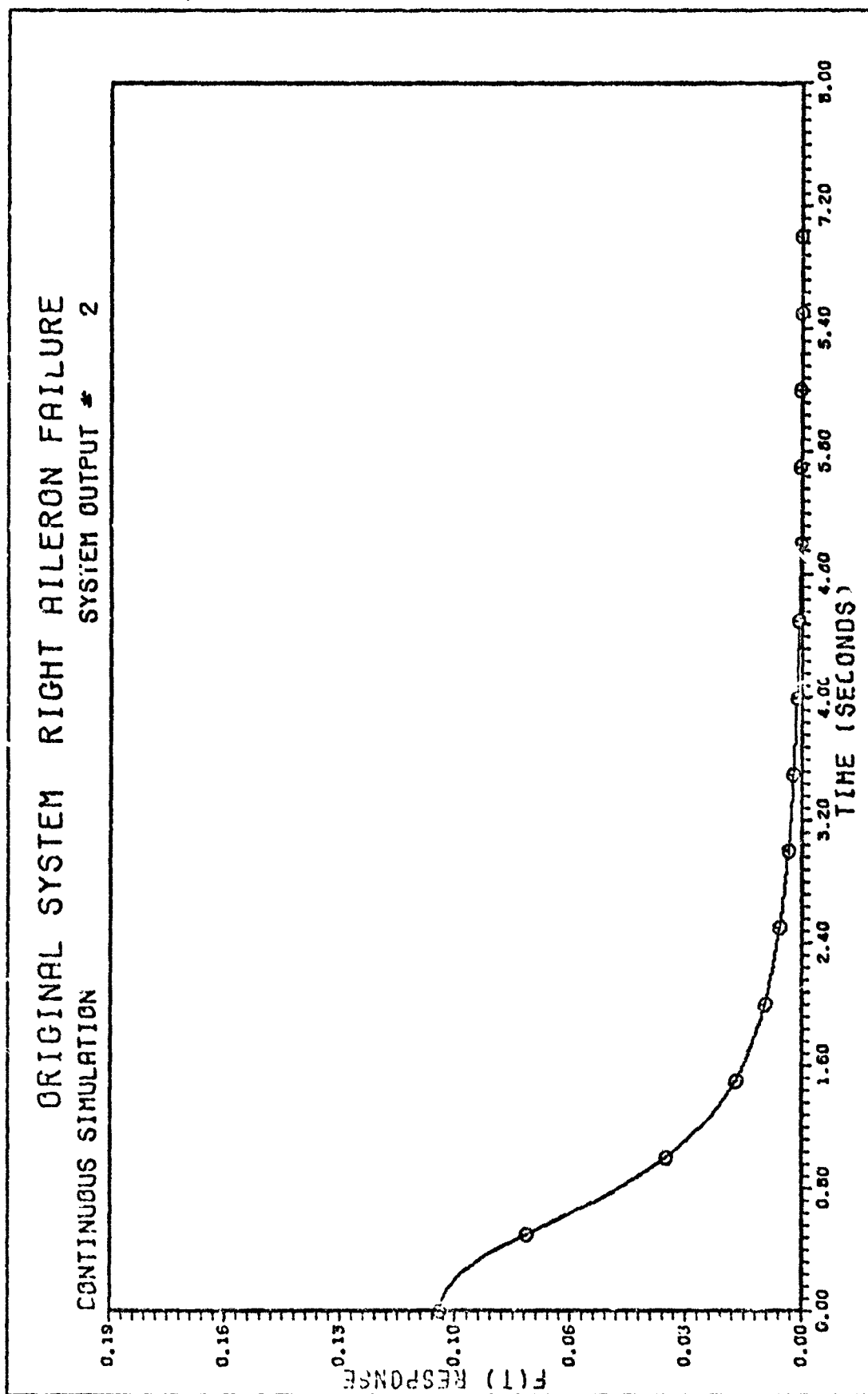


Figure 12a. Pitch Angle, Initial Condition 0.1 Rad vs. t

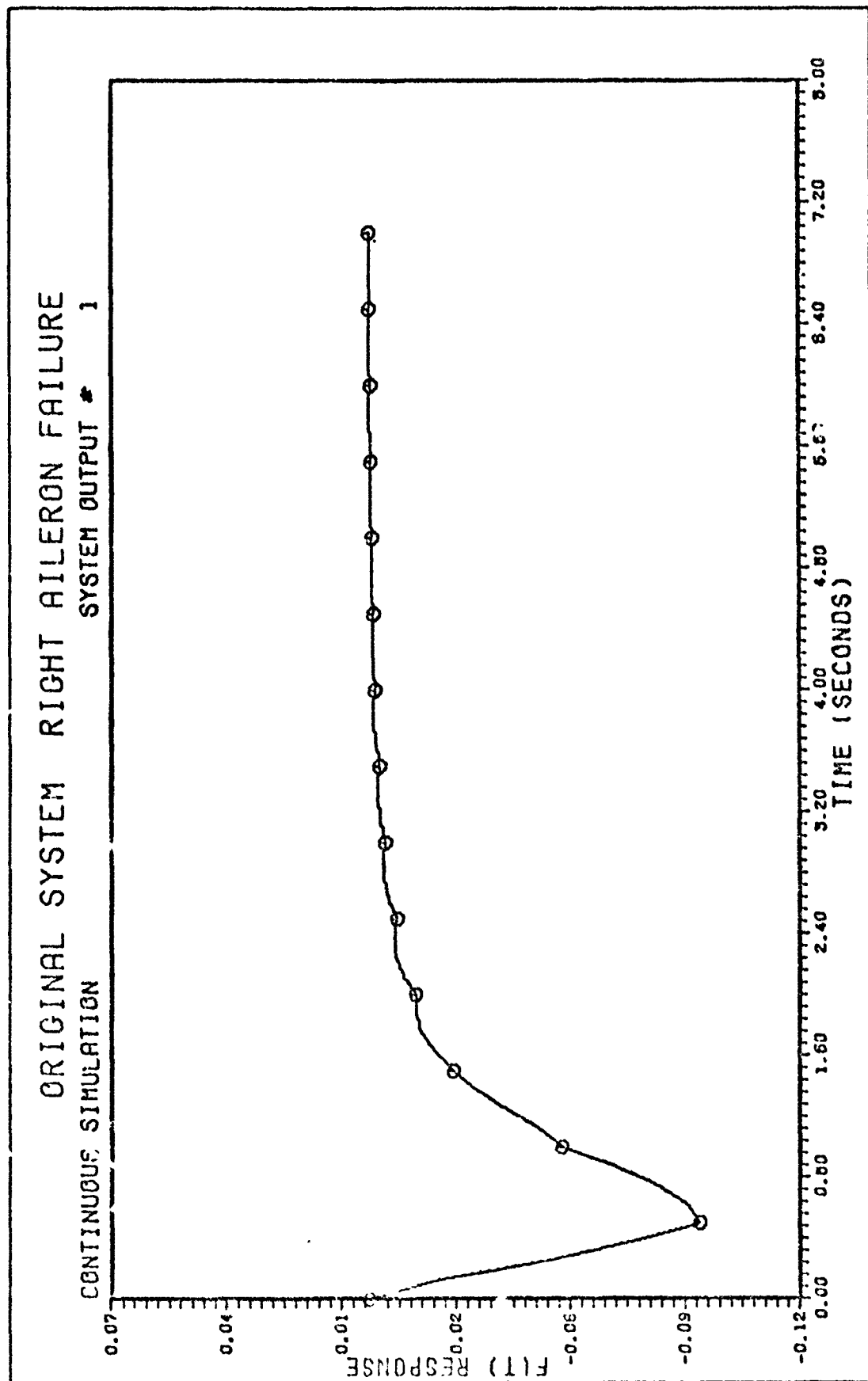


Figure 12b. Pitch Rate vs. t

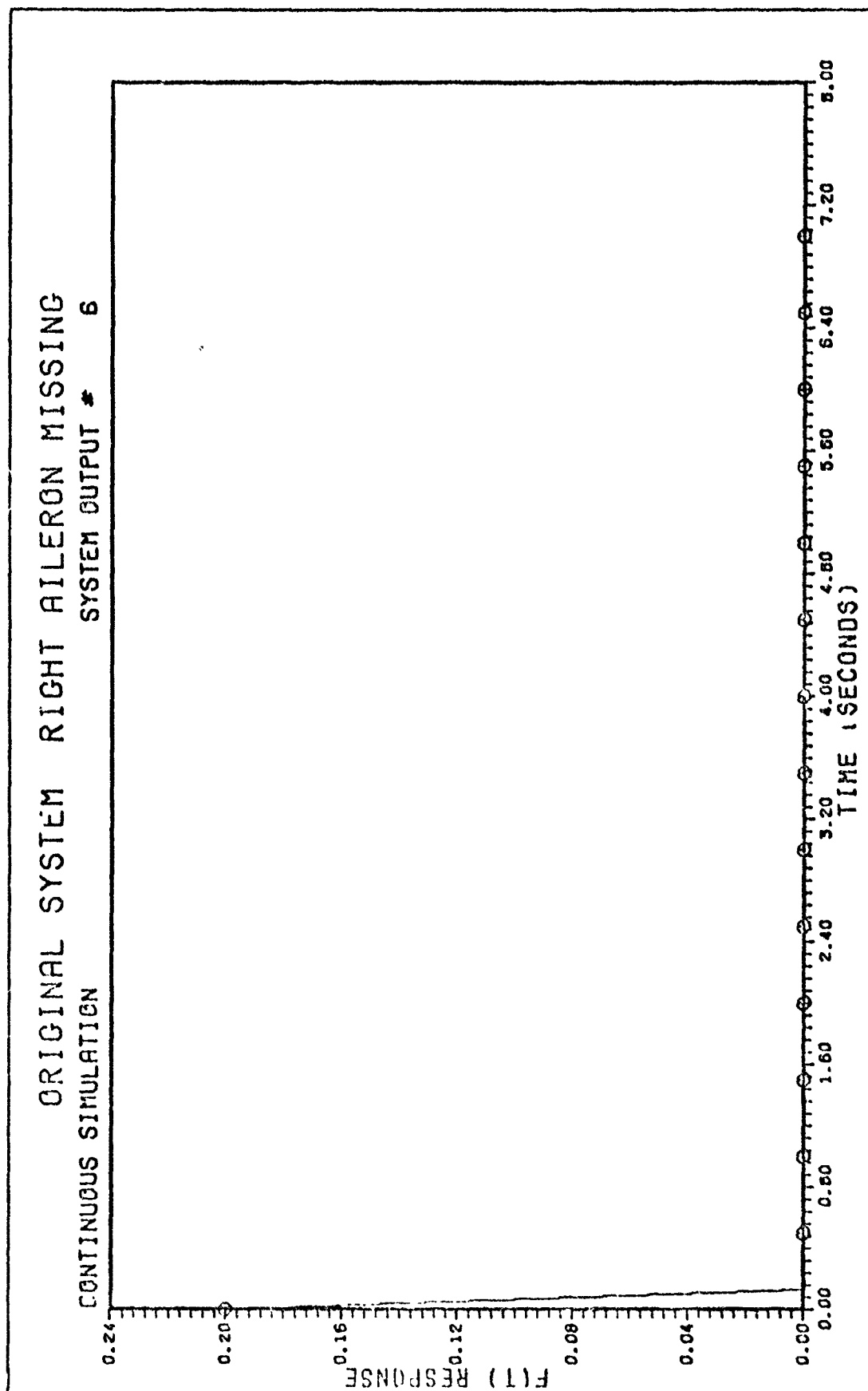


Figure 12c. Roll Angle, Initial Conditions .2 Rad vs. t

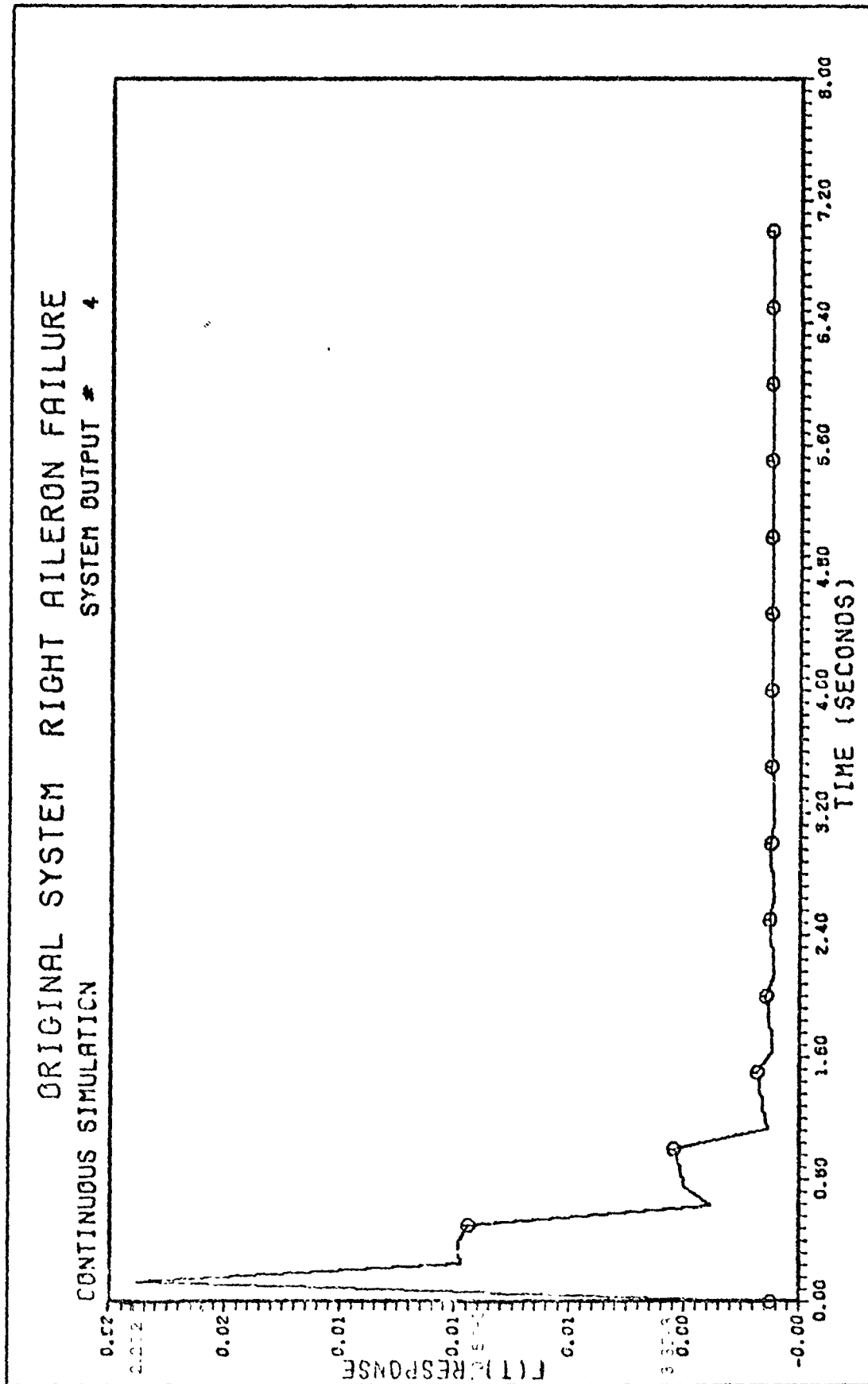


Figure 12d. Roll Rate Angle vs. t

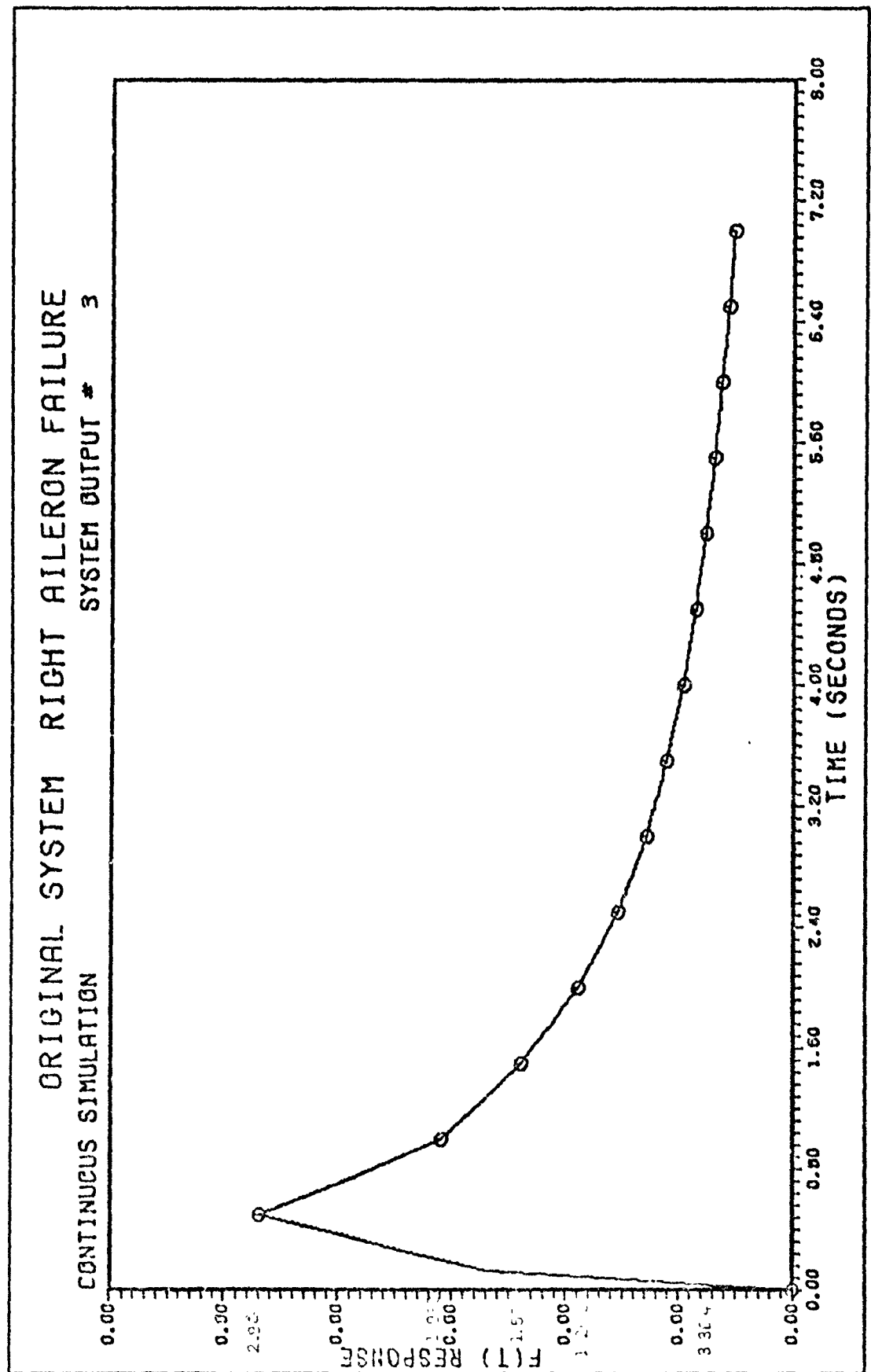


Figure 12e. Sideslip Angle vs. t

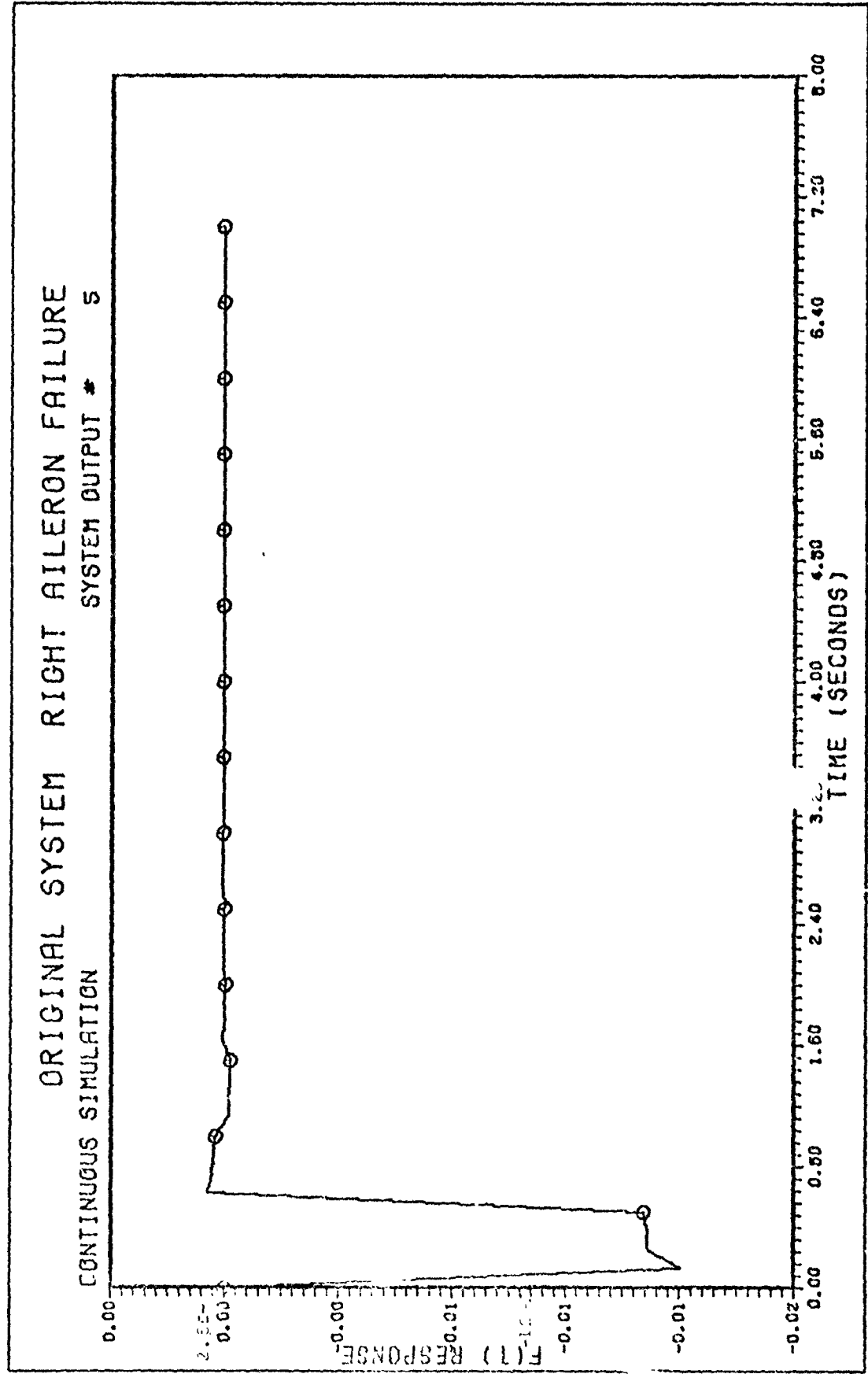


Figure 12f. Yaw Rate vs. t

equation for the balanced system is, as follows:

$$\dot{x}'(t) = (T^{-1}AT)x'(t) + (T^{-1}B)u(t) \quad (63)$$

$$y(t) = CT \ x'(t) \quad (64)$$

and the control law in the discrete-time domain is

$$u(kt) = K'x'(kt) \quad (65)$$

The actual magnitude of the control input is required in order to determine if the designed control law exceeds the physical limits of the actuators. Therefore, since  $x'(kt) = T^{-1} x(kt)$ ,

$$u(kt) = K'T^{-1} x(kt) = Kx(kt) \quad (66)$$

Also, the initial condition inputs for the balanced system must be transformed into the new coordinate system by

$$x'(0) = T^{-1}x(0) \quad (67)$$

Proceeding with the regulator design for the internally balanced system using Equation (A-25 through A-27), the closed-loop eigenvalue spectrum is

$$\sigma(F + G_0 K) = \{0.005, 0.007, 0.009, 0.01, 0.03, 0.05, 0.07, 0.09\} \quad (68)$$

Assigning the eigenvector for each  $\lambda_i$  of Equation (59), the matrix  $X'$  of eigenvectors is

$$X' = \begin{bmatrix} 0.2264E-01 & -0.7282E-01 & -0.3186E-02 & 0.3118 \\ -0.2095E-02 & -0.1041 & -0.9799E-02 & 0.1621 \\ -0.1516 & -0.1033E-01 & -0.3112E-02 & -0.1016E-01 \\ 0.2754 & 0.1845E-01 & 0.1480E-01 & 0.2166E-01 \\ 0. & 1.000 & 0. & 0. \\ 0.7869 & 0.9943E-02 & -0.3865E-01 & 0.1089 \\ 1.000 & 0. & 0. & 0. \\ 0. & 0. & 0. & 1.000 \end{bmatrix}$$

$$\begin{bmatrix} -0.1738E-03 & 0.3050 & 0.3684E-03 & -0.2891E-02 \\ -0.9793E-03 & 0.1577 & 0.9896E-03 & -0.1042E-01 \\ -0.2651E-03 & -0.1012E-01 & 0.9387E-03 & -0.4218E-02 \\ -0.5001E-03 & 0.2096E-01 & -0.3472E-02 & 0.1800E-01 \\ 0. & 0. & 0. & 0. \\ 0.1549E-02 & 0.1077 & 0.7428E-02 & -0.3664E-01 \\ 0. & 0. & 0. & 0. \\ 0. & 1.000 & 0. & 0. \end{bmatrix}$$

(69)

and the associated  $\Omega$  matrix is

$$\Omega' = \begin{bmatrix} 0.8855 & 0.3501E-01 & -1.241 & -0.2361E-01 \\ 0. & 0. & 1.000 & 0. \\ 0.1126 & 0.4050 & -0.2651 & 0.9257E-01 \\ 0.3665 & 0.1383 & -0.9529 & -0.2482 \\ 0. & 0. & 0. & 0. \\ 0. & 0. & 0. & 0. \end{bmatrix}$$

$$\begin{bmatrix} -0.4475E-01 & -0.1168E-01 & -0.7149E-02 & -1.238 \\ 0. & 0. & 0. & 1.000 \\ 0.4621E-02 & 0.9389E-01 & -0.1168E-01 & -0.2644 \\ -0.8522E-01 & -0.1959 & 0.6394E-01 & -0.9519 \\ 0. & 0. & 1.00 & 0. \\ 1.000 & 0. & 0. & 0. \end{bmatrix}$$

(70)

The feedback matrix of Equation (65)

$$K = \begin{bmatrix} -131.8 & 213.0 & -403.8 & -79.73 \\ 93.20 & -157.2 & 376.8 & 85.95 \\ -28.07 & 48.09 & -131.6 & -30.82 \\ -93.77 & 129.5 & -64.27 & 7.069 \\ 402.0 & -725.2 & 2233. & 495.0 \\ 249.8 & -281.3 & -1757. & -650.0 \\ \\ 7.978 & -9.034 & -27.82 & 5.146 \\ -5.473 & 8.870 & 24.02 & -2.573 \\ 1.960 & -4.226 & -7.283 & .8373 \\ 5.601 & 7.432 & -14.77 & 6.376 \\ -22.72 & 160.5 & 65.12 & -13.27 \\ -25.46 & -56.75 & -48.79 & -29.86 \end{bmatrix} \quad (71)$$

The average gain for Equation (71) is 199. Using the inverse of the transformation matrix  $T$ , the matrix  $K$  given in Equation (66) is obtained where  $T^{-1}$  is

$$T^{-1} = \begin{bmatrix} 3.1310E-5 & -1.8741E-2 & 3.1528E-3 & 2.2038E-2 \\ -1.5149E-5 & 1.6794E-2 & -1.9646E-3 & -1.8162E-2 \\ -2.5606E-3 & 4.3495E-1 & -4.6060E-3 & -4.5933E-1 \\ 5.6238E-4 & -7.7507E-1 & 1.1906E-1 & 9.1296E-1 \\ -3.4657E-5 & 1.8281E-2 & -2.9889E-3 & -2.0732E-2 \\ -1.6022E-4 & -5.1974E-4 & 2.9203E-1 & -7.4909E-2 \\ 2.8776E-4 & -1.0776 & 9.3580E-2 & 1.8823E-1 \\ -1.4248E-5 & -4.0350E-2 & -3.6914E-2 & -1.4945E-2 \\ \\ -7.8563E-2 & 6.2237E-2 & 4.6185E-1 & 1.0295 \\ -2.4268E & 3.4092E-2 & 1.8894E-1 & -1.8377 \\ -7.9595E-3 & 4.1505E-4 & -3.6800E-3 & 1.7059E-2 \\ -3.8466E-2 & -9.9916E-5 & 7.4374E-3 & -8.2169E-2 \\ 6.4536E-1 & -3.4859E-2 & 6.8651E-1 & 9.1750E-2 \\ 1.2719E-1 & 1.4930E-2 & 2.9657E-2 & 3.3226E-3 \\ -8.3743E-2 & -9.2893E-3 & -1.6389E-2 & -8.4078E-3 \\ 1.3260 & 1.8622E-1 & 3.6654E-1 & -2.2451E-2 \end{bmatrix} \quad (72)$$

This results in the actual feedback matrix K as illustrated in Equation (66). Then the actual controls can be analyzed to ensure that they do not exceed the physical limits of the actuators.

$$K = \begin{bmatrix} 0.9734 & -77.87 & 2.817 & 101.1 \\ -0.9011 & 67.00 & -1.570 & -85.69 \\ 0.3159 & -24.20 & 0.2630 & 29.75 \\ 0.1591 & -13.74 & 3.788 & 28.01 \\ -5.396 & 497.7 & 12.30 & -550.8 \\ 4.133 & -216.5 & -15.08 & 220.3 \\ \\ -487.1 & -0.2977 & -12.18 & -520.4 \\ 360.0 & 0.2104 & 7.765 & 377.8 \\ -110.0 & 0.5744E-01 & -1.053 & -112.7 \\ -292.4 & -0.2085 & -11.91 & -334.7 \\ 1674. & 1.287 & 27.34 & 1708. \\ 642.8 & 0.2244 & 34.55 & 823.1 \end{bmatrix} \quad (73)$$

Using the  $K'$  feedback matrix, the closed-loop plant matrix has the specified eigenvalues of Equation (68):

$$[F' + G'_0 K'] = \begin{bmatrix} -2.118 & 0.4608 & 0.2956E-01 & 0.1507 \\ -1.094 & 0.2927 & -0.9719E-01 & -0.1276 \\ 0.8791E-01 & -0.1925E-01 & 0.2463E-01 & -0.8952E-01 \\ -0.2155 & 0.3584E-01 & 0.6555E-01 & 0.4149 \\ -0.5578E-12 & 0.4317E-12 & -0.1007E-11 & 0.1473E-11 \\ -0.6021 & 0.1319 & -0.6959E-01 & -0.7137 \\ 0.9511E-12 & -0.1619E-11 & 0.3949E-11 & 0.7017E-13 \\ -6.994 & 1.482 & 0.1815 & 0.7074 \\ \\ -0.1102 & 0.1138 & -0.7759E-01 & 0.5732 \\ -0.4885E-01 & -0.2275E-01 & 0.6369E-01 & 0.2996 \\ 0.6697E-02 & -0.3791E-01 & 0.5543E-01 & -0.1807E-01 \\ -0.2005E-01 & 0.1588 & -0.2230 & 0.3598E-01 \\ 0.7000E-02 & 0.3382E-12 & -0.9993E-12 & 0.1066E-13 \\ -0.1553E-01 & -0.2425 & 0.3947 & 0.2086 \\ -0.7200E-13 & -0.2984E-12 & 0.5100E-02 & -0.2665E-14 \\ -0.3699 & 0.4572 & -0.3656 & 1.887 \end{bmatrix} \quad (74)$$

Before the continuous-time simulation is carried out, the initial conditions of Equation (62) are transformed by Equation (67) to

$$x'(0) = \begin{bmatrix} 0.20810 \\ -0.36936 \\ -0.04218 \\ 0.07486 \\ 0.01628 \\ -6.826E-3 \\ 0.817141 \\ -5.9848E-3 \end{bmatrix} \quad (75)$$

The continuous time plots of the balanced system are shown in Figure 13. The eigenvalue spectrum, Equation (68), for this regulator

design was located close to the origin in the Z-plane. These eigenvalues have a faster transient time than the previous design. Thus, the control law realized drives the response of the system harder between the sampling periods to a settling time of about 4 sec causing what appears to be the short period or dutch roll oscillation. However, that is not the case. The increased magnitude of the piecewise-constant control inputs are overdriving the system, producing the oscillations and not the aircraft modes. An important result in all the balanced responses is that the initial conditions are approximately the same as for the original system. Thus, the transformation of Equation (67) on the initial conditions and the internally balanced matrices do represent the original system. The responses differ from the original system because of a different eigenvalue spectrum and eigenvectors. In general, disregarding the overshoots produced by the increased constant piecewise-constant inputs, the responses, Figure 13, do show an improvement in the settling time of the system.

The internally balanced matrices of Equation (A-25 through 27) were reduced to seven states as illustrated in Equation (43). Using the following closed-loop eigenvalue spectrum:

$$\sigma(F_R^* + G_R^* K_R^*) = \{0.005, 0.007, 0.009, 0.01, 0.03, 0.05, 0.07\} \quad (76)$$

The eigenvectors of Equation (57) were assigned for each  $\lambda_i$  of Equation (76) and resulted in the following eigenvector matrix  $X^*$

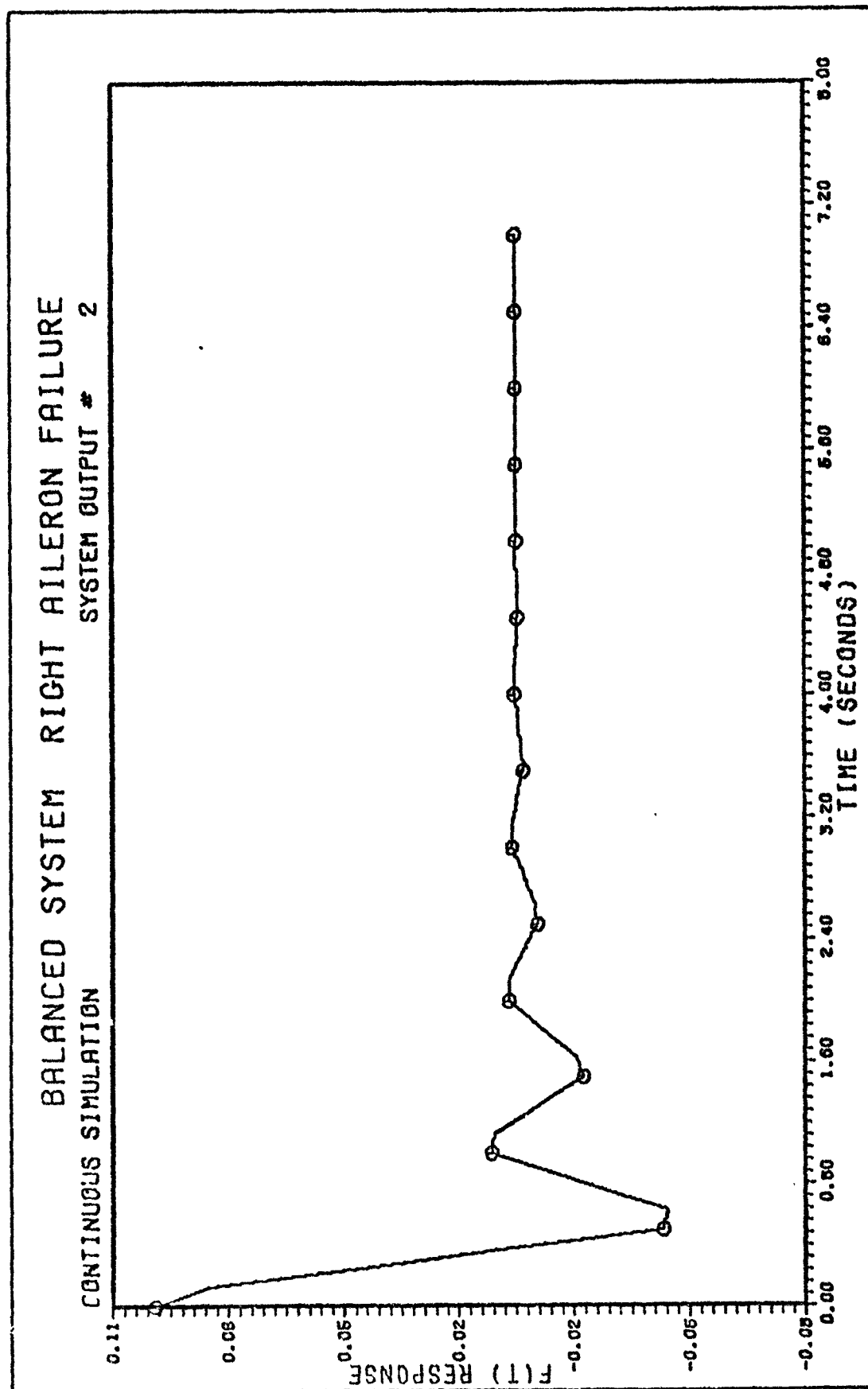


Figure 13a. Pitch Angle vs. t

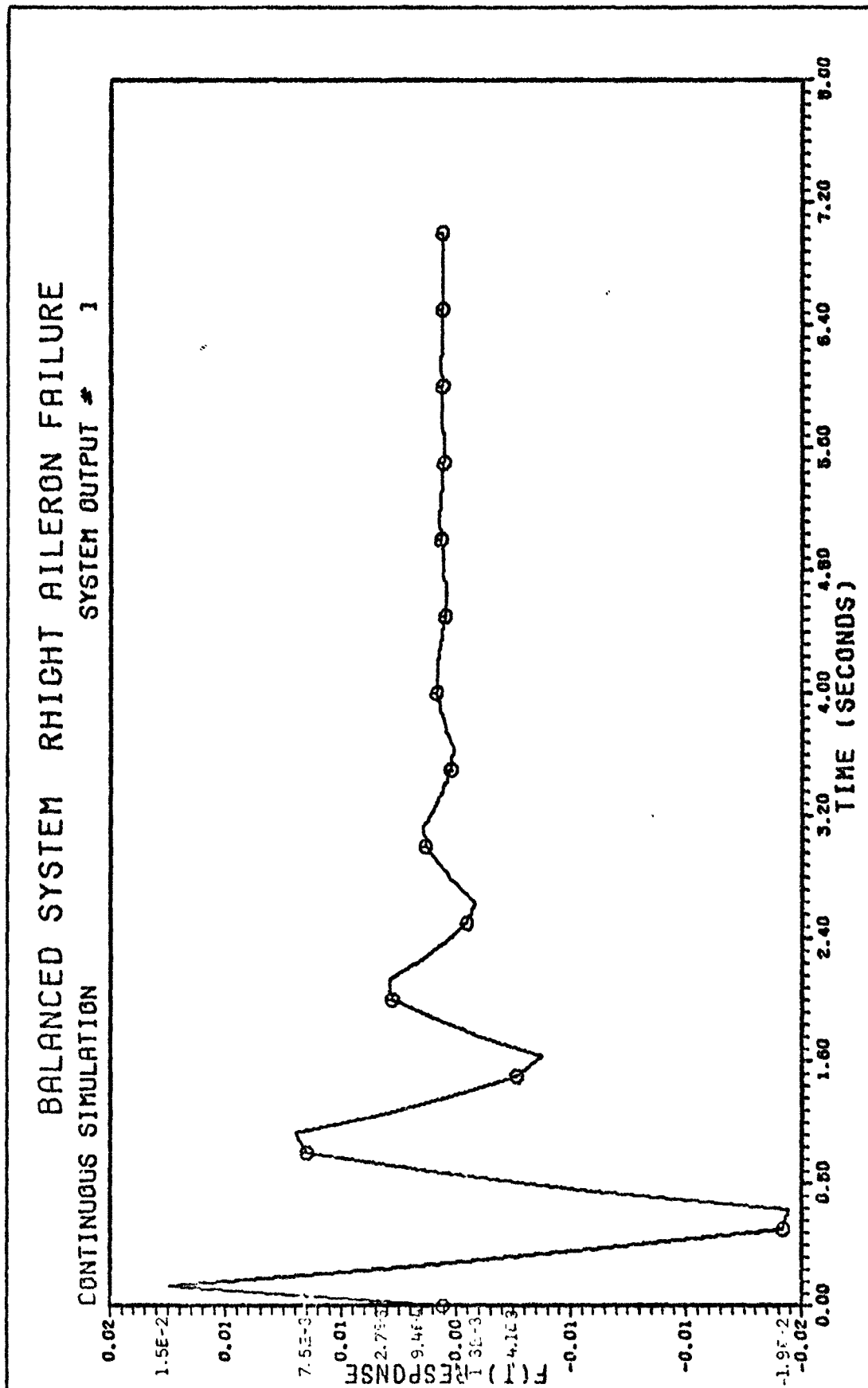


Figure 13b. Pitch Rate vs. t

# BALANCED SYSTEM RIGHT AILERON FAILURE CONTINUOUS SIMULATION SYSTEM OUTPUT # 5

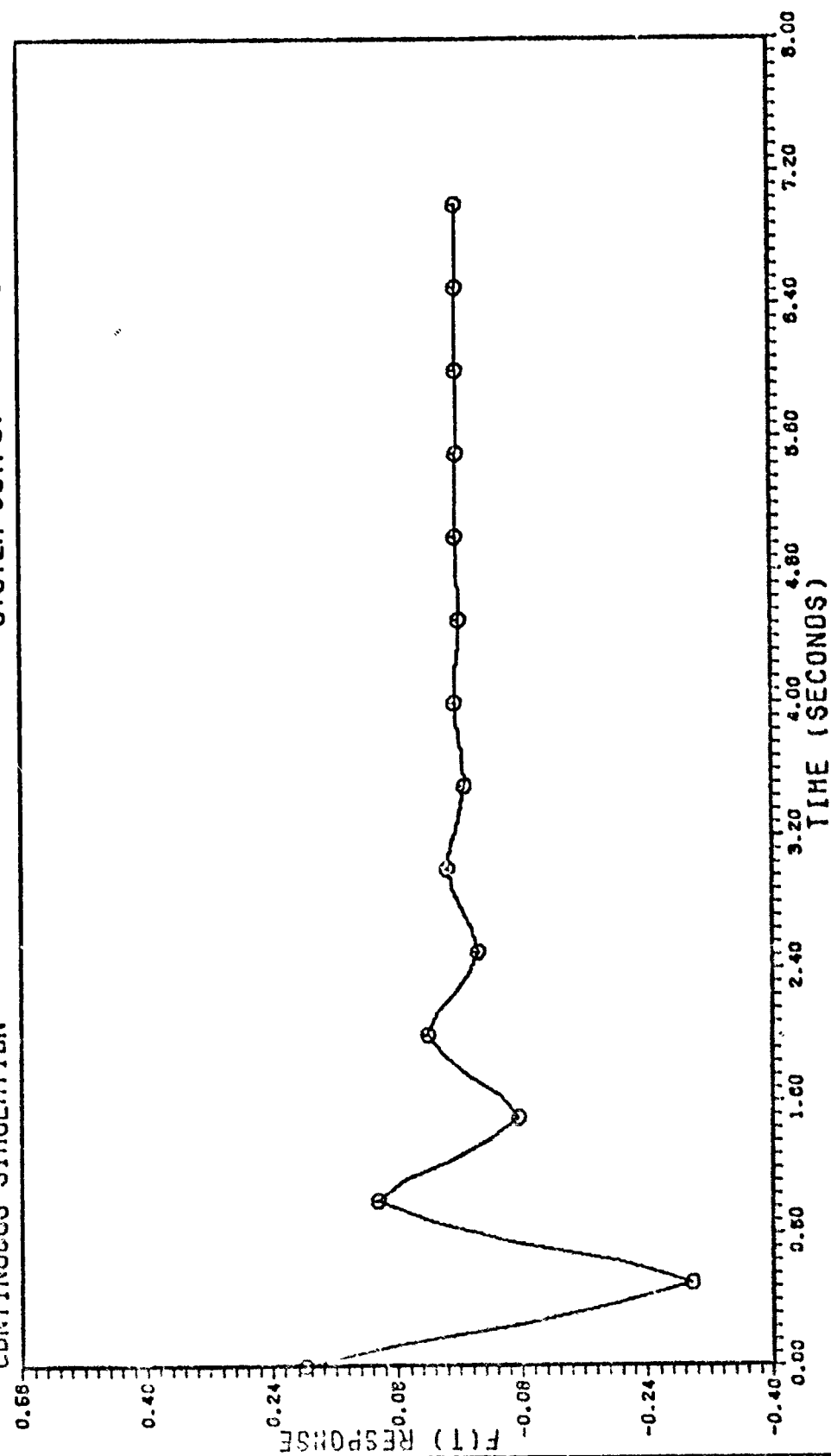


Figure 13c. Roll Angle vs. t

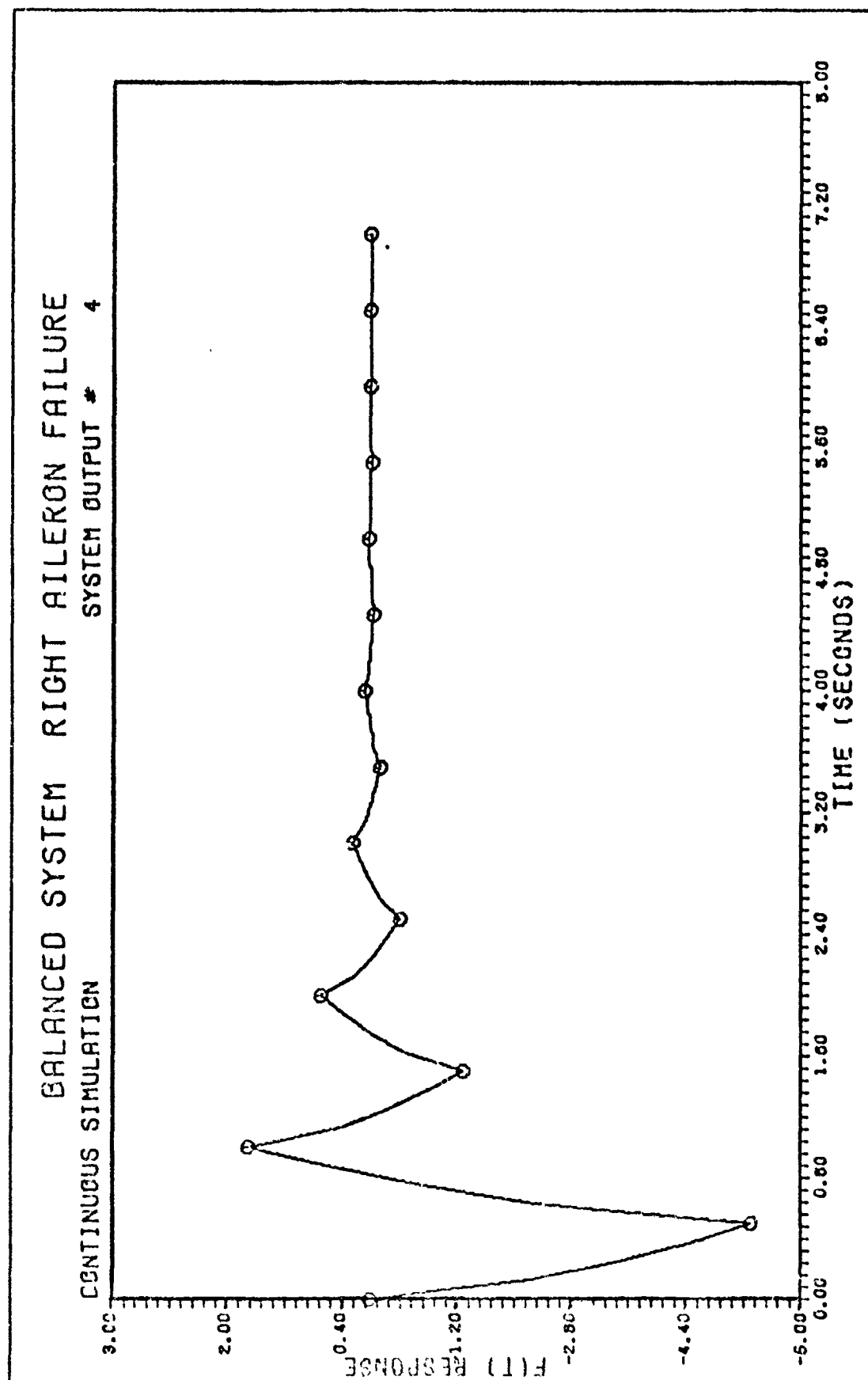


Figure 13d. Roll Rate vs. t

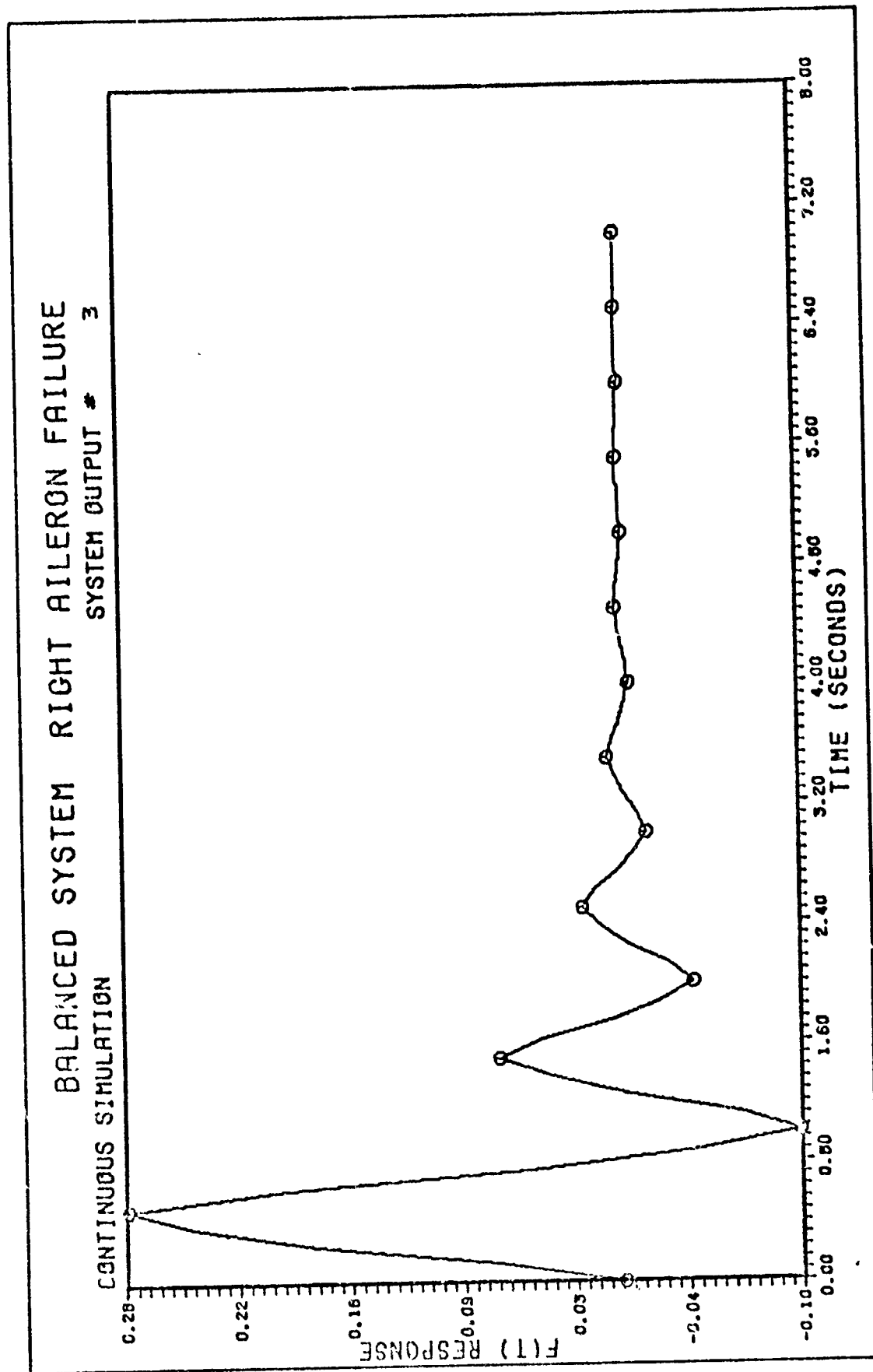


Figure 13e. Sideslip vs. t

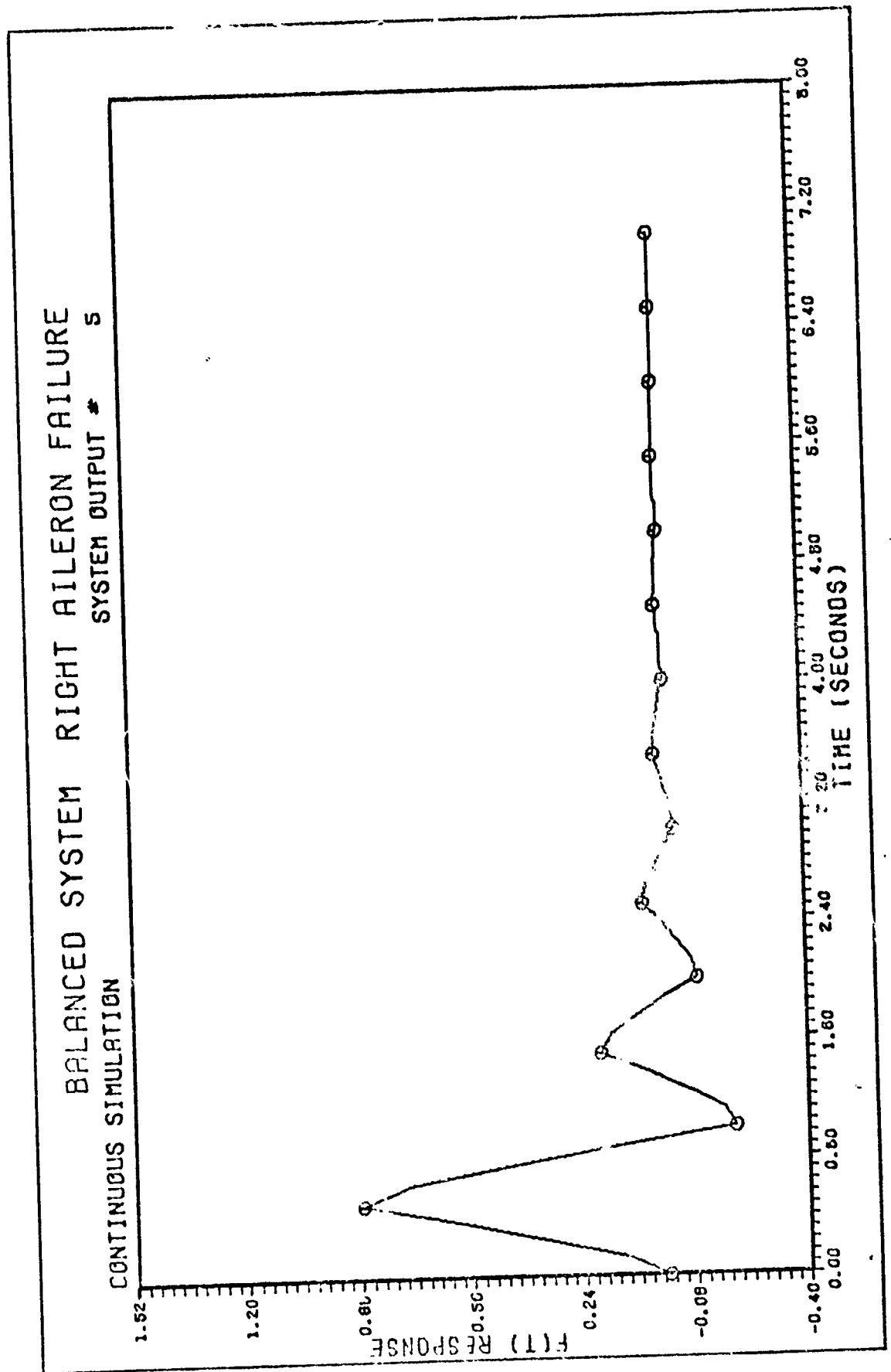


Figure 13f. Yaw Rate vs. t

$$X_R' = \begin{bmatrix} 0.2293 & 0.5702E-02 & -0.5106 & -0.5323 \\ 0.1166 & -0.5313E-01 & -0.3096 & -0.3148 \\ -0.1502 & -0.1484E-01 & -0.7938E-02 & -0.5111E-02 \\ 0.2752 & 0.1838E-01 & 0.1839E-01 & 0.3865E-02 \\ 0. & 1.000 & 0. & 0. \\ 0.8248 & 0.2442E-01 & -0.1227 & -0.8793E-01 \\ 1.000 & 0. & 0. & 0. \\ & -0.4551E-01 & -0.5428 & 0.3549E-01 \\ & -0.2850E-01 & -0.3238 & 0.2201E-01 \\ & -0.7559E-03 & -0.6274E-02 & 0.1376E-02 \\ & -0.1669E-03 & 0.6174E-02 & -0.3136E-02 \\ & 0. & 0. & 0. \\ & -0.5911E-02 & -0.8523E-01 & 0.1282E-01 \\ & 0. & 0. & 0. \end{bmatrix} \quad (77)$$

and the associated matrix  $\Omega$  of the Equation (59) is

$$\Omega_R = \begin{bmatrix} 0.7783 & -0.3428E-02 & -0.9561 & 0.2996 \\ 0. & 0. & 1.000 & 0. \\ 0.1013 & 0.4008 & -0.2206 & 0.4709E-01 \\ 0. & 0. & 0. & 1.000 \\ 0. & 0. & 0. & 0. \\ 0. & 0. & 0. & 0. \\ & -0.1872E-01 & 0.3042 & -0.2672E-01 \\ & 0. & 0. & 0. \\ & 0.9154E-02 & 0.5832E-01 & -0.1475E-01 \\ & 0. & 1.000 & 0. \\ & 0. & 0. & 1.000 \\ & 1.000 & 0. & 0. \end{bmatrix} \quad (78)$$

The  $K_R'$  matrix of Equation (65) is

$$K_R' = \begin{bmatrix} -106.5 & 176.1 & -294.3 & 23.13 \\ 78.12 & -131.7 & 299.4 & 12.99 \\ -23.28 & 39.44 & -105.1 & -5.832 \\ -68.78 & 105.8 & -0.4973 & 66.33 \\ 329.0 & -588.0 & 1810. & 97.25 \\ 144.7 & -181.6 & -2025. & -899.4 \end{bmatrix}$$

$$\begin{bmatrix} 5.335 & 29.11 & -69.93 \\ -3.452 & -18.26 & 53.91 \\ 1.250 & 5.071 & -17.52 \\ 4.506 & 29.13 & -38.92 \\ -11.28 & 12.40 & 221.1 \\ -21.29 & -147.6 & 53.05 \end{bmatrix} \quad (79)$$

The closed-loop discrete plant matrix of the reduced balanced system for the assigned eigenvalues is

$$[F_R' + G_R' K_R'] = \begin{bmatrix} -0.7759 & 1.965 & -6.184 & -5.884 \\ -0.4539 & 1.054 & -3.565 & -3.491 \\ 0.9498E-02 & -0.1083E-01 & 0.5284E-01 & -0.5843E-01 \\ -0.6378E-01 & 0.1065 & -0.2890 & 0.6867E-01 \\ 0.5862E-12 & -0.9184E-12 & 0.4164E-11 & 0.1756E-11 \\ 0.2704E-01 & 0.4203E-01 & -0.2270 & -0.9062 \\ 0.9532E-12 & -0.1353E-11 & 0.3867E-11 & 0.5089E-12 \end{bmatrix}$$

$$\begin{bmatrix} 0.1881 & -2.174 & 2.433 \\ 0.1121 & -1.294 & 1.462 \\ 0.1652E-02 & -0.2330E-01 & 0.4193E-01 \\ 0.5358E-03 & 0.2438E-01 & -0.7374E-01 \\ 0.7000E-02 & 0.3064E-13 & -0.7352E-12 \\ 0.2383E-01 & -0.3308 & 0.4811 \\ -0.5118E-13 & -0.3197E-12 & 0.5000E-02 \end{bmatrix} \quad (80)$$

The initial condition vector  $x'(0)$  of Equation (75) was reduced by removal of the last element for the continuous-time simulation. Figure 14 is the time response plot for the reduced balanced system and is compared to the previous cases for improved or deteriorated responses.

The regulator design for the reduced balanced system exhibits approximately the same initial conditions as the two previous designs. Due to the fast transient responses of the eigenvalue spectrum, the feedback matrix  $K'_R$  produces a control law that overdrives the system during the first two sampling periods only. The pitch angle, Figure 14a, differs from Figure 13b only little in the initial response and the settling time is decreased from 4.0 sec to 1.5 sec since the control input induced oscillation is not present. For the remainder of the outputs, the settling time decreased from 4.0 sec to 2.5 sec. By removing the roll subsidence state, which had a low degree of controllability, the aircraft model was not degraded. Thus, the magnitude of the control inputs was decreased sufficiently to remove the oscillation caused by the control inputs of the balanced system.

To transform the reduced balanced feedback matrix ( $K'_R$ ) in the new coordinate system back to the original coordinate system the following transformation is applied. First the reduced balanced state vector is obtained as follows,

$$x'_R(t) = \begin{bmatrix} I_{n-j, n-j} & 0_{n-j, j} \end{bmatrix} x'(t) \quad (81)$$

where  $j$  is the number of balanced states to be removed,  $n$  is the dimension of the original plant matrix,  $I$  is an identity matrix, and  $j$  is the number of zero (0) vectors. The state equations for the reduced

balanced system are,

$$\dot{x}_R'(t) = A_R' x_R'(t) + B_{O_R}' u(t) \quad (82)$$

where the matrices of Equation (82) are obtained as shown in Equation (43) and  $x_R' \in \mathbb{R}^7$ . The eigenvalues of the reduced model are shifted, hopefully only by a small amount and still retaining the characteristics of the model. The control law for the reduced system is

$$u(t) = K_R'(t) x_R'(t) \quad (83)$$

where  $K_R'$  is of dimension  $w \times (n-j)$ , and  $w$  is the column dimension of the control input matrix. The transformation of the control law to the balanced system, using Equation (81) is

$$u(t) = K_R' \begin{bmatrix} I_{n-j, n-j} & 0_{n-j, j} \end{bmatrix} x'(t) \quad (84)$$

To obtain the actual  $K$  matrix in the original state coordinate system,  $x' = T^{-1}x$  is substituted into Equation (84) to form

$$u(t) = \left( K_R' \begin{bmatrix} I_{n-j, n-j} & 0_{n-j, j} \end{bmatrix} T_{nxn}^{-1} \right) x(t) \quad (85)$$

Therefore,

$$u(t) = K_{wxn} x(t) \quad (86)$$

once the transformation of the reduced balanced system control law to the original system is completed. The time responses produced by the transformed control law can then be compared to the original time responses. This allows one to investigate the effects of using a reduced feedback matrix, transformed back into the original state

coordinate system in the control laws.

### Summary

By increasing the control input capabilities of the CESA arrays and determining the degree of controllability of the aircraft states, a multivariable control law was designed. The time response plots of the original, and internally balanced systems proved that the state coordinate system can be changed without modifying the system characteristics. The control laws designed for a sampled data regulator and tracker illustrate the capabilities of the entire eigenstructure assignment design method. The assignment of the eigenvalue spectrum and associated eigenvectors points out their effect on the closed-loop system as shown in the time response plots for the different regulator cases. Due to the large difference in the eigenvalue spectra used in the regulator designs, the system responses exhibit an acceptable settling time and a decrease in the overshoots. The desirable feedback matrix should have an average gain about 1.0, due to the eigenvectors selected, and would constitute an acceptable control law.

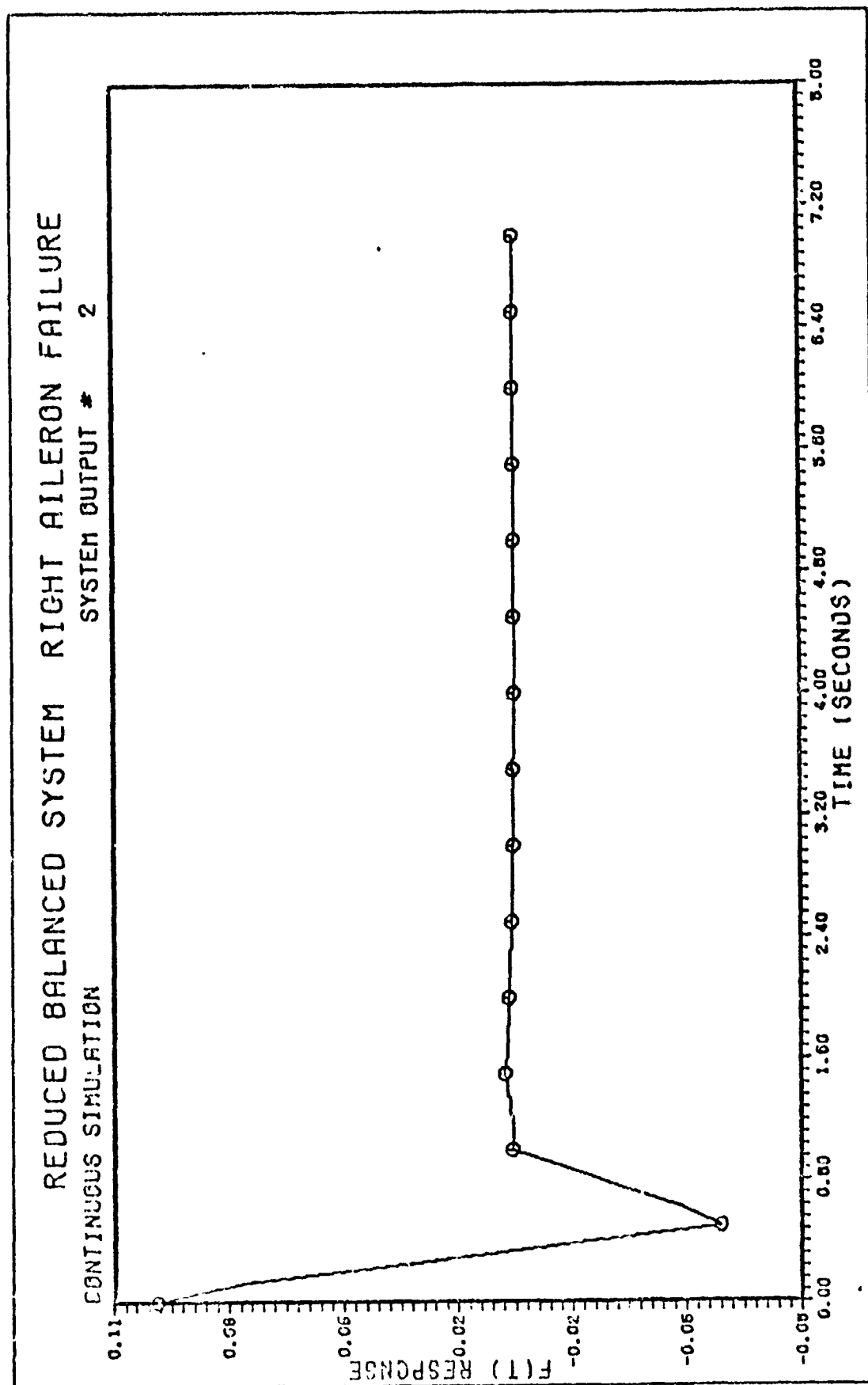


Figure 14a. Pitch Angle vs. t

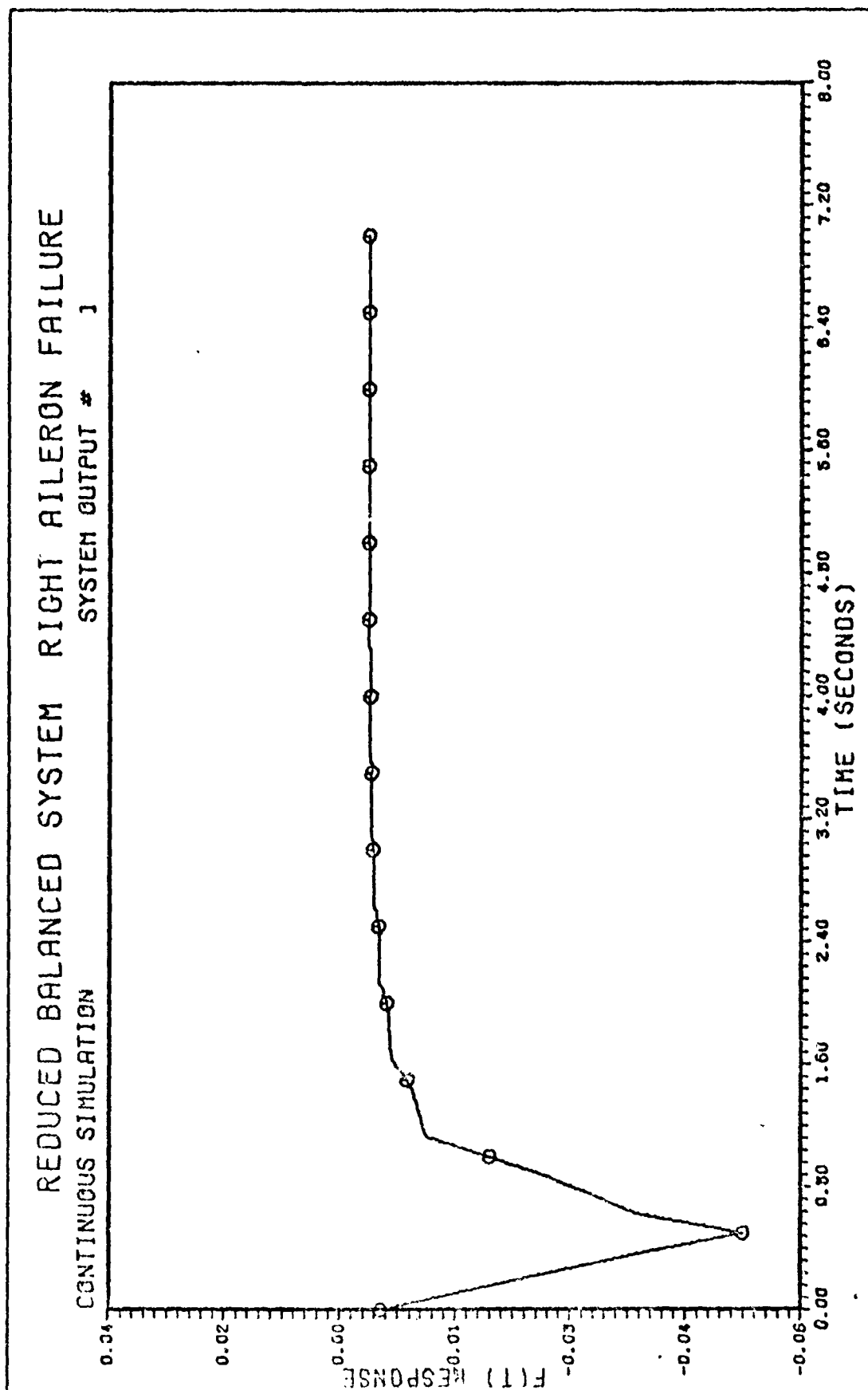


Figure 14b. Pitch Rate vs. t

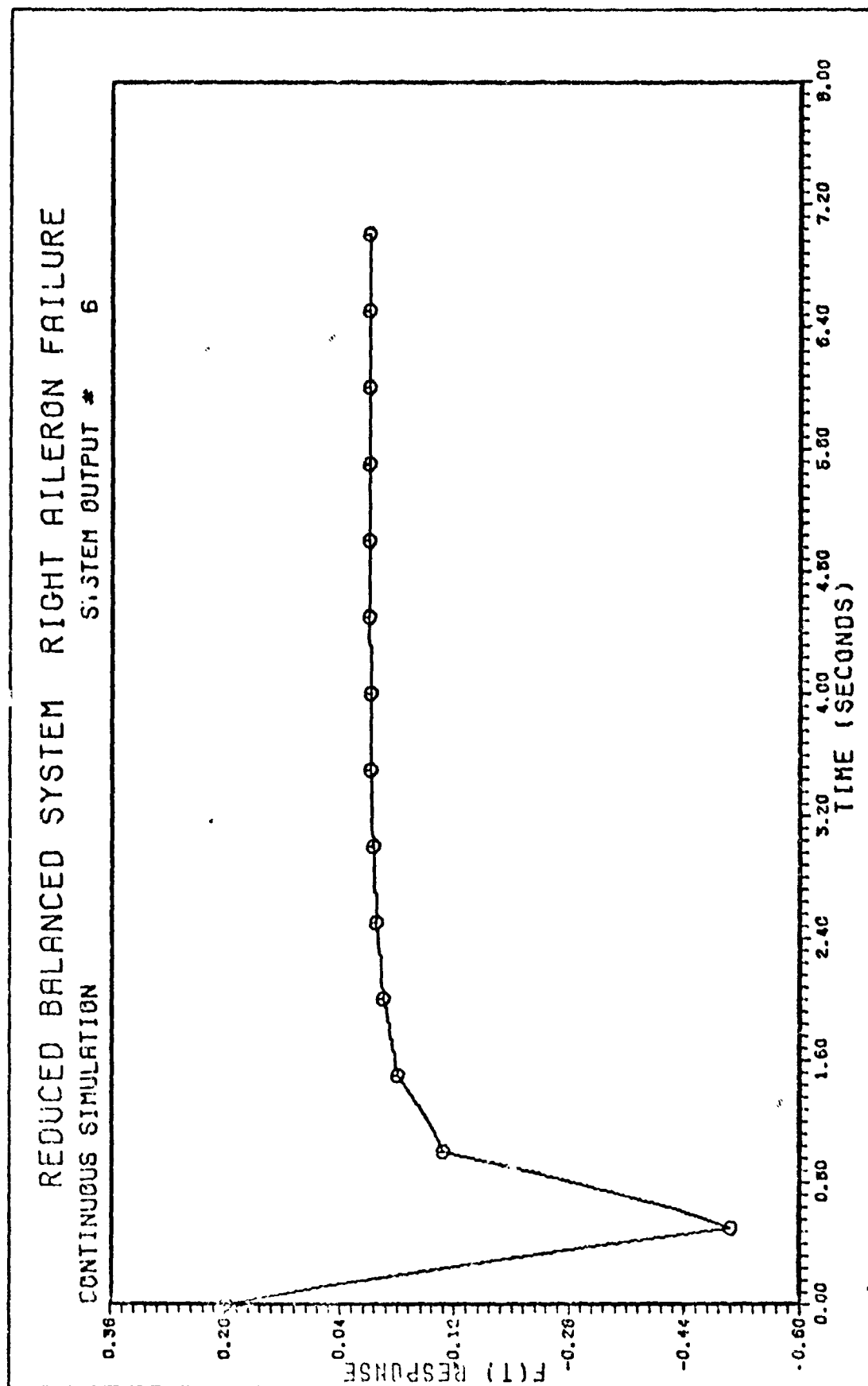


Figure 14c. Roll Angle vs. t

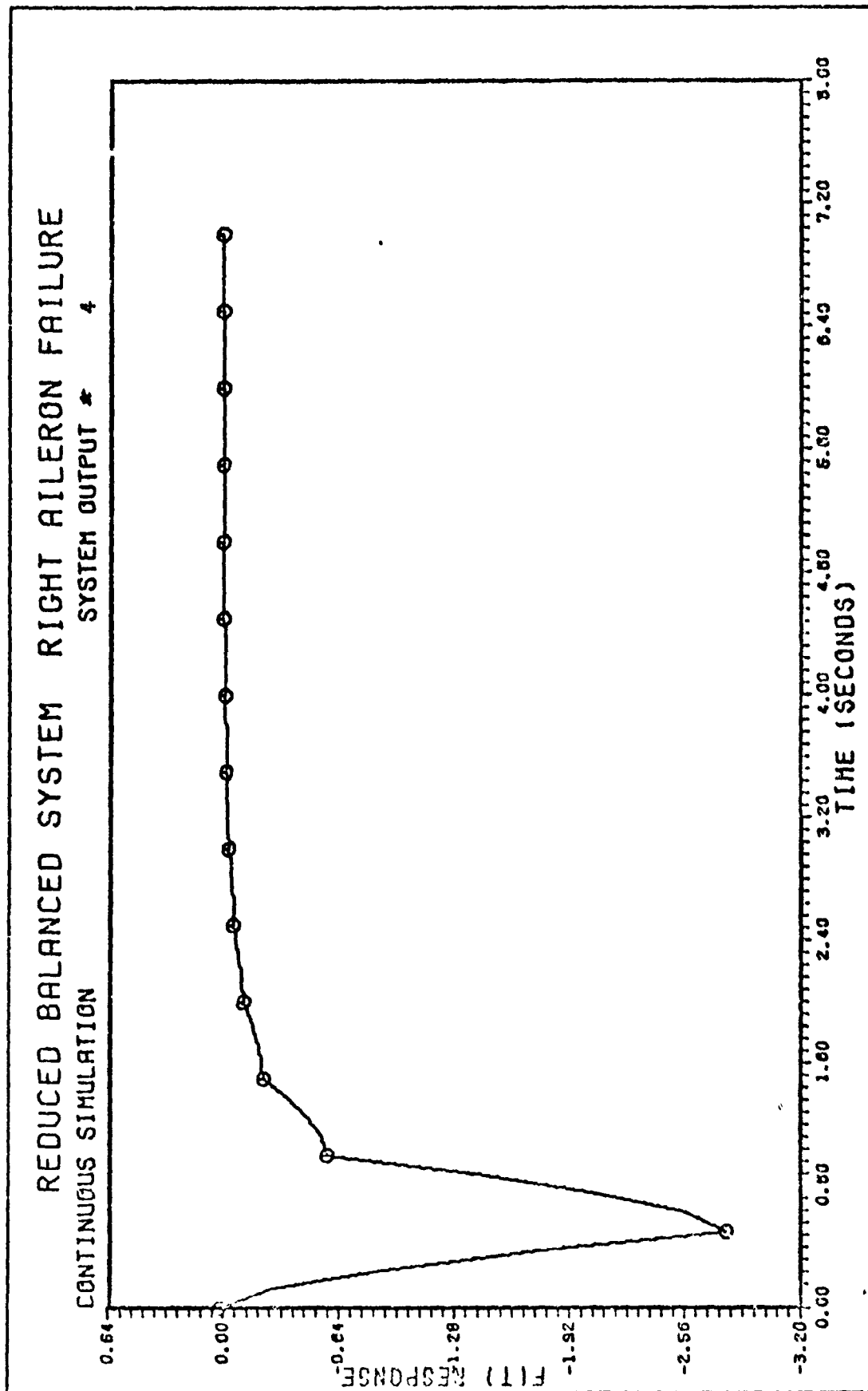


Figure 14d. Roll Rate vs. t

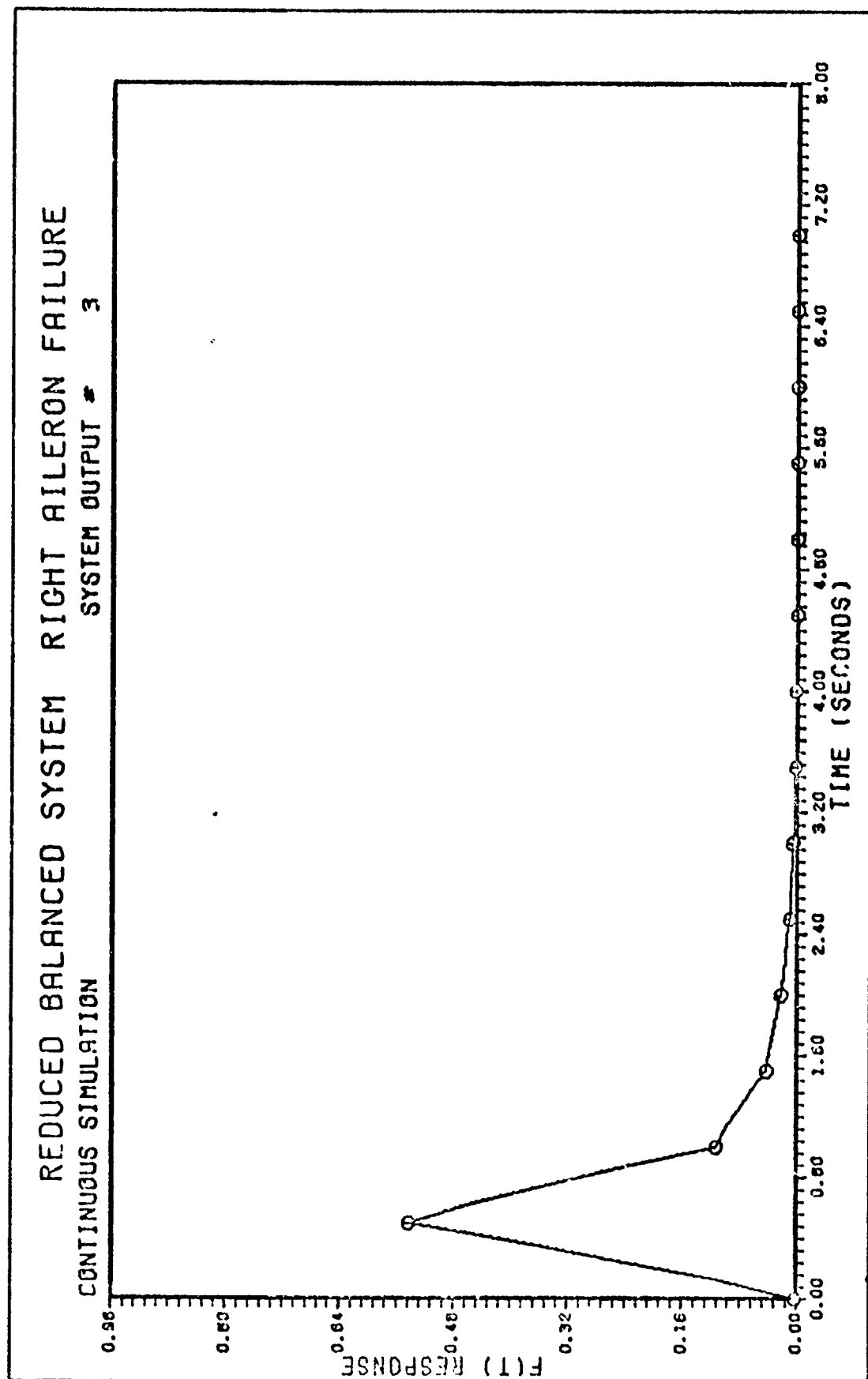


Figure 14e. Sideslip Angle vs.  $t$

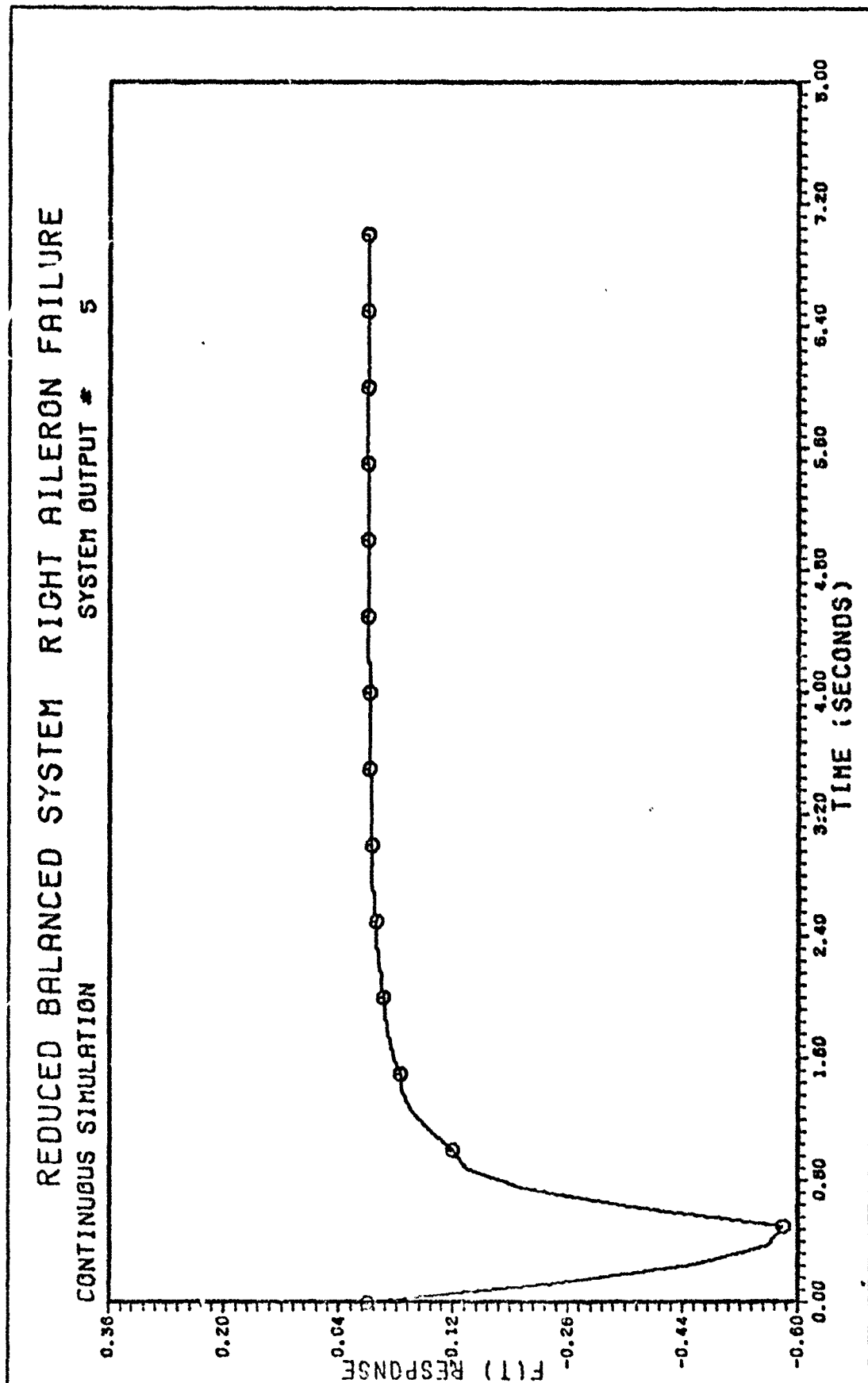


Figure 14f. Yaw Rate

## V. Conclusions and Recommendations

### Conclusions

Reconfiguring the control surfaces response to compensate for a primary surface failure required a comprehensive aircraft model. Using the left and right control surfaces as independently maneuverable inputs in the six degree-of-freedom aircraft equations of motion, an accurate aircraft model was developed in Chapter II. The importance of coupling all the control surface inputs to both the longitudinal and lateral axes is illustrated by the time responses for the uncontrolled original system in Chapter III. Therefore, the equations of motion cannot be decoupled when a sampled-data controller is designed. Inclusion of this coupling between the axes required the derivation of several new non-dimensional control derivatives. The new dimensional control derivatives were then calculated for use in the aircraft model. Using the geometrical properties of the aircraft and the Digital Datcom computer program, the needed control derivatives were derived as shown in Appendix B.

A comprehensive review of entire eigenstructure assignment is presented in Chapter III. The use of this method for designing multivariable control laws is feasible since there is complete freedom in assigning the eigenvalues and the eigenvectors must be within specified sub spaces. With a comprehensive model now available, the entire eigenstructure assignment method was used to assign both the eigenvalues and eigenvectors to the closed-loop plant matrix by synthesizing a state variable feedback control law for a regulator and tracker. Using the interactive computer program CESA, a direct

digital design of both a sampled-data regulator and tracker were attempted in Chapter IV. Considering the number of control inputs, the degree of controllability of the states was established by the singular value decomposition of the  $H_{INF}$  matrix by means of Moore's algorithm for internally balanced matrices. Model reduction is then possible by removing the state(s) of low controllability as indicated by the magnitude of the singular values.

With the degree of controllability of the system determined, the regulator control law design should be carried out first to uncover any mathematical problems with a new system. The regulator designs for reconfiguring the control surfaces of this aircraft model results in a zero steady state error. However, the "proper" selection of the eigenvectors would improve the magnitude of the initial control inputs so that the physical limits of the actuator are not exceeded. Were it not for the time limit at this point in the thesis, it would be possible to reimplement the tracker design for a reconfigurable control law. Plots of the regulator designs are included in this thesis.

#### Recommendations

The aircraft model developed in this thesis and the attempt to design a sampled-data controller by the entire eigenstructure assignment method paves the way for further studies in the area of reconfigurable control laws. Areas that need further investigation and development are:

1. During the design of an aircraft, more extensive wind tunnel testing is necessary to provide the data for the additional control

derivatives in order to obtain a more accurate aircraft model driven by individual control surfaces.

2. The development of the criteria for the selection of the eigenvalues and eigenvectors assigned to the closed-loop plant matrix to insure the design of a realizable multivariable control law. This includes the further study of the entire eigenstructure assignment method to modify the control surface input to compensate for a particular control surface failure.

3. The development of a fault and isolation detection system that monitors the control surface responses. This would determine which control surface is not following the command inputs. This may be accomplished by means of a Kalman filter.

4. The investigation of a digital design method that uses the plant and the measurement (sensor) outputs as feedback which are compared with the input commands for the design of an error-actuated controller as it would apply to reconfigurable tracker control laws.

5. The modification of the interactive program CESA to facilitate the transformation of the reduced feedback balanced matrix to the original state coordinate system. Then apply the transformed state feedback to the original system and compare its response with that of the reduced system.

## Bibliography

1. Bender, M., et al. Flight Test Evaluation of a Digital Multimode Flight Control System for the A-7D Aircraft. Volume I - Design, Analysis, and Ground Test Phase. AFFDL-TR-7597. Air Force Flight Dynamics Laboratory, Wright-Patterson AFB, OH, August 1975.
2. Blakelock, John H. Automatic Control of Aircraft and Missiles. New York: John Wiley & Sons, Inc., 1965.
3. Boudreau, J. A., Berman. Dispersed and Reconfigurable Digital Flight Control System Study, Volume I, Grumman Aerospace Corporation, Bethpage, NY, September 1979.
4. Bradshaw, A. and B. Porter. "Design of Linear Multivariable Discrete-Time Tracking System," International Journal of Systems Science, 6:117-125 (1975).
5. Clarke, R., et al. Flight Test Evaluation of a Digital Multimode Flight Control System for the A-7D Aircraft. Volume II - Flight Test. AFFDL-TR-97. Air Force Flight Dynamics Laboratory, Wright-Patterson AFB, OH, November 1975.
6. D'Azzo, J. J. Synthesis of Linear Multivariable Sampled-Data Feedback Control Systems by Entire Eigenstructure Assignment. Ph.D. dissertation. Salford, England: The University of Salford, 1978.
7. Kennedy, Tom A. The Design of Digital Controllers for the C-141 Aircraft using Entire Eigenstructure Assignment and the Development of an Inter-Active Computer Design Program. M.S. Thesis. Air Force Institute of Technology, Wright-Patterson AFB, OH, March 1979.
8. Kennedy, T. A. CESA - An Interactive Computer for Complete Eigenstructure Assignment to Aid in Designing State-Space Control Law for MIMO Systems. Master Thesis. Air Force Institute of Technology, Wright-Patterson AFB, OH, March 1979.
9. Larimer, S. J. TOTAL - An Interactive Computer Aided Design Program for Digital and Continuous Control System Analysis and Synthesis. Master Thesis. Air Force Institute of Technology, Wright-Patterson AFB, OH, March 1978.
10. Lipari, Louis J. DIGITAC II Phase I, Yaw Control Laws and Analytical Redundancy Evaluation. AFFDL-TR-79-5. Air Force Flight Dynamics Laboratory, Wright-Patterson AFB, OH, April 1979.
11. ITV Vought Aeronautics Division; A-7 Aero-Dynamic Data Report. Rpt No. 2-53310/5R-1981, 21 May 1965.

12. McClendon, J. R. Model Order Reduction Using the Balanced State Representation: Theory, Application, and Interactive Software Implementation. Master Thesis. Air Force Institute of Technology, Wright-Patterson AFB, OH, December 1979. (AD A080371).
13. McClendon, J. R. MIMO - An Interactive Program for Model Order Reduction and Singular Value Analysis at Multivariable, Linear, Time-Invariant System. Master Thesis. Air Force Institute of Technology, Wright-Patterson AFB, OH, December 1979.
14. McDonnell Douglas Corporation; The USAF Stability and Control Digital Datcom. Volume I User's Manual, AFFDL-TR-76-45, Air Force Flight Dynamics Laboratory, Wright-Patterson AFB, OH, 1976.
15. Moore, B. C. Singular Value Analysis of Linear Systems. Part I: External Variables. Systems Control Report No. 7801. Department of Electrical Engineering, University of Toronto, Toronto, Ontario. (1978).
16. Moore, B. C. Singular Value Analysis of Linear Systems. Part II: Controllability, Observability, and Model Reduction. Systems Control Report No. 7802, Department of Electrical Engineering, University of Toronto, Toronto, Ontario. (1978).
17. Porter, B. and A. Bradshaw. "Disturbance Rejection Characteristics of Linear Discrete-Time Systems Incorporating Integral Feedback," Electronic Letters, 11:27-28 (1975).
18. Porter, B. and H. M. Power. "Controllability of Multivariable Systems Incorporating Integral Feedback," Electronic Letters, 6:689-690 (1970).
19. Roskam, Jan. Airplane Flight Dynamics and Automatic Flight Controls. Lawrence, KS: Roskam Aviation and Engineering Corporation, 1976.
20. Seth, W. A. A-7D Estimated Flying Qualities. Report No. 2-53300/8R-8039. Dallas, TX: Vought Aeronautics Division, LTV Aerospace Company, February 19, 1962. (AD 847912).
21. Bender, M. A., Wolf. Flight Test Evaluation of a Digital Flight Control System for the A-7D Aircraft Simulation Test Plan. Contract F33615-73-C-3098. Aeronautical Systems Division, Wright-Patterson AFB, OH, 15 February 1974.
22. Dongarra, J. J., et al. LINPACK User's Guide. Philadelphia: Siam, 1979.

## APPENDIX A

### Introduction

This appendix presents a model of the A-7D using the linearized aircraft equations of motion. Coupling between the longitudinal and the lateral-directional axes is through the control surfaces described earlier. The linearized differential equations of motions are then used to derive the continuous state space model.

### Equations of Motion

The lateral-directional and longitudinal equations are developed with coupling between the axes through the non-traditional control inputs (Ref 4). These equations assume:

1. X, Y, and Z axes are in the plane of symmetry and the origin of the axes is at the center of gravity of the aircraft.
2. The mass of the aircraft is constant.
3. The aircraft is a rigid body.
4. The earth is an inertial reference.
5. The perturbations from equilibrium are small.
6. The flow is quasisteady (Ref 2). The linearized longitudinal equations of motion are as follows:

$$\begin{aligned}\dot{u} = & -g\theta\cos\theta_1 + X_u u + X_\alpha \alpha + X_{\dot{\alpha}} \dot{\alpha} + X_{\delta_{it}} \delta_{it} + X_{\delta_r} \delta_r + X_{\delta_a} \delta_a \\ & + X_{\delta_s} \delta_s + X_{\delta_f} \delta_f\end{aligned}\quad (A-1)$$

$$\begin{aligned}\dot{w} = & U_1 q - g\theta\sin\theta_1 + Z_u u + Z_\alpha \alpha + Z_{\dot{\alpha}} \dot{\alpha} + Z_q q + Z_{\delta_{it}} \delta_{it} + Z_{\delta_r} \delta_r \\ & + Z_{\delta_a} \delta_a + Z_{\delta_s} \delta_s + Z_{\delta_f} \delta_f\end{aligned}\quad (A-2)$$

The dimensional stability derivatives for the aircraft model are given in Table I. Excluded are the dimensional control derivatives which are derived in Appendix B. All of the derivatives relating to angles are per radian measure (Ref 21). The continuous state space of the model is now formed.

#### Continuous State Space

The aircraft model has eight state variables and the control inputs are defined as pairs as shown below. When used as independent control surfaces,  $\delta_{it}$  becomes the  $\delta_{h_l}$  (left) and  $\delta_{h_r}$  (right) horizontal stabilizer. The remaining sets of control surfaces, except the rudder, are split into the left and right control surface when the multi-variable control laws are designed. The states are:

1.  $u$  Perturbation Forward Velocity
2.  $\alpha$  Perturbation Angle of Attack
3.  $q$  Perturbation Pitch Rate
4.  $\theta$  Perturbation Pitch Angle
5.  $\beta$  Perturbation Sideslip
6.  $p$  Perturbation Roll Rate
7.  $r$  Perturbation Yaw Rate
8.  $\phi$  Perturbation Roll Angle

The control inputs are:

1.  $\delta_{it}$  Horizontal Stabilizer Deflection
2.  $\delta_r$  Rudder Deflection
3.  $\delta_a$  Aileron Deflection
4.  $\delta_s$  Spoiler Deflection
5.  $\delta_f$  Flap Deflection

The dimensional stability derivatives for the aircraft model are given in Table I. Excluded are the dimensional control derivatives which are derived in Appendix B. All of the derivatives relating to angles are per radian measure (Ref 21). The continuous state space of the model is now formed.

#### Continuous State Space

The aircraft model has eight state variables and the control inputs are defined as pairs as shown below. When used as independent control surfaces,  $\delta_{it}$  becomes the  $\delta_{h_l}$  (left) and  $\delta_{h_r}$  (right) horizontal stabilizer. The remaining sets of control surfaces, except the rudder, are split into the left and right control surface when the multi-variable control laws are designed. The states are:

1.  $u$  Perturbation Forward Velocity
2.  $\alpha$  Perturbation Angle of Attack
3.  $q$  Perturbation Pitch Rate
4.  $\theta$  Perturbation Pitch Angle
5.  $\beta$  Perturbation Sideslip
6.  $p$  Perturbation Roll Rate
7.  $r$  Perturbation Yaw Rate
8.  $\phi$  Perturbation Roll Angle

The control inputs are:

1.  $\delta_{it}$  Horizontal Stabilizer Deflection
2.  $\delta_r$  Rudder Deflection
3.  $\delta_a$  Aileron Deflection
4.  $\delta_s$  Spoiler Deflection
5.  $\delta_f$  Flap Deflection

TABLE I

Cruise Configuration  
Dimensional Stability Derivatives

$X_u$	-0.00829 *
$X_\alpha$	5.47751
$g$	32.2 ft/sec <sup>2</sup>
$Z_u$	-0.11324
$Z_\alpha$	-632.63786
$Z_q$	0.0
$M_u$	0.00036
$M_\alpha$	-8.15547
$M_\alpha^\circ$	-0.11565
$M_q$	-0.59329
$Y_\beta$	-102.69611
$Y_p$	0.56427
$Y_r$	1.35163
$L_\beta$	-25.73501
$L_p$	-3.00146
$L_r$	0.90217
$N_\beta$	3.9975
$N_p$	-0.0067
$N_r$	-0.5096

\*units rad<sup>-1</sup>

Flight conditions for Table I are given in Appendix B, Table I.

The continuous state space equations of motion are derived from Equations (A-1 - A-6). The state equations are then developed for use with the CESA interactive computer program CESA, so that a discrete-time state variable feedback control law can be designed.

To derive the state space equations, one must solve for the time derivatives of  $u$ ,  $\alpha$ ,  $q$ ,  $\theta$ ,  $\beta$ ,  $r$ ,  $p$ , and  $\phi$ . This derivation assumes  $\dot{X}_a$ ,  $\dot{Z}_a$ , and  $\dot{Z}_q$  are zero (Ref 21). Also, for a steady level flight condition,  $U_1 = \text{constant}$ ,  $V_1 = 0$ ,  $W_1 = 0$ , using the stability axis,  $\theta_1 = 0$ ,  $\phi_1 = 0$ , and  $P_1 = Q_1 = R_1 = 0$ .

Equation (A-1) solved for  $\dot{u}$ :

$$\begin{aligned} \dot{u} = & -g\theta + X_u u + X_\alpha \alpha + X_{\delta_{it}} \delta_{it} \\ & + X_{\delta_r} \delta_r + X_{\delta_a} \delta_a + X_{\delta_s} \delta_s + X_{\delta_f} \delta_f \end{aligned} \quad (A-9)$$

Equation (A-2) is solved for  $\dot{\alpha}$ :

Letting  $w = u\alpha$  implies  $\dot{w} = U_1 \dot{\alpha} + \dot{u} \alpha_1$  where  $\dot{u} \alpha_1 = 0$ . Since  $\alpha_1$  at equilibrium is zero, therefore,  $\dot{w} = U_1 \dot{\alpha}$ . Substituting into Equation (A-2) yields

$$\begin{aligned} U_1 \dot{\alpha} = & U_1 q + Z_u u + Z_\alpha \alpha + Z_{\delta_{it}} \delta_{it} + Z_{\delta_r} \delta_r \\ & + Z_{\delta_a} \delta_a + Z_{\delta_s} \delta_s + Z_{\delta_f} \delta_f \end{aligned} \quad (A-10)$$

Dividing through by  $U_1$  yields

$$\begin{aligned} \dot{\alpha} = & q + \frac{1}{U_1} \left[ Z_u u + Z_\alpha \alpha + Z_{\delta_{it}} \delta_{it} + Z_{\delta_r} \delta_r \right. \\ & \left. + Z_{\delta_a} \delta_a + Z_{\delta_s} \delta_s + Z_{\delta_f} \delta_f \right] \end{aligned} \quad (A-11)$$

Equation (A-3) is solved for  $\dot{q}$ .

$$\begin{aligned}\dot{q} = & M_u u + M_\alpha \alpha + M_{\dot{\alpha}} \dot{\alpha} + M_q q + M_{\delta_{it}} \delta_{it} + M_{\delta_r} \delta_r \\ & + M_{\delta_a} \delta_a + M_{\delta_s} \delta_s + M_{\delta_f} \delta_f\end{aligned}\quad (A-12)$$

To express  $\dot{q}$  in terms of  $U_1 \alpha$ ,  $q$  Equation (A-11) is substituted into Equation (A-12) for  $\dot{\alpha}$ , then regrouping the terms;

$$\begin{aligned}\dot{q} = & M_u u + M_\alpha \alpha + M_{\dot{\alpha}} \left( q + \frac{Z_u}{U_1} U + \frac{Z_\alpha}{U_1} \alpha \right) + M_q q \\ & + \left( \frac{M_{\dot{\alpha}} Z_{\delta_{it}}}{U_1} + M_{\delta_{it}} \right) \delta_{it} + \left( \frac{M_{\dot{\alpha}} Z_{\delta_r}}{U_1} + M_{\delta_r} \right) \delta_r + \left( \frac{M_{\dot{\alpha}} Z_{\delta_a}}{U_1} + M_{\delta_a} \right) \delta_a \\ & + \left( \frac{M_{\dot{\alpha}} Z_{\delta_s}}{U_1} + M_{\delta_s} \right) \delta_s + \left( \frac{M_{\dot{\alpha}} Z_{\delta_f}}{U_1} + M_{\delta_f} \right) \delta_f\end{aligned}\quad (A-13)$$

The final equation needed in the longitudinal state space representation is

$$\dot{\theta} = q \quad (A-14)$$

Equation (A-5) is solved for  $\dot{\beta}$ :

Let  $\dot{V} = U_1 \dot{\beta}$ , which is substituted into Equation (A-4)

$$\begin{aligned}\dot{\beta} = & \frac{1}{U_1} \left( Y_\beta \beta + g\phi + Y_p p \right) + \left( \frac{Y_{r-1}}{U_1} \right) r \\ & + \frac{1}{U_1} \left[ Y_{\delta_{it}} \delta_{it} + Y_{\delta_r} \delta_r + Y_{\delta_a} \delta_a + Y_{\delta_s} \delta_s + Y_{\delta_f} \delta_f \right]\end{aligned}\quad (A-15)$$

Equation (A-6) is solved for  $\dot{r}$ :

The  $EL = \dot{p} - \frac{I_{xz}}{I_{xx}} \dot{r}$  and to simplify use, a new set of primed stability

derivatives (Ref 6) are used:

$$\begin{aligned} L'_i &= L_i + \frac{\frac{I_{xz}}{I_{xx}} N_i}{1 - \frac{I_{xz}^2}{I_{xx}(I_{zz})}} \text{ and} \\ N'_i &= N_i + \frac{\frac{I_{xz}}{I_{zz}} L_i}{1 - \frac{I_{xz}^2}{I_{xx}(I_{zz})}} \end{aligned} \quad (A-16)$$

where  $i$  represents  $\beta$ ,  $p$ ,  $r$ ,  $\delta_{it}$ ,  $\delta_a$ ,  $\delta_r$ ,  $\delta_s$ , and  $\delta_f$ .

$$\begin{aligned} \dot{r} &= L'_\beta \beta + L'_p p + L'_r r + L'_{\delta_{it}} \delta_{it} + L'_{\delta_r} \delta_r \\ &\quad + L'_{\delta_a} \delta_a + L'_{\delta_s} \delta_s + L'_{\delta_f} \delta_f \end{aligned} \quad (A-17)$$

Equation (A-7) is solved for  $\dot{p}$ :

The  $EN = \dot{r} - \frac{I_{xz}}{I_{zz}} \dot{p}$  and simplify Equation (A-6) as above.

$$\begin{aligned} \dot{p} &= N'_\beta \beta + N'_p p + N'_r r + N'_{\delta_{it}} \delta_{it} + N'_{\delta_r} \delta_r \\ &\quad + N'_{\delta_a} \delta_a + N'_{\delta_s} \delta_s + N'_{\delta_f} \delta_f \end{aligned} \quad (A-18)$$

The last equation for the lateral axis equation is:

$$\begin{aligned}\dot{\phi} &= p + r \tan \theta_1 \\ \dot{\phi} &= p\end{aligned}\quad (A-19)$$

The equations for  $\dot{u}$ ,  $\dot{\alpha}$ ,  $\dot{q}$ ,  $\dot{\theta}$ ,  $\dot{\beta}$ ,  $\dot{r}$ ,  $\dot{p}$ , and  $\dot{\phi}$  are put in the matrix form

$$\dot{\mathbf{x}} = \mathbf{A}\mathbf{x} + \mathbf{B}\mathbf{u} \quad (A-20)$$

where

$$\begin{bmatrix} \dot{u} \\ \dot{\alpha} \\ \dot{q} \\ \dot{\theta} \\ \dot{\beta} \\ \dot{p} \\ \dot{r} \\ \dot{\phi} \end{bmatrix} = \begin{bmatrix} X_u & X_\alpha & 0 & -g & 0 & 0 & 0 & 0 \\ Z_u/U_1 & Z_\alpha/U_1 & 1 & 0 & 0 & 0 & 0 & 0 \\ \left( \frac{M_u + M_\alpha Z_u}{U_1} \right) & \left( \frac{M_\alpha + M_\alpha Z_\alpha}{U_1} \right) & M_q & 0 & 0 & 0 & 0 & 0 \\ 0 & 0 & 1 & 0 & 0 & 0 & 0 & 0 \\ 0 & 0 & 0 & 0 & \frac{v_\beta}{U_1} & \frac{Y_p}{U_1} & \frac{Y_{r-1}}{U_1} & \frac{g}{U_1} \\ 0 & 0 & 0 & 0 & L'_\beta & L'_p & L'_r & 0 \\ 0 & 0 & 0 & 0 & N'_\beta & N'_p & N'_r & 0 \\ 0 & 0 & 0 & 0 & 0 & 0 & 1 & 0 \end{bmatrix} \begin{bmatrix} u \\ \alpha \\ q \\ \theta \\ \beta \\ p \\ r \\ \phi \end{bmatrix} +$$

$$\begin{bmatrix} X_{\delta_{it}} & X_{\delta_r} & X_{\delta_a} & X_{\delta_s} & X_{\delta_f} \\ Z_{\delta_{it}}/U_1 & Z_{\delta_r}/U_1 & Z_{\delta_a}/U_1 & Z_{\delta_s}/U_1 & Z_{\delta_f}/U_1 \\ \left( \frac{M_\alpha Z_{\delta_{it}} + M_{\delta_{it}}}{U_1} \right) & \left( \frac{M_\alpha Z_{\delta_r} + M_{\delta_r}}{U_1} \right) & \left( \frac{M_\alpha Z_{\delta_a} + M_{\delta_a}}{U_1} \right) & \left( \frac{M_\alpha Z_{\delta_s} + M_{\delta_s}}{U_1} \right) & \left( \frac{M_\alpha Z_{\delta_f} + M_{\delta_f}}{U_1} \right) \\ 0 & 0 & 0 & 0 & 0 \\ Y_{\delta_{it}}/U_1 & Y_{\delta_r}/U_1 & Y_{\delta_a}/U_1 & Y_{\delta_s}/U_1 & Y_{\delta_f}/U_1 \\ L_{\delta_{it}} & L_{\delta_r} & L_{\delta_a} & L_{\delta_s} & L_{\delta_f} \\ N_{\delta_{it}} & N_{\delta_r} & N_{\delta_a} & N_{\delta_s} & N_{\delta_f} \\ 0 & 0 & 0 & 0 & 0 \end{bmatrix} \begin{bmatrix} \delta_{it} \\ \delta_r \\ \delta_a \\ \delta_s \\ \delta_f \end{bmatrix} \quad (A-21)$$

The A matrix for the system is, as follows:

$$A = \begin{bmatrix} -0.8290E-2 & 5.478 & 0. & -32.20 \\ -0.1784E-3 & -0.9966 & 1.000 & 0 \\ 0.3806E-3 & -8.155 & -0.5933 & 0 \\ 0 & 0 & 1.000 & 0 \\ 0 & 0 & 0 & 0 \\ 0 & 0 & 0 & 0 \\ 0 & 0 & 0 & 0 \\ 0 & 0 & 0 & 0 \end{bmatrix}$$

$$\begin{bmatrix} 0 & 0 & 0 & 0 \\ 0 & 0 & 0 & 0 \\ 0 & 0 & 0 & 0 \\ 0 & 0 & 0 & 0 \\ -0.1618 & 0.8900E-3 & -0.9979 & 0.5072E-1 \\ -26.23 & -3.008 & 0.9610 & 0 \\ 4.547 & 0.5678E-1 & -0.5310 & 0 \\ 0 & 0 & 1.000 & 0 \end{bmatrix} \begin{bmatrix} u \\ \alpha \\ q \\ \theta \\ \beta \\ p \\ r \\ \phi \end{bmatrix}$$

(A-22)

With a  $\delta_{ar}$  failure the B matrix is:

$$B^* = \begin{bmatrix} -16.43 & -16.43 & -7.506 & 0. \\ -0.6730E-1 & -0.6730E-1 & 0 & -0.4788E-1 \\ -7.955 & -7.955 & 0 & 1.860 \\ 0 & 0 & 0 & 0 \\ 0 & 0 & 0.4530E-1 & -0.5816E-2 \\ -8.040 & 8.040 & 5.967 & 17.19 \\ 0.6014 & -0.6014 & -5.198 & 0.2985E-1 \\ 0 & 0 & 0 & 0 \end{bmatrix}$$

$$\begin{bmatrix} 260 & -1.260 & -9.3423 & -9.3423 \\ -0.9707E-2 & -0.9707E-2 & -0.9351E-1 & -0.9351E-1 \\ -0.2013 & -0.2013 & -1.0488 & -1.0488 \\ 0 & 0 & 0 & 0 \\ 0.1424E-2 & -0.1424E-2 & 0 & 0 \\ -1.099 & 1.099 & -5.3212 & 5.3212 \\ -0.5335E-1 & 0.5335E-1 & 0.1571 & -0.1571 \\ 0 & 0 & 0 & 0 \end{bmatrix} \begin{bmatrix} \delta_{h_l} \\ \delta_{h_r} \\ \delta_r \\ \delta_{a_l} \\ \delta_{s_l} \\ \delta_{s_r} \\ \delta_{f_l} \\ \delta_{f_r} \end{bmatrix}$$

\*See page 116.

(A-23)

where the failed right aileron control input is missing. The sign convention for the control surface is: positive  $\delta_h$ ,  $\delta_{a_l}$ , and  $\delta_f$  is trailing edge down; positive  $\delta_r$  is trailing edge left; positive  $\delta_s$  is spoiler up.

For the regulator design the left and right flap inputs are dropped to resolve the controllability and eigenvector problems associated with the tracker design.

The tracker output equation is:

$$Cx = \begin{bmatrix} 0 & -1 & 0 & 1 & 0 & 0 & 0 & 0 \\ 0 & 0 & 0 & 0 & 1 & 0 & 0 & 0 \\ 0 & 0 & 0 & 0 & 0 & 0 & 1 & 0 \\ 0 & 0 & 0 & 0 & 0 & 0 & 0 & 1 \end{bmatrix} \begin{bmatrix} u \\ \alpha \\ q \\ \theta \\ \beta \\ p \\ r \\ \phi \end{bmatrix} \quad (A-24)$$

and the desired command input for the tracker is:

$$v(t) = \begin{bmatrix} 1 \\ 0 \\ 0 \\ 0 \end{bmatrix} = \begin{bmatrix} \theta - \alpha = \gamma \\ \beta \\ r \\ \phi \end{bmatrix} \quad (A-25)$$

where  $\gamma = \theta - \alpha$  is the flight path angle. The regulator output matrix  $C$  is:

$$Cx = \begin{bmatrix} 0 & 0 & 1 & 0 & 0 & 0 & 0 & 0 \\ 0 & 0 & 0 & 1 & 0 & 0 & 0 & 0 \\ 0 & 0 & 0 & 0 & 1 & 0 & 0 & 0 \\ 0 & 0 & 0 & 0 & 0 & 1 & 0 & 0 \\ 0 & 0 & 0 & 0 & 0 & 0 & 1 & 0 \\ 0 & 0 & 0 & 0 & 0 & 0 & 0 & 1 \end{bmatrix} \begin{bmatrix} u \\ \alpha \\ q \\ \theta \\ \beta \\ p \\ r \\ \phi \end{bmatrix} \quad (A-26)$$

The following equations are for the internally balanced matrices of the system generated by MIMO (Ref 13). The plant matrix is:

$$A' = \begin{bmatrix} -0.1695 & -0.2289E-2 & -0.1297E-1 & 0.1447E-1 \\ -0.2146 & -0.7590E-4 & -0.6469E-2 & 0.1587E-1 \\ 0.2143E-1 & 0.9030E-2 & 0.5677E-1 & 0.1149 \\ -0.3819E-1 & -0.2011E-1 & -0.7662E-1 & -0.8726E-1 \\ -1.663 & -1.004 & -0.2189E-1 & 0.5202E-1 \\ -0.6214E-1 & -0.2490E-1 & 0.2280 & -0.5543 \\ -0.1076E-1 & -0.2002E-2 & 0.3949E-1 & -0.2044 \\ -0.2895 & -0.1751 & 0.1538E-1 & -0.3358E-1 \end{bmatrix}$$
  

$$\begin{bmatrix} 1.718 & -0.5732E-1 & 0.4076E-1 & -0.4794 \\ 1.025 & -0.3078E-1 & 0.1075E-1 & -0.2376 \\ 0.2811E-1 & -0.3121E-1 & 0.7517E-2 & -0.8604E-2 \\ -0.4492E-1 & 0.1865 & 0.2124 & 0.7503E-2 \\ -0.7259 & 0.1813 & -0.1018 & 1.360 \\ -0.2004E-1 & -1.450 & 2.701 & 0.4078E-1 \\ 0.3793E-1 & -3.051 & -0.193 & 0.3932 \\ -0.2407 & -0.3918 & -0.1836 & -2.784 \end{bmatrix} \quad (A-27)$$

The  $B'_0$  input matrix is:

$$B'_0 = \begin{bmatrix} -0.2470 & 0.1983 & -2.033 \\ -0.1457 & 0.1752 & -0.8886 \\ 0.3737 & 0.3848 & 0.4047E-1 \\ -0.8989 & -0.9095 & -0.4522E-1 \\ 0.7163 & -0.6700 & -3.747 \\ -2.423 & -2.218 & -0.5811E-1 \\ -0.6118 & -0.7415 & 0.2381E-1 \\ -0.9802 & 1.573 & 0.7340 \end{bmatrix}$$
  

$$\begin{bmatrix} 0.9265E-1 & 1.091 & -0.9363E-1 \\ 0.5125E-1 & 0.6013 & -0.5074E-1 \\ 0.8547E-2 & -0.9944E-1 & 0.8005E-2 \\ -0.1681E-1 & 0.2573 & -0.1749E-1 \\ -0.2134E-2 & -0.5889 & 0.3069E-2 \\ -0.4078E-1 & 0.8001 & -0.7639E-1 \\ -0.1970E-1 & 0.6600E-1 & 0.2221E-2 \\ 0.2301 & 3.137 & -0.2145 \end{bmatrix} \begin{bmatrix} \delta_{h_1} \\ \delta_{h_r} \\ \delta_r \\ \delta_{a_1} \\ \delta_{s_1} \\ \delta_{s_r} \end{bmatrix}$$

(A-28)

The  $C'_0$  matrix is:

$$C'_0 x = \begin{bmatrix} 0.2767E-1 & 0.1357E-1 & -0.1832 & 0.2226 \\ -0.4228E-1 & -0.3246E-1 & 0.2157 & 1.366 \\ -0.4086 & -0.2212 & -0.7995E-2 & 0.1546E-1 \\ 2.183 & 0.9912 & 0.2776E-3 & 0.3343E-1 \\ 0.4128 & 0.2848 & -0.7939E-2 & 0.1697E-1 \\ 0.6222 & -0.2040 & 0.1058E-1 & -0.2820E-1 \\ -0.1859E-1 & 3.339 & -0.2253 & -0.2936 \\ -0.2395E-1 & -0.2415 & -0.8955 & -0.3772E-1 \\ 0.2191 & 0.2959E-1 & -0.1504E-1 & 0.2150 \\ -3.747 & 0.4795 & -0.2491 & 3.707 \\ 1.093 & 0.2318E-2 & -0.101E-3 & 0.1423E-1 \\ -0.2464 & -0.2907E-1 & 0.1439E-1 & -0.2137 \end{bmatrix} \begin{bmatrix} u \\ \alpha \\ q \\ \theta \\ \beta \\ p \\ r \\ \phi \end{bmatrix}$$

(A-29)

After final review of the B matrix, it was determined that the signs of the lateral-directional coefficients  $[\delta_{h_1}, \delta_{h_r}, \delta_{f_1}, \delta_{f_r}]$  and the longitudinal coefficients  $[\delta_{a_1}$  (pitching moment) and  $\delta_{s_1}, \delta_{s_r}$  (lift)] required a sign change. Also the  $\delta_{a_1}$  (pitching moment) coefficient was corrected. The time response plots for this thesis were obtained using the B matrix of Equation (A-23). The following B matrix should be used for future studies of reconfigurable multivariable

control laws:

$$B = \begin{bmatrix} -16.43 & -16.43 & -7.506 & 0 \\ -0.6730E-1 & -0.6730E-1 & 0 & -0.4788E-1 \\ -7.955 & -7.955 & 0 & -0.3944 \\ 0 & 0 & 0 & 0 \\ 0 & 0 & 0.4530E-1 & -0.5816E-2 \\ 8.040 & -8.040 & 5.967 & 17.19 \\ -0.6014 & 0.6014 & -5.198 & 0.2985E-1 \\ 0 & 0 & 0 & 0 \\ -1.260 & -1.260 & -9.3423 & -9.3423 \\ 0.9707E-2 & 0.9707E-2 & -0.9351E-1 & -0.9351E-1 \\ -0.2013 & -0.2013 & -1.0488 & -1.0488 \\ 0 & 0 & 0 & 0 \\ 0.1424E-2 & -0.1424E-2 & 0 & 0 \\ -1.099 & 1.099 & 5.3212 & -5.3212 \\ -0.5335E-1 & 0.5335E-1 & -0.1571 & 0.1571 \\ 0 & 0 & 0 & 0 \end{bmatrix}$$

(A-30)

## APPENDIX B

### Introduction

At this point, one should remember that the control surface inputs will be separated into independent variable left and right control surfaces. When this is done, caution must be exercised in assigning the correct sign to the left and right control derivative. For example, the derivative  $L'_{\delta_a}$ , the change of rolling moment due to aileron deflection, is -34.4 for both surfaces. This indicates that the right aileron is down and the left aileron is up causing a rolling moment to the left. When the aileron surfaces are treated as independent controls, the rolling moment coefficient due to the right aileron ( $L'_{\delta_{ar}}$ ) has a value of -17.2 and the left aileron 17.2. This assumes the sign convention is trailing edge down and represents a positive deflection.

This appendix presents the equations used to derive the dimensional control derivatives and the derivation of the non-dimensional control derivatives for non-traditional control surfaces used as input in the aircraft equations of motion.

### Dimensional Control Derivatives Equations

The equations for the longitudinal dimensional control derivatives are, as follows:

Let  $X = \bar{q}S/m$  then;

$$X_{\delta} = -XC_{D_{\delta}} \quad (B-1)$$

Where  $\delta = \delta_{it}, \delta_r, \delta_a, \delta_s, \delta_f$ , which remains the same for the remainder

of the equations illustrated.

For the Z force inputs, let  $Z = \bar{q}S/m$  then,

$$Z_{\delta} = -ZC_{L_{\delta}} \quad (B-2)$$

and for the M torque inputs, let  $M = \bar{q}Sc/I_{yy}$ ,

$$M_{\delta} = MC_{m_{\delta}}. \quad (B-3)$$

Continuing with the lateral-directional control derivatives, let

$$Y = \bar{q}S/m$$

$$Y_{\delta} = YC_{y_{\delta}} \quad (B-4)$$

and for the L and N torque inputs, let  $L = \bar{q}Sb/I_{zz}$  then,

$$L_{\delta} = LC_{l_{\delta}} \quad (B-5)$$

and

$$N_{\delta} = NC_{n_{\delta}}. \quad (B-6)$$

The data for use with the above equations is given in Table I, (Ref 21).

TABLE I

## Aircraft Data Cruise Configuration

ALTITUDE	15,000 ft.
MACH	.6
WEIGHT	25,338 lbs.
c.g.	28.71% of mgc
$\bar{q}$	300.88 lbs/ft <sup>2</sup>
s	375 ft. <sup>2</sup>
b	38.73 ft.
$\bar{c}$	10.84 ft.
$I_{xx}$	15,365 Slug ft. <sup>2</sup>
$I_{zz}$	79,005 Slug ft. <sup>2</sup>
$I_{yy}$	69,528 Slug ft. <sup>2</sup>
$I_{xz}$	-1,664 Slug ft. <sup>2</sup>

Now the method mentioned in Chapter II is used to obtain the new non-dimensional control derivatives.

#### Derivation of Non-Dimensional Control Derivatives

The control derivatives of Table II are for the aircraft at a cruise configuration of 0.6 Mach, angle of attack at  $4.2^\circ$  and flying at 15K feet from the following three references: digital DATCOM (Ref 14), A-7 Aerodynamic Data (Ref 11), and from (Ref 21). The digital DATCOM program was used to find those non-dimensional control derivatives not available from the other reference sources. Therefore, only those

TABLE II

## Non-Dimensional Control Derivatives\*

LONGITUDINAL		LATERAL-DIRECTIONAL	
$C_{D\delta_{hr}}$	0.1146	$C_{y\delta_{hr}}$	0.0
$C_{L\delta_{hr}}$	0.29796	$C_{l\delta_{hr}}$	-0.02827
$C_{m\delta_{hr}}$	-0.45276	$C_{n\delta_{hr}}$	-0.01087
$C_{D\delta_r}$	0.05233	$C_{y\delta_{ar}}$	0.02505
$C_{L\delta_r}$	0.0	$C_{l\delta_{ar}}$	-0.06045
$C_{m\delta_r}$	0.0	$C_{n\delta_{ar}}$	0.0071
$C_{D\delta_{ar}}$	0.0	$C_{y\delta_r}$	0.20055
$C_{L\delta_{ar}}$	0.2120	$C_{l\delta_r}$	0.01902
$C_{m\delta_{ar}}$	-0.0229	$C_{n\delta_r}$	-0.0917
$C_{D\delta_{sr}}$	8.7859E-3	$C_{y\delta_{sr}}$	-6.303E-3
$C_{L\delta_{sr}}$	-0.04297	$C_{l\delta_{sr}}$	3.8636E-3
$C_{m\delta_{sr}}$	-0.01146	$C_{n\delta_{sr}}$	1.9100E-3
$C_{D\delta_{fr}}$	0.06515	$C_{y\delta_{fr}}$	0.0
$C_{L\delta_{fr}}$	0.41399	$C_{l\delta_{fr}}$	-0.01865
$C_{m\delta_{fr}}$	-0.06024	$C_{n\delta_{fr}}$	3.0879E-4

\*Units  $\text{rad}^{-1}$ , right control surface, except rudder

control derivatives found with digital DATCOM will be addressed here.

The following derivatives were derived using digital DATCOM:  $C_{D_{\delta_h}}$ ,  $C_{D_{\delta_r}}$ ,  $C_{D_{\delta_f}}$ ,  $C_{L_{\delta_f}}$ ,  $C_{m_{\delta_f}}$ ,  $C_{l_{\delta_h}}$ ,  $C_{n_{\delta_f}}$  and  $C_{l_{\delta_f}}$  since this data is not usually available from wind tunnel testing. To establish confidence in this method, a comparison was done on  $C_{n_{\delta_s}}$  between digital DATCOM and the A-7 aerodynamic data, which is shown later in this Appendix. For the longitudinal mode, digital DATCOM provided the data for the following non-dimensional control derivatives:  $C_{D_{\delta_h}}$ ,  $C_{D_{\delta_r}}$ ,  $C_{D_{\delta_f}}$ ,  $C_{m_{\delta_f}}$ , and  $C_{L_{\delta_f}}$ . The drag for the horizontal stabilizer is usually considered zero. But to be thorough, as many control derivatives as possible were implemented in the aircraft equations of motion. Thus,  $C_{D_{\delta_h}}$  was derived using the following equation and the data is in Table III.

$$C_{D_{\delta_h}} = \frac{\Delta C_D|_{i_h} = i_{h|x} + i_{h_T} - C_D|_{i_h}}{\Delta X} \quad (B-7)$$

Where  $C_D$  is 0.035 with a trim angle of attack at  $i_{h_T}$   $4.35^\circ$ ,  $\Delta X$  is the change in the tail incidence angle, and  $C_{D_{i_h}}$  is the drag of the unit horizontal tail (UHT) at the incidence angle in question. The average is then taken on the summation of the results from the data in Table III for each angle change to determine  $C_{D_{\delta_h}}$ . Using the average applies to the derivation of all the remaining control derivatives that follow, except for  $C_{n_{\delta_h}}$  and  $C_{D_{\delta_s}}$ .

The derivation of  $C_{D_{\delta_r}}$  required that the vertical tail be modeled

as a wing in order to obtain this control derivative using the following formula.

$$C_{D_{\delta_r}} = \frac{\Delta C_{D_{min}} + C_{D_i}}{\Delta \delta_r} \quad (B-8)$$

Where  $C_{D_i}$  is the induced drag coefficient and  $C_{D_{min}}$  is the change in minimum drag due to a change in control surface deflection,  $\delta_r$ . Table IV contains the data used to find  $C_{D_{\delta_r}}$ .

For  $C_{D_{\delta_f}}$  change in drag due to flap deflection was found using Equation (B-8) only  $\delta_r$  is now  $\delta_f$ . The data used in the derivation of  $C_{D_{\delta_f}}$ ,  $C_{L_{\delta_f}}$ , and  $C_{m_{\delta_f}}$  is in Table IV. The following equations were used for the derivation of  $C_{L_{\delta_f}}$  and  $C_{m_{\delta_f}}$  are:

$$C_{L_{\delta_f}} = \frac{\Delta C_L}{\Delta \delta_f}$$

$$C_{m_{\delta_f}} = \frac{\Delta C_m}{\Delta \delta_f} \quad (B-9)$$

TABLE III

DATCOM Data for  $C_{D\delta_h}$  and  $C_{D\delta_r}$ 

$C_{D\delta_h}$		$C_{D\delta_r}$		
$\delta_h$	$C_D$	$\delta_r$	$C_{D_{min}}$	$C_{D_i}$
4.0° Ref	0.035	-6.0	0.00547	9.57E-6
6.0	0.039	-4.0	0.00337	3.88E-6
8.0	0.043	-2.0	0.00154	6.917E-7
10.0	0.047	0	0	0
12.0	0.050	2.0	0.00154	1.8E-6
15.0	0.055	4.0	0.00337	6.1E-6
		6.0	0.00547	1.29E-6

\*Units  $\text{deg}^{-1}$

TABLE IV

DATC OM Data for  $C_{D\delta_f}$ ,  $C_{L\delta_f}$ , and  $C_{m\delta_f}$ 

	$C_{D\delta_f}$		$C_{L\delta_f}$	$C_{m\delta_f}$
$\delta_f$	$C_{D_{min}}$	$C_{D_1}$	$C_L$	$C_m$
5			0.094	-0.0137
10	0.00583	6.19E-4	0.187	-0.0273
15	0.01356	1.47E-3	0.276	-0.0402
20	0.02294	2.59E-3	0.361	-0.0526
25	0.03453	3.93E-3	0.439	-0.064
30	0.04743	5.25E-3	0.502	-0.0732
35	0.06203	6.34E-3	0.549	-0.0801
40	0.07578	7.04E-3	0.578	-0.0843

\*Units  $\text{deg}^{-1}$ 

The lateral control derivatives  $C_{l\delta_h}$ ,  $C_{n\delta_f}$ , and  $C_{l\delta_f}$  were derived with the data in Table V and the following equations:

$$C_{l\delta_h} = \frac{\Delta C_l}{\Delta \delta_h}$$

$$C_{n\delta_f} = \frac{\Delta C_n}{\Delta \delta_f}$$

$$C_{l\delta_f} = \frac{\Delta C_l}{\Delta \delta_f}$$

(B-10)

The  $C_{n\delta_h}$  control derivative was calculated using the following equation,

$$C_{n\delta_h} = \frac{-C_{l_{it}} \cdot C_{D_{it}}}{C_{l_{it}} \cdot 2} \quad (B-11)$$

where  $C_{l_{it}} = 0.5937/\text{rad}$ ,  $C_{D_{it}} = 0.2292/\text{rad}$  from (Ref 21) and  $C_{l_{it}}$  is twice  $C_{l\delta_h}$ . The 2 is divide through to obtain the magnitude for one control surface and the minus sign indicates the direction of yaw with the left UHT down.

TABLE V

DATCOM Data for  $C_{l\delta_h}$ ,  $C_{n\delta_f}$ , and  $C_{l\delta_f}$

$C_{l\delta_h}$			$C_{n\delta_f}$	$C_{l\delta_f}$
$\delta_h$	$C_l$	$\delta_f$	$C_n$	$C_l$
6.8	3.329E-3	5	-1.228E-4	2.8309E-3
5.0	2.466E-3	10	-2.456E-4	5.6617E-3
0	0	15	-3.601E-4	8.3004E-3
7.5	-3.699E-3	20	-4.193E-4	9.6722E-3
10.0	-4.932E-3	25	-4.402E-4	1.0157E-3
12.5	-6.164E-3	30	-4.791E-4	1.1054E-3
15.0	-7.397E-3	35	-5.215E-4	1.2031E-3
17.5	-8.630E-3	40	-5.646E-4	1.3026E-3
20.0	-9.860E-3			
22.5	-1.110E-2			

\*Units  $\text{deg}^{-1}$

TABLE VI

Data for  $C_{n\delta_s}$ 

$C_{n\delta_s}$		
$\delta_s$	$C_n$ (DATCOM)	$C_n$ (Ref 2)
10	3.47E-4	3.0E-4
20	6.84E-4	7.0E-4
30	1.0E-3	1.8E-3
40	1.285E-3	2.0E-3
50	1.53E-3	2.5E-3
60	1.73E-3	3.5E-3

\*Unit  $\text{deg}^{-1}$ 

To obtain a degree of confidence in the data being used, a comparison was made between the A-7D Aerodynamic Data (Ref 11:206) and the digital DATCOM data for  $C_n$  vs.  $\delta_s$ . The following equation, along with the data from Table VI was used to derive  $C_{n\delta_s}$ .

$$C_{n\delta_s} = \frac{\Delta C_n}{\Delta \delta_s} \quad (\text{B-12})$$

Since the data of (Ref 11) for  $C_n$  is for a spoiler deflector, the average value had to be divided by a scale factor of 1.75, (Ref 14:62) in order to obtain a  $C_{n\delta_s}$  for the spoiler alone. The values are 1.91E-3/rad and 1.652E-3/rad for the A-7 Aerodynamic and DATCOM data

respectively, with a difference of  $3.58\text{E-}4/\text{rad}$ . This is an acceptable difference considering the different methods used in their derivation.

The  $C_{D_{\delta_s}}$  was derived with the following equation

$$C_{D_{\delta_s}} = \frac{C_{n_{\delta_s}} \cdot b}{\text{OBS}} \quad (\text{B-13})$$

where  $b$  is the wing span and OBS is the out board end of the spoiler which is 43.46% of the semispan.

This completes the derivation of the dimensional control derivative equations, and the non-dimensional control derivatives not available in (Ref 11) or (Ref 21). After reexamination of the  $C_{D_{\delta_r}}$  coefficient (which may be zero), it is suggested that this control derivative be further investigated in future studies.

### Vita

David W. Potts was born in New York City, New York on August 28, 1942. He entered the Air Force in October 1961. In December 1976, he received his B.S. degree in electrical engineering from the Oklahoma State University, Oklahoma. He received a Commission in the United States Air Force after completion of OTS in March 1977. He was then assigned to the 552nd AWACS as Chief, Battle Staff Section, responsible for the battlestaff software programs of the airborne operational computer program (AOCP). Upon completion of the guidance and control graduate program at the Air Force Institute of Technology, he is being assigned to the AFWAL/Flight Dynamics Laboratory.

UNCLASSIFIED

SECURITY CLASSIFICATION OF THIS PAGE (When Data Entered)

REPORT DOCUMENTATION PAGE		READ INSTRUCTIONS BEFORE COMPLETING FORM
1. REPORT NUMBER AFIT/GE/EE/80D-36 ✓	2. GOVT ACCESSION NO. AD-A100794	3. RECIPIENT'S CATALOG NUMBER
4. TITLE (and Subtitle) DIRECT DIGITAL DESIGN METHOD FOR RECONFIGURABLE MULTIVARIABLE CONTROL LAWS FOR THE A-7D DIGITAC II AIRCRAFT		5. TYPE OF REPORT & PERIOD COVERED MS Thesis
7. AUTHOR(s) David W. Potts		6. PERFORMING ORG. REPORT NUMBER
9. PERFORMING ORGANIZATION NAME AND ADDRESS Air Force Institute of Technology (AFIT-EN) Wright-Patterson AFB, Ohio 45433		8. CONTRACT OR GRANT NUMBER(s)
11. CONTROLLING OFFICE NAME AND ADDRESS Control Systems Development Br/Flight Control Div. Flight Dynamics Lab., AF Wright Aeronautical Lab. (AFWAL/FIGL), Wright-Patterson AFB, Ohio 45433		10. PROGRAM ELEMENT, PROJECT, TASK AREA & WORK UNIT NUMBERS
14. MONITORING AGENCY NAME & ADDRESS (if different from Controlling Office)		12. REPORT DATE December 1980
		13. NUMBER OF PAGES
		15. SECURITY CLASS. (of this report) UNCLASSIFIED
		15a. DECLASSIFICATION/DOWNGRADING SCHEDULE
16. DISTRIBUTION STATEMENT (of this Report)  Approved for public release; distribution unlimited		
17. DISTRIBUTION STATEMENT (of the abstract entered in Block 20, if different from Report)		
18. SUPPLEMENTARY NOTES  Approved for public release; IAW AFR 190-17 <i>Fredric C. Lynch</i> FREDRIC C. LYNCH, Major, USAF Director of Public Affairs		
19. KEY WORDS (Continue on reverse side if necessary and identify by block number) CONTROL LAW A-7D RECONFIGURABLE CONTROL LAWS REGULATOR CONTROL LAW DIRECT DIGITAL DESIGN 6 D-O-F A/C EQUATIONS MULTIVARIABLE CONTROL LAW ENTIRE EIGENSTRUCTURE ASSIGNMENT 21 MAY 1981		
20. ABSTRACT (Continue on reverse side if necessary and identify by block number) This thesis investigates control of an aircraft when there is a primary control surface failure. The object of this study is to reconfigure the remaining control surfaces to compensate for the additional forces and moments generated by the inoperative control surface. To study this flight control problem, a comprehensive aircraft model is required which considers each control surface operating individually.  A six degree-of-freedom aircraft model is developed, including all the		

UNCLASSIFIED

SECURITY CLASSIFICATION OF THIS PAGE (When Data Entered)

UNCLASSIFIED

SECURITY CLASSIFICATION OF THIS PAGE(When Data Entered)

Block 20 - Continued

individual control surfaces. A control surface input can produce both a lateral and/or a longitudinal response. Thus, the equations of motion cannot be decoupled for the design of the control laws. The coupling between the axes requires the derivation of several new non-dimensional control derivatives. Using the geometrical properties of the aircraft and the Digital Datcom computer program, the needed control derivatives are derived.

With a comprehensive aircraft model now available, the entire eigenstructure assignment method is used to assign both the eigenvalues and the eigenvectors to the closed-loop plant matrix. This method is used for the direct digital design of a multivariable discrete regulator and tracker control law. The effect of increasing the number of control inputs on the relative degree of controllability of the states was determined by singular value decomposition.

This thesis concludes that a direct digital design for reconfiguring the multivariable control law is feasible. However, more wind tunnel data is essential to derive the additional control derivatives for a more accurate aircraft model driven by individual control surfaces. Further work is also necessary to perfect the assignment of the closed-loop eigenvalues and eigenvectors.

UNCLASSIFIED

SECURITY CLASSIFICATION OF THIS PAGE(When Data Entered)